

CR-189334

IN-35
2948

FINAL REPORT

DEFORMED ELLIPSOIDAL DIFFRACTION GRATING BLANK

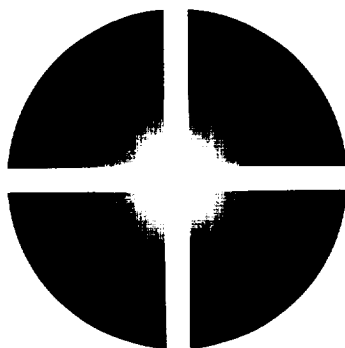
Contract No. NAS5-31790

(NASA-CR-189334) DEFORMED
ELLIPSOIDAL DIFFRACTION GRATING
BLANK Final Report (Space Optics
Research Labs.) 113 p

N94-29872

Unclass

G3/35 0003848



FINAL REPORT

DEFORMED ELLIPSOIDAL DIFFRACTION GRATING BLANK

Contract No. NAS5-31790

Submitted by:

**SPACE OPTICS RESEARCH LABS
AN INTERGRAPH DIVISION
7 STUART ROAD
CHELMSFORD, MA 01824**

Alan E. DeCew, Jr.
General Manager

FINAL REPORT

DEFORMED ELLIPSOIDAL DIFFRACTION GRATING BLANK

Contract No. NAS5-31790

TABLE OF CONTENTS

1.0	Introduction
2.0	Applicable Documents
3.0	Program Summary
3.1	Fabrication planning
3.2	Fabrication and initial testing
3.2.1	The holographic interferometer
3.2.2	The aspheric figuring
3.2.3	The testing metrology
3.3	Final testing
4.0	Specification Compliance
4.1	Surface figure
4.2	Figure error
4.2.1	Overall Peak to Valley
4.2.2	Midfrequency roughness
4.2.3	Microroughness
5.0	Recommendations
5.1	Fabrication times and techniques
5.2	Figure error metrology
6.0	Conclusion

TABLE OF APPENDICES

Appendix A	DEGB surface figure calculations
Appendix B	Manufacturing and test plan
Appendix C	Figuring cycles to fabricate DEGB
Appendix D	Interferometer for aspheric testing
Appendix E	Optical test set up configuration
Appendix F	An alternate test method
Appendix G	Surface scan data for midfrequency
Appendix H	Contract statement of work
Appendix I	Quality assurance documentation

1.0 Introduction

The Deformed Ellipsoidal Grating Blank (DEGB) is the primary component in an ultraviolet spectrometer. Since one of the major concerns for these instruments is throughput, significant efforts are made to reduce the number of components and subsequently reflections. Each reflection results in losses through absorption, and scattering. It is these two sources of photon loss that dictated the requirements for the DEGB.

The first goal is to shape the DEGB in such a way that the energy at the entrance slit is focused as well as possible on the exit slit. This is a geometrical problem which must account for the diffraction angle of the radiation. The result was the shape defined in the specification. This shape is a non-rotationally symmetric general asphere. This unusual surface requires an unusual test and unusual test equipment to verify the shape.

The second goal is to produce a surface smooth enough to minimize the photon loss due to scattering. The production techniques to produce these surfaces are often held in the craftsmanship of the optician. The measurement is accomplished with modern scanning interferometric methods.

2.0 Applicable Documents

3.0 Program Summary

The program was accomplished in three phases. The first phase was the fabrication planning. The second phase was the actual fabrication and initial testing. The last phase was the final testing of the completed DEGB.

3.1 Phase 1 -- Fabrication planning

The project actually began at the proposal stage. At that time, SORL calculated the asphericity of the DEGB and used the results to verify the values presented in the RFP. These calculations and calculation methods are shown in Appendix A. This led to many of the conclusions regarding the test methods and equipment requirements.

First, we saw that the underlying ellipsoid for the DEGB is an optic which can be tested in a very conventional null test. The ellipsoid is generated by taking the ellipse and spinning it around its long axis. The section of the ellipsoid we are fabricating is taken from around the minor axis. A double pass test can be used by placing an interferometer at one focus and a retroreflecting sphere centered on the other focus.

We also saw that the difference between the minor axis ellipse and a circle which best fits that ellipse is only 0.11μ ($\lambda/5.75$ @ $\lambda=.633\mu$). This is a good approximation for estimating the wavefront over the entire piece if the part is generated as a "football torrus". This is where the longer radius is used as the generating surface, and the shorter radius is used to locate the generating axis. This method of generating a torrus closely approximates the method of making the ellipsoid of revolution which can be tested with the previously mentioned null test. The same radii can also be used to generate a "bagel torrus", and as might be expected in this case, the shorter radius is used as the generating surface, and the longer radius is used to locate the generating axis.

The deformation factor is an additive expression combined with the standard equation for an ellipsoid. The deformation along the edge of the clear aperture as defined by the specification showed a maximum deviation of about 2.41μ or 3.81λ . This would show up as 15.25 fringes in an interferogram. A simulated interferogram is presented in figure 1.

SORL prepared a fabrication and test plan. This is included in appendix B. The plan included both the fabrication steps and the testing steps which were intended to be used for the completion of the project. The plan includes drawings of the test configuration and the DEGB component. This plan was delivered 15 November 1991.

3.2 Phase 2 -- Fabrication and initial testing

The actual fabrication was carried out along the guidelines put forth in the fabrication plan. The primary goal of this phase was to create the optical figure. The geometry of this figure was worked out during the proposal and phase 1. This led to the conclusion that ordinary interferometry, even with phase shifted data would not be sufficient to meet the accuracy requirements of the surface. Therefore the holographic approach to the testing was adopted. The principles of operation of this instrument are described in the first paper in Appendix D.

3.2.1. The Holographic Interferometer

Negotiations for the procurement of the holographic interferometer as proposed began shortly after receipt of the contract. The purchase order to APA optics for the holographic interferometer and all the necessary holograms and accessories was dated 10 Oct 1991. The promised delivery date was 17 Jan 1992

Almost immediately the delivery of the interferometer began to slip. By November, the delivery was targeted for February. In order to ameliorate this slip, SORL sent our optician, Bob Scannell, who was to work on the figuring to have a hand on session with a demonstration unit which was at a trade show in California. The visit was successful with regard to the training. After this trip which occurred in January, we learned that the delivery of our interferometer would be 16 March 1994. In February Alan DeCew traveled to Florida to again observe the APA Interferometer for Aspheric Testing (IAT) at a nother trade show. He was also able to talk to APA's other customer for an IAT, Martin Marieta. By March the delivery hasd slipped to 16 April 1992.

On 22 May 1992 the IAT was installed at SORL. The hologram for the DEGB was not completed, and delivery was scheduled for mid-June. By June, the delivery of the hologram was slipped to July. Then other technical issues arose such as the calibration. The F/4 objective was not fully characterized and would have to be replaced. A new schedule for completing these tasks pushed the IAT qualification out to 24 Sep 1994. The new objective and holograms were actually ready for testing at SORL the first week in November. Unfortunately, the holograms were wrong. A correct hologram did not arive until 23 February, 1993.

Other problems with the IAT also surfaced. The fringes were almost impossible to see. After lengthy negotiations with APA, the instrument was returned to APA. It was to be replaced with a new unit. Delivery was promised for 1 June 1993. The unit was actually set up and working 26 August 1993, more than 19 months after promised delivery. It took APA about 7 times as long as they originally projected to produce a working IAT for SORL.

The Calibration of the unit was performed at APA. The results are presented in Appendix D along with a paper by Steve Arnold describing the calibration procedure.

3.2.2 The aspheric figuring

The Zerodur® blanks for the DEGB were ordered from Schott in November 1991. The delivery was scheduled for January 1992, and arrived on schedule. By February, the spherical shape had been generated into the blanks, concave on one, convex on the other. The blanks were then delivered into the hands of the optician, Bob Scannell for figuring.

The first step was to generate a toroidal shape into the blanks. A number of preliminary forays into developing a process were attempted from March through June. The conclusion was that it was no advantage working on the positive and negative blanks together. Using a combination of full size tools and sub-aperture tools seemed necessary to make predictable progress.

The progress of the grinding was monitored with a programable 3-axis coordinate measurement machine. The sag of the part was measured in three positions. The part was rotated 90° and measured again. These results were studied by the optician to determine the next step of the grinding. The results also averaged and plotted to give an indication of the general direction of the progress. The charts are presented in Appendix C.

This was the state of the optic until the holographic interferometer was finally ready for use. At that point progress became rapid and steady. The goal for the optician was to make the fringes straight. The progress over time can be seen in the interferograms shown in Appendix C.

One interesting development of the testing metrology which starts with the null configuration for the underlying ellipse is that the image of the ellipse as seen by the camera in the LUPI is foreshortened. The fringes which normally would be evenly spaced, appear to radiate from the vanishing point of the circumscribed rectangle.

The verification of this is to look at the null fringe case. The interferogram is difficult to read even in the original copy since it is a null. The visual inspection clearly showed that the wavefront was adequate to show a complete null. This confirmed the foreshortening phenomenon. Reading the interferograms in the normal manner would indicate huge errors on the order of 1 wave. The reading also becomes worse the more tilt fringes are introduced into the interferogram.

3.2.3 The testing metrology

Obtaining the proper shape required the proper instrument, a trained optician, and finally, a careful set up of the equipment. The positions on the table and the procedure for placing the components is given in appendix E.

3.3 Phase 3 -- Final testing

The surface figure was established during Phase 2. In Phase 3 the object was to verify all the other requirements of the DEGB. This effort began immediately after establishing that we had met the surface figure requirement.

All the remaining requirements were relatively easy to establish with the exception of the midfrequency. To measure this we contracted with Bauer Associates to use their Model 100 scanner. This was a particularly good choice since Goddard SFC has a similar machine. We could be quite sure that measurements taken at Bauer would correspond closely with measurements taken at GSFC. A number of delays in the program occurred due to the lack of availability of this machine, including the fact that at one point the only available working sources had to go to GSFC to upgrade their Model 100 instrument. The final measurements were made 12 November 1994. This completed the tasks on the contract.

4.0 Specification Compliance

All the specification requirements are called out in Attachment 3 of the Statement of Work (Appendix H). These requirements were measured and the results are shown in the QA documentation which was provided with the part. A copy of the documentation is included as Appendix I.

In determining the mechanical requirements standard mechanical metrology tools were used to determine compliance. The blank diameter was measured with a vernier. The center thickness was measured with a drop gauge. The conjugate distances for the ellipsoid were measured with radius rods. The QA Documentation showing the results of these measurements is included in Appendix I.

4.1 Surface Figure

The actual shape produced depended on the correct set up of the optics and interferometer according to the set up shown in Appendix E. This was verified by independent verification of the set up by a second test technician. The positions of the conjugate points relative to the optic are within the nominal settings.

4.2 Figure error

The figure was toleranced in three spatial wavelength areas. On the overall figure level the requirement is for 1/8 wave. The midfrequency covers spatial wavelengths from .5mm to 10mm. Microroughness covers spatial wavelengths less than .5mm.

4.2.1 Overall Peak to Valley

As pointed out in a previous section, the fringes did not appear as evenly spaced straight fringes. As a result a manual reduction of the fringes was done. This construction is presented in the QA documentation. It was concluded that the surface figure met the 1/8 wave requirement.

4.2.2 Midfrequency roughness

Probably the second most important parameter after the surface figure is the midfrequency ripple. The specification for this is 2nm rms. The measurements were made on a Bauer Model 100 noncontact profilometer, and the results are shown in Appendix G. The data shown was taken from a scan from {-25,50} to {+25,50} in the {Y,Z} plane of the ellipsoid as described in the Statement of Work (Appendix H). It is appropriate to remove polynomial 0 through 6 since these polynomials represent spatial wavelengths greater than 10mm. A plot of exactly what each polynomial takes out of the data is included as part of Appendix G.

4.2.3 Microroughness

The microroughness was not directly measured. The results of the Model 100 instrument were below the microroughness requirement. The shorter spatial frequencies typically show smaller rms roughness values. This result is also presented in the QA Documentation.

5.0 Recommendations

5.1 Fabrication times and techniques

While considerable more time was spent on the first unit, the estimate of labor hours needed to complete a similar DEGB is 260 hours. There is also associated engineering of 50 hours needed to specify the testing and hologram from APA. Assuming there are quality assurance provisions commensurate with a space flight hardware, and applying industry rates, the selling price for other DEGBs will be about \$50,000.

5.2 Figure error metrology

The holographic approach to surface metrology proved quite adequate after the developmental nature of the interferometer was overcome. There are other ways of implementing holographic testing and one is presented in Appendix F.

APPENDIX A
DEGB SURFACE FIGURE CALCULATIONS

- 1) Geometric properties of underlying ellipse
- 2) Comparison of ellipse to circle
- 3) Deformation from ellipse

1) Geometric properties of underlying ellipse

From the parameters supplied in the contract Statement of Work other descriptors of the ellipse were generated. In particular, the conic constant "K" which is used in the sag equation was calculated. The vertex curvature is "c" and the radial distance from the optical axis is "Y".

$$Sag = \frac{cY^2}{1 + \sqrt{1 - (1+K)c^2Y^2}}$$

The vertex radii were also calculated for both the minor axis and the major axis. The calculations match the SOW perfectly.

===== VARIABLE SHEET =====
 St Input---- Name--- Output--- Unit----- Comment-----

Filename: < CONIC2.TK > Rev. 8/8/88

```

1672.92      a
1523.081     b
0            z
0            x
            K
            C
Rmajor      1386.6627
Rminor      1837.5
EVF         980.9044
EFF         1384.0312

```

```

***** ELLIPSE *****
semi-major axis
semi-minor axis
Sag of point on ellipsoid
radial coordinate of point on ellipsoi
conic constant
vertex curvature
Vertex radius at major axis
Vertex radius at minor axis
Focus to Vertex distance
Focus to Focus distance

```

===== RULE SHEET =====
 S Rule-----

```

;Ellipse
Z = C * X^2 / (1 + Sqrt(1 - (K + 1) * C^2 * X^2))
K = ( b^2 - a^2) / a^2
C = 1 / ((K+1) * a)
Rmajor=1/C
EFF =2* SQRT(a^2-b^2)
EVF = a-EFF/2
Rminor = a^2/b
Rmajor = b^2/a

```

```

===== VARIABLE SHEET =====
St Input--- Name--- Output--- Unit----- Comment-----
Filename: < CONIC2.TK > Rev. 21 Feb 94

```

```

1523.081 a
1672.92 b
100 X
      Z 2.7235235
      K .20643616
      C .00054422
      Rmajor 1837.5
      Rminor 1386.6627
      EFF 1384.0312
      EVF 'OBLATE

```

```

***** ELLIPSE *****
semi-major axis (Horizontal Axis)
semi-minor axis (Vertical Axis)
Sag of point on ellipse (Horiz Coord)
Vertical coordinate of point on ellips
conic constant
vertex curvature
Vertex radius at major axis
Vertex radius at minor axis
Focus to Focus distance
Focus to Vertex distance

```

```

===== RULE SHEET =====
S Rule-----
;Ellipse
Z = C * X^2 / (1 + Sqrt(1 - (K + 1) * C^2*X^2))
K = ( b^2 - a^2) / a^2
C = 1/((K+1)*a)
Rmajor=1/C
Rminor = a^2/b
Rmajor = b^2/a
EFF =2* SQRT(abs(a^2-b^2))
IF K>0 THEN EVF = 'OBLATE ELSE EVF = a-EFF/2

```

2) Comparison of ellipse to circle

Three graphs are presented. The first shows the actual sags of the ellipsoid in two axes. The second shows the difference between the two sags. This is valuable to the optician since it tells how much stock must be removed from his starting point which is a sphere. The third shows the difference between the ellipse and a circle which best fits the ellipse along a cut which includes the major axis. This is essentially the difference between an ellipsoid and a torrus.

===== VARIABLE SHEET =====

St Input----- Name----- Unit----- Comment-----

Filename: Tansph2.TK Rev 10 July 90

.20643616	K		Conic Constant	0=Sphere, -1=Parabola
	C	.00054422	Vertex Curvature	
1837.5	RV		Vertex Radius	
	Parf1	918.75	Paraxial focal length	
	OffAXAn	0	Angle of chief ray to axis (degrees)	
	CRL	918.75	Chief ray length (Surface to Focus)	
	OED	-101.6	Off-Edge distance	
203.2	DIAM		Diameter of Mirror	
0	ACD		Axis to Center distance	
72	Ytan		Distance from center to tangent point	
	Rc	1837.2088	Radius of tangent sphere	
0	K2		Conic Constant of 2nd Asphere	
	C2	.00065656	Vertex curvature	
1523.081	RV2		Vertex Radius	
	Parf12	761.5405	Paraxial Focal length	
L 100	Y		Radial distance from axis	
L	Z	2.7235235	Sag of conic	
L	Zcir	2.7234266	Sag of circle	
L	dZdy	.05451926	Slope of conic at <Z,Y>	
L	DZcir	.0545112	Slope of circle	
L	Dsag	.00009689	Sag Difference (Asphere - Sphere)	
L	Dslope	8.0537E-6	Slope Difference (Asphere - Sphere)	

===== RULE SHEET =====

S Rule-----

$$\text{DIAM}/2 + \text{OED} = \text{ACD}$$

$$\text{Parfl} = 1/(c*2)$$

$$\text{RV} = 1/c$$

$$\text{CRL} = \text{Parfl} + (\text{ACD}^2 / (2 * \text{RV}))$$

$$\text{Sind}(\text{OffAxAng}) = \text{ACD} / \text{CRL}$$

$$\text{rxtan} = \text{SQRT}(1 - (K+1) * c^2 * \text{Ytan}^2)$$

$$\text{Ztan} = c * \text{Ytan}^2 / (1 + \text{rxtan})$$

$$\text{Zcirtan} = 0 - \text{Sgn}(c) * \text{SQRT}(\text{Rc}^2 - \text{Ytan}^2)$$

$$\text{Ztan} = \text{Zcirtan}$$

$$\text{dZdYtan} = c * \text{Ytan} / \text{rxtan}$$

$$\text{DZcirtan} = \text{Sgn}(c) * \text{Ytan} / \text{SQRT}(\text{Rc}^2 - \text{Ytan}^2)$$

$$\text{dZdYtan} = \text{DZcirtan}$$

$$\text{rx} = \text{SQRT}(1 - (K+1) * c^2 * \text{Y}^2)$$

$$\text{Z} = c * \text{Y}^2 / (1 + \text{rx})$$

$$\text{dZdY} = c * \text{Y} / \text{rx}$$

$$\text{Zcir} = 0 - \text{Sgn}(c) * \text{SQRT}(\text{Rc}^2 - \text{Y}^2)$$

$$\text{DZcir} = \text{Sgn}(c) * \text{Y} / \text{SQRT}(\text{Rc}^2 - \text{Y}^2)$$

$$\text{Dsag} = \text{Z} - \text{Zcir}$$

$$\text{Dslope} = \text{dZdY} - \text{DZcir}$$

$$\text{rx2} = \text{SQRT}(1 - (K2+1) * c2^2 * \text{Y}^2)$$

$$\text{Z2} = c2 * \text{Y}^2 / (1 + \text{rx2})$$

$$\text{Dsag2} = \text{Z2} - \text{Zcir}$$

$$\text{RV2} = 1/c2$$

$$\text{Parfl2} = 1/(c2 * 2)$$

$$\text{dZdY2} = c2 * \text{Y} / \text{rx2}$$

$$\text{rx2tan} = \text{SQRT}(1 - (K2+1) * c2^2 * \text{Ytan}^2)$$

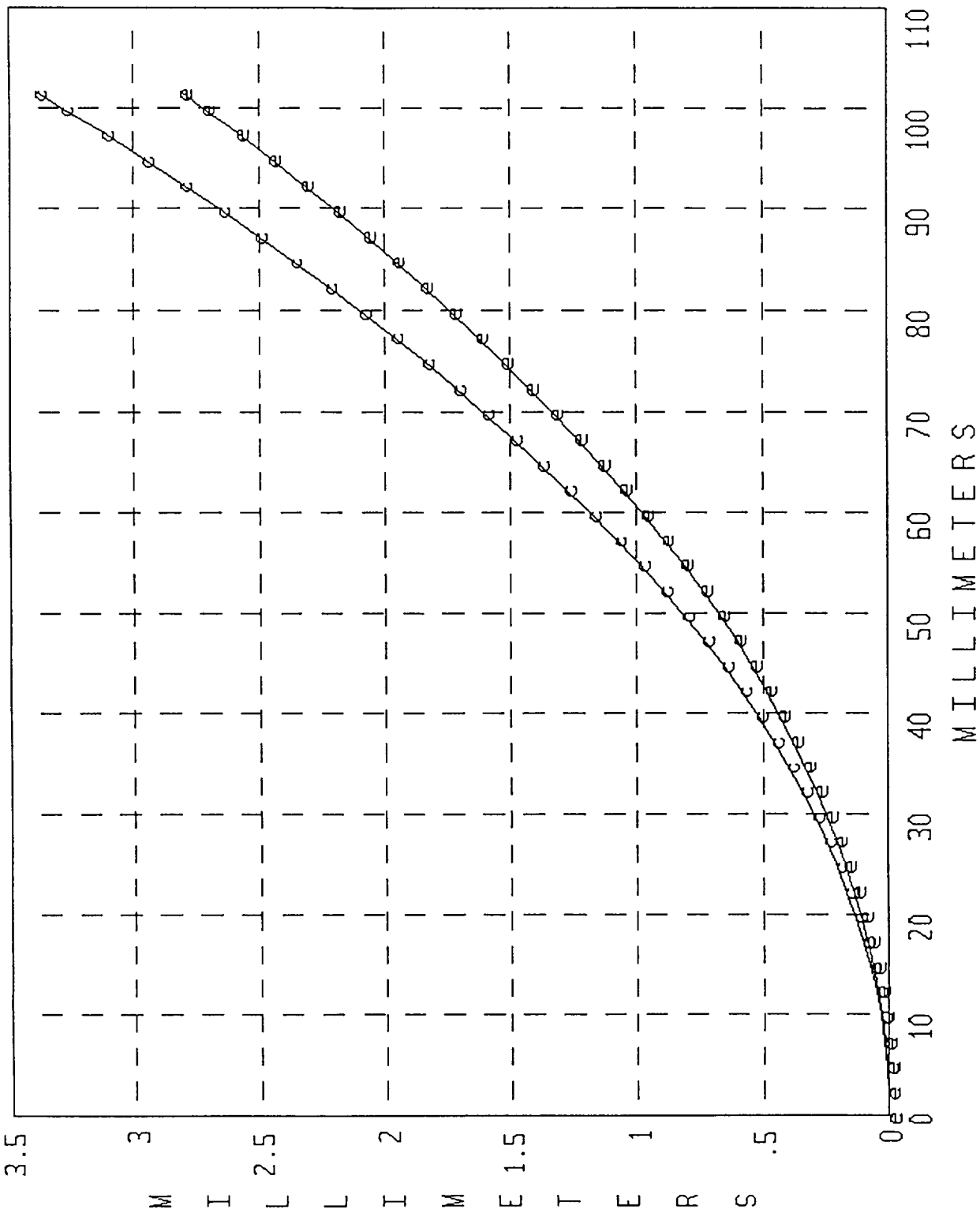
$$\text{Z2tan} = c2 * \text{Ytan}^2 / (1 + \text{rx2tan})$$

$$\text{D2sag} = \text{Z2} - \text{Z}; - (\text{Z2tan} - \text{Ztan})$$

SAG FOR TANGENT SPHERE, ASPHERE1 AND ASPHERE2

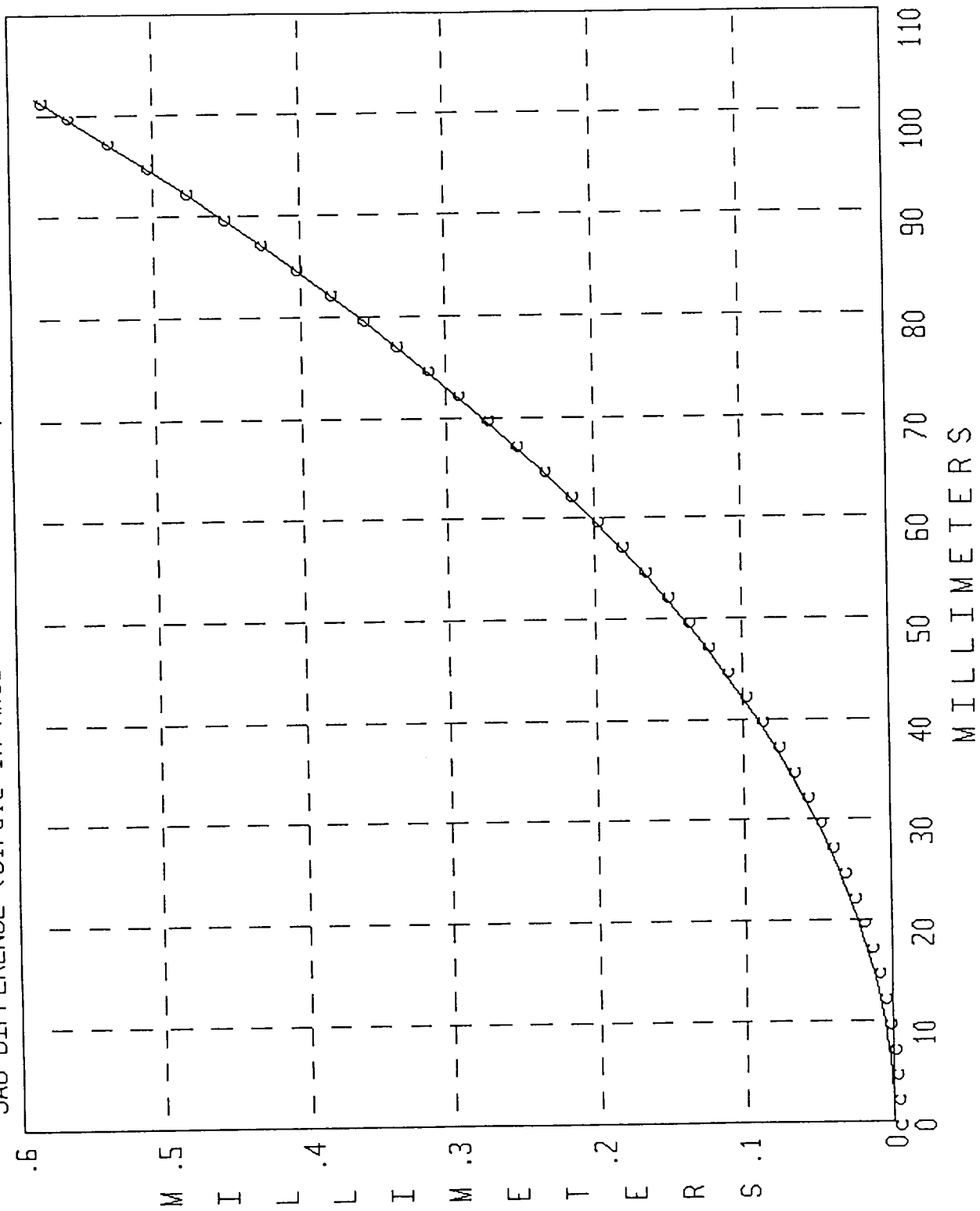
Y	Zcir	Z	Dsag	Z2	D2sag
0	-.00011190	0.00000000	.00011190	0.00000000	0.00000000
2.5	.00158905	.00170068	.00011163	.00205176	.00035108
5	.00669192	.00680274	.00011082	.00820707	.00140433
7.5	.01519672	.01530620	.00010948	.01846597	.00315977
10	.02710350	.02721113	.00010762	.03282855	.00561742
12.5	.04241234	.04251760	.00010526	.05129492	.00877732
15	.06112332	.06122572	.00010240	.07386523	.01263951
17.5	.08323654	.08333561	.00009908	.10053967	.01720405
20	.10875212	.10884743	.00009531	.13131844	.02247101
22.5	.13767021	.13776133	.00009112	.16620181	.02844047
25	.16999096	.17007752	.00008656	.20519004	.03511252
27.5	.20571457	.20579622	.00008165	.24828346	.04248724
30	.24484121	.24491765	.00007644	.29548242	.05056477
32.5	.28737112	.28744209	.00007097	.34678729	.05934520
35	.33330453	.33336982	.00006529	.40219849	.06882868
37.5	.38264169	.38270114	.00005945	.46171648	.07901533
40	.43538288	.43543639	.00005351	.52534172	.08990533
42.5	.49152839	.49157593	.00004753	.59307474	.10149881
45	.55107854	.55112012	.00004158	.66491609	.11379597
47.5	.61403365	.61406937	.00003572	.74086634	.12679697
50	.68039408	.68042410	.00003002	.82092611	.14050201
52.5	.75016019	.75018475	.00002456	.90509605	.15491130
55	.82333237	.82335180	.00001943	.99337685	.17002505
57.5	.89991103	.89992573	.00001470	1.08576921	.18584348
60	.97989660	.97990706	.00001046	1.18227388	.20236682
62.5	1.06328952	1.06329633	.00000681	1.28289166	.21959533
65	1.15009025	1.15009409	.00000383	1.38762334	.23752926
67.5	1.24029929	1.24030093	.00000164	1.49646979	.25616886
70	1.33391712	1.33391746	.00000034	1.60943189	.27551443
72.5	1.43094428	1.43094430	.00000002	1.72651055	.29556625
75	1.53138130	1.53138211	.00000081	1.84770673	.31632462
77.5	1.63522874	1.63523156	.00000282	1.97302140	.33778984
80	1.74248719	1.74249336	.00000617	2.10245559	.35996223
82.5	1.85315723	1.85316821	.00001098	2.23601034	.38284213
85	1.96723949	1.96725688	.00001739	2.37368675	.40642988
87.5	2.08473461	2.08476012	.00002551	2.51548594	.43072582
90	2.20564323	2.20567873	.00003550	2.66140904	.45573031
92.5	2.32996604	2.33001352	.00004748	2.81145727	.48144374
95	2.45770373	2.45776534	.00006161	2.96563183	.50786649
97.5	2.58885700	2.58893503	.00007803	3.12393397	.53499894
100	2.72342660	2.72352349	.00009689	3.28636500	.56284151
101.6	2.81134438	2.81145470	.00011032	3.39248831	.58103361

SAG OF ELLIPSOID IN BOTH AXES



MILLIMETERS

SAG DIFFERENCE (Circle in Axis 2 - Oblate Ellipse in Axis 1)



3) Deformation from ellipse

In these calculations, the departure from the ellipse is calculated. It is calculated at points around the clear aperture and then at points around the edge of the blank. The graphs of this computation are used to show the maximum departure. The basic deformation equation was also used to generate the points of equal deformation which were used to produce the topographical map of the surface and simulated fringe map.

===== VARIABLE SHEET =====
 St Input---- Name---- Output--- Unit----- Comment-----

Filename < DEGB.TK > Rev. 22 Feb 94

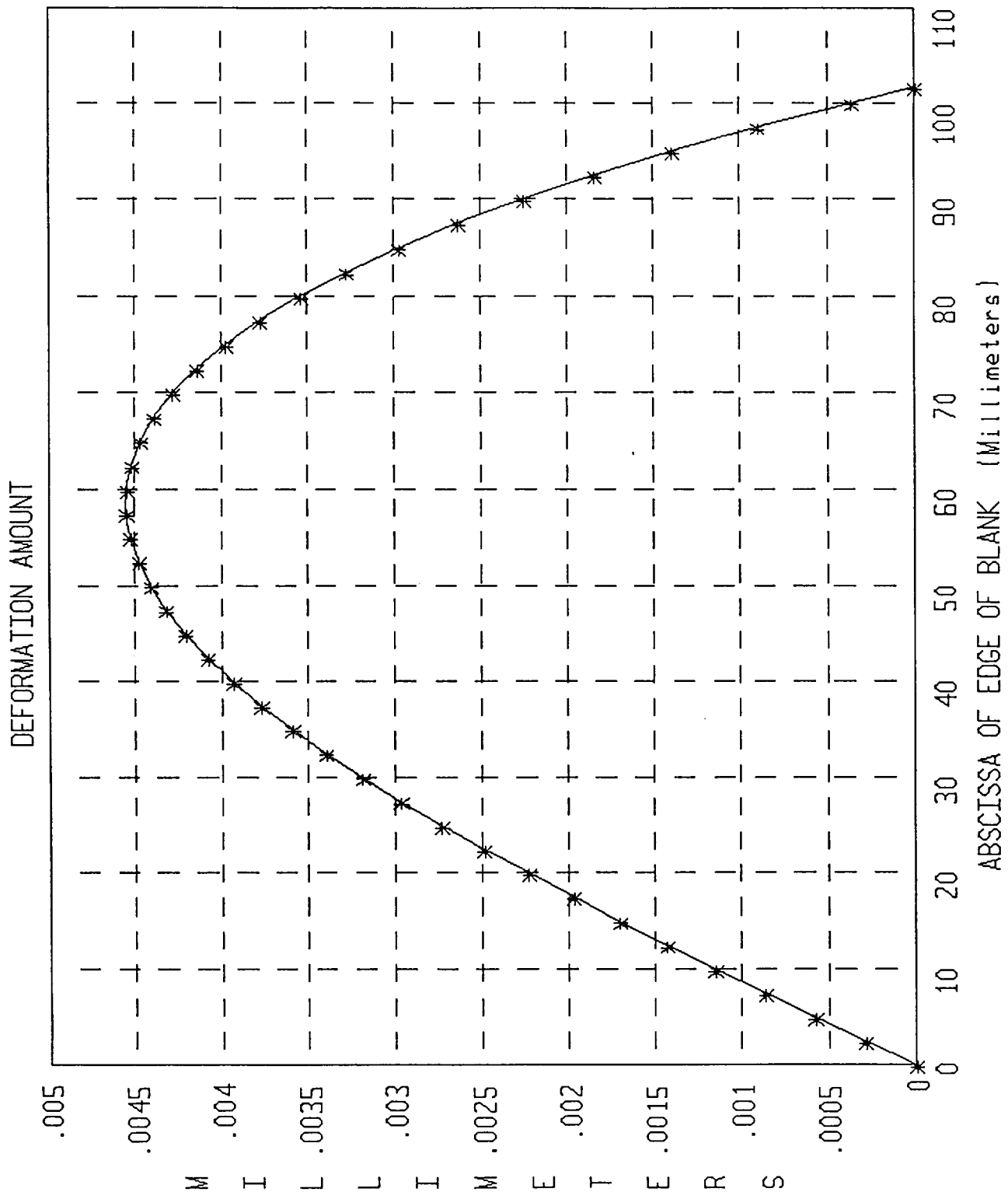
L	1.128E-8	DEFORM	e	1.023E-14	Departure from ellipsoid along CA
L	92.5		Y		Deformation Coefficient
LG	9.9016E-5		Z		Y coordinate of CA
L	92.5	DEFORMA	Yb	.00184297	Z coordinate of CA
LG	42.027491		Zb		Departure from ellipsoid along edge
					Y coordinate of edge of blank
					Z coordinate of edge of blank

===== RULE SHEET =====
 S Rule-----

* DEFORM = e*y*z*z
 * 1 = Y*Y/92.5^2 + z*z/77.5^2
 * DEFORMAX = e*yb*z*b*z
 * 1 = Yb*yb/101.6^2 + zb*z*b/101.6^2

DEFORMATION FROM ELLIPSOID

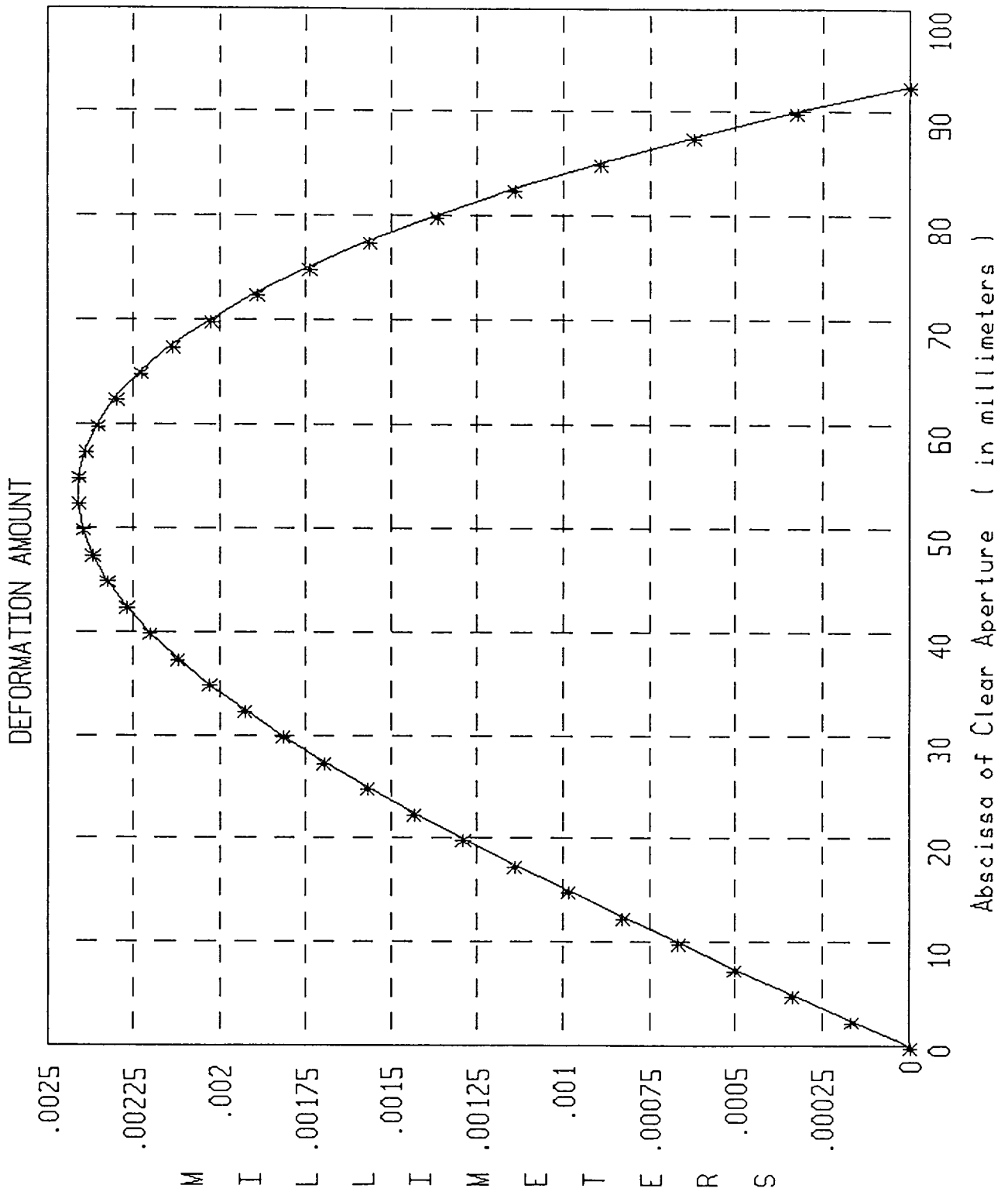
Y	Z	DEFORM	Yb	Zb	DEFORMAX
0	77.5	0	0	101.6	0
2.5	77.4716895	.000169253	2.5	101.569237	.00029092
5	77.3866958	.000337763	5	101.476894	.000580782
7.5	77.2448319	.000504788	7.5	101.322801	.00086853
10	77.0457836	.000669587	10	101.106676	.001153105
12.5	76.7891062	.000831416	12.5	100.828121	.00143345
15	76.4742195	.000989533	15	100.486616	.001708507
17.5	76.1004008	.001143197	17.5	100.081517	.00197722
20	75.6667767	.001291664	20	99.6120475	.00223853
22.5	75.1723124	.001434192	22.5	99.0772931	.002491379
25	74.6157982	.00157004	25	98.47619	.002734712
27.5	73.9958343	.001698464	27.5	97.807515	.002967469
30	73.3108108	.001818722	30	97.0698717	.003188594
32.5	72.5588852	.001930073	32.5	96.2616746	.003397029
35	71.7379537	.002031773	35	95.3811302	.003591717
37.5	70.8456176	.00212308	37.5	94.4262146	.003771599
40	69.8791415	.002203252	40	93.3946465	.003935619
42.5	68.8354025	.002271547	42.5	92.2838556	.004082719
45	67.7108279	.002327222	45	91.0909436	.004211841
47.5	66.5013167	.002369535	47.5	89.8126383	.004321929
50	65.2021426	.002397744	50	88.4452373	.004411924
52.5	63.8078287	.002411106	52.5	86.9845389	.004480769
55	62.3119889	.002408879	55	85.4257572	.004527406
57.5	60.7071188	.002390321	57.5	83.7634168	.004550779
60	58.9843193	.002354689	60	81.991219	.004549829
62.5	57.1329233	.002301241	62.5	80.1018726	.004523499
65	55.1399789	.002229234	65	78.0868747	.004470731
67.5	52.9895175	.002137927	67.5	75.9362232	.004390468
70	50.6614845	.002026576	70	73.6380337	.004281653
72.5	48.1301195	.001894441	72.5	71.1780163	.004143228
75	45.3613948	.001740777	75	68.5387482	.003974136
77.5	42.3087369	.001564844	77.5	65.6986301	.003773318
80	38.9053679	.001365898	80	62.6303441	.003539718
82.5	35.0492714	.001143197	82.5	59.2984823	.003272278
85	30.5696017	.000895999	85	55.6557275	.002969941
87.5	25.1351351	.000623562	87.5	51.6363244	.002631648
90	17.8962241	.000325143	90	47.1440346	.002256343
92.5	9.90161E-5	1.023E-14	92.5	42.027491	.001842968
			95	36.0216602	.001390465
			97.5	28.5711393	.000897778
			100	17.9599555	.000363848
			101.6	0	0



DEFORMATION AMOUNT

ABSCISSA OF EDGE OF BLANK (Millimeters)

M I L L I M E T E R S



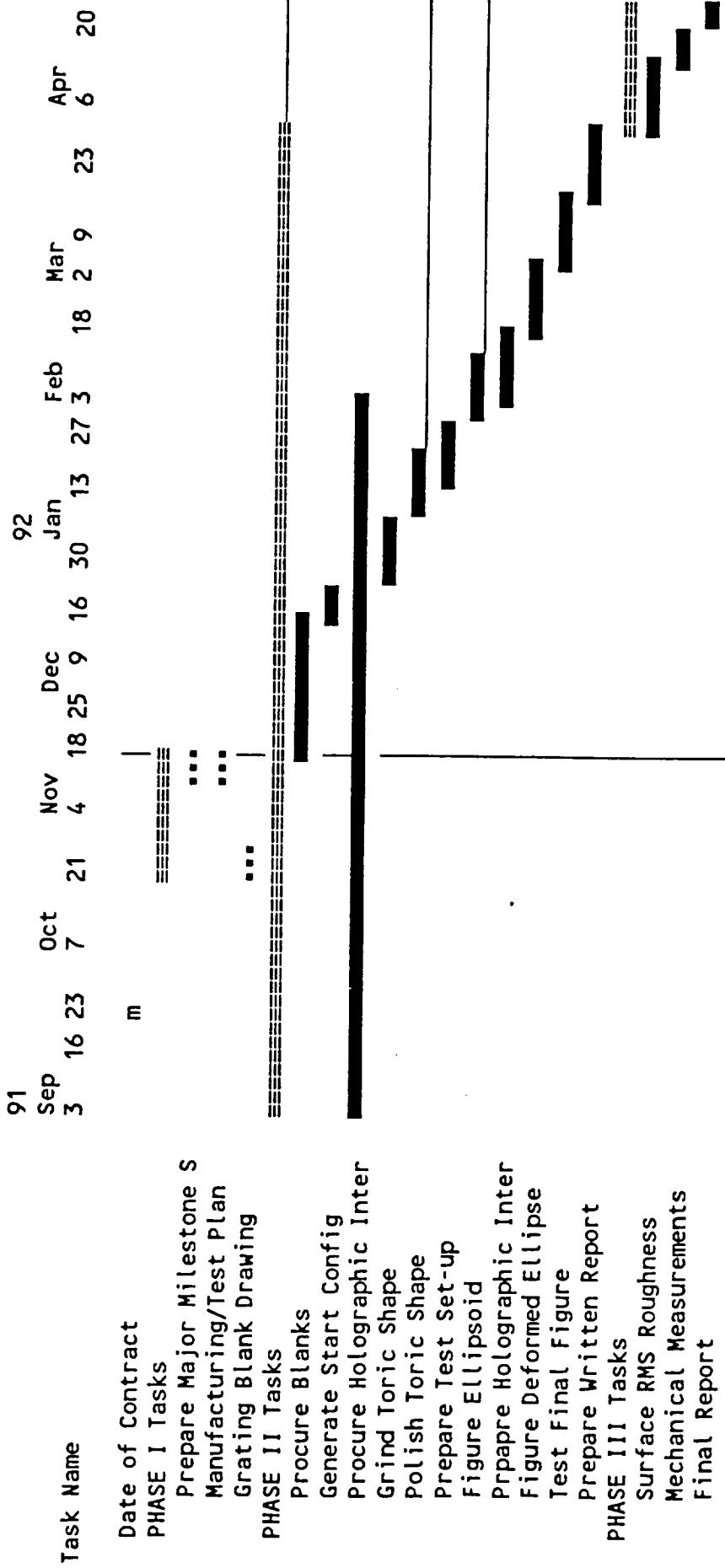
M I L L I M E T E R S

APPENDIX B

MANUFACTURING AND TEST PLAN

Schedule Name : DEFORMED ELLIPSOIDAL DIFFRACTION GRATING BLANK
 Responsible : Alan DeCew, Jr.
 As-of Date : 15-Nov-91 9:00am Schedule File : C:\TL3\DATA\TEMPLATE

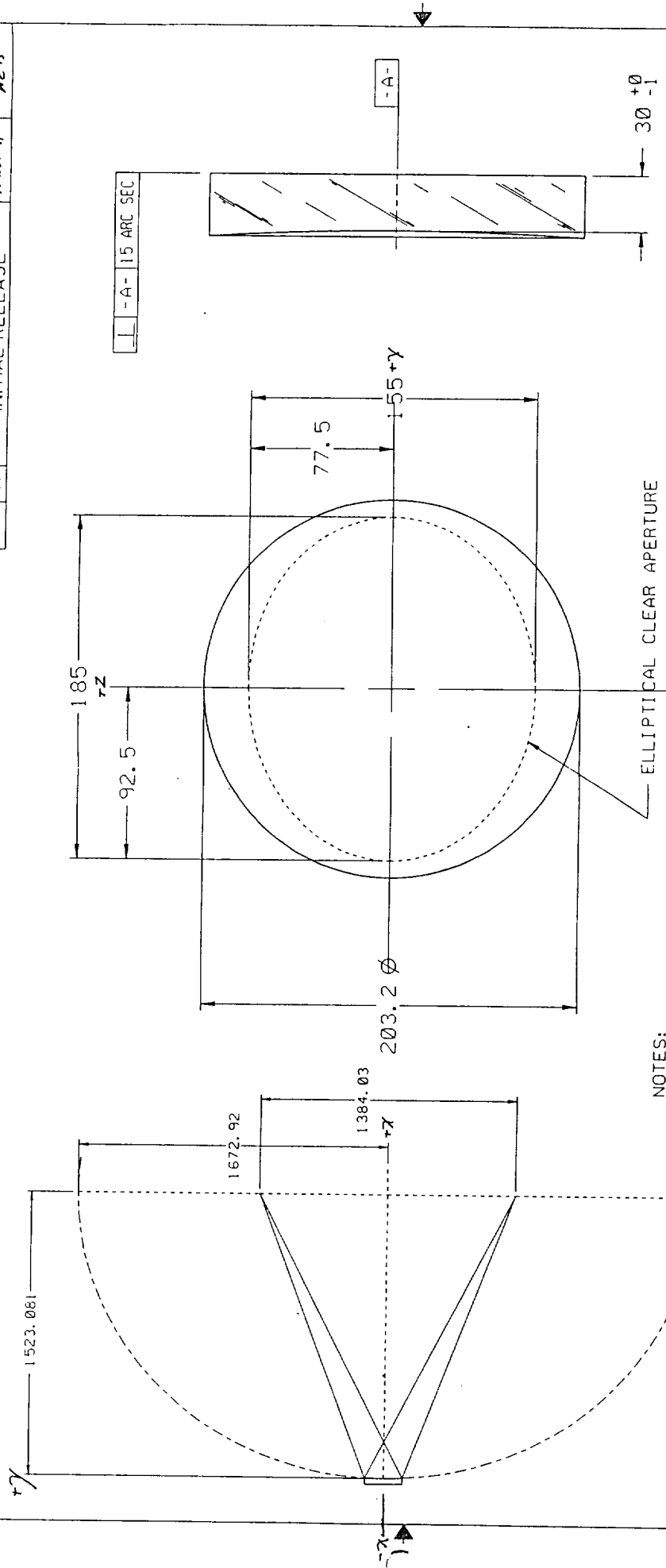
NASA GODDARD SPACE FLIGHT CENTER



----- Scale: 2 days per character -----

■ Detail Task ■ Summary Task M Milestone
 ■ (Started) ■ (Started) >>> Conflict
 ■ (Slack) ■ (Slack) .. Resource delay

REVISIONS		
ZONE	REV	DESCRIPTION
	A	INITIAL RELEASE
		DATE
		APPROVED



NOTES:

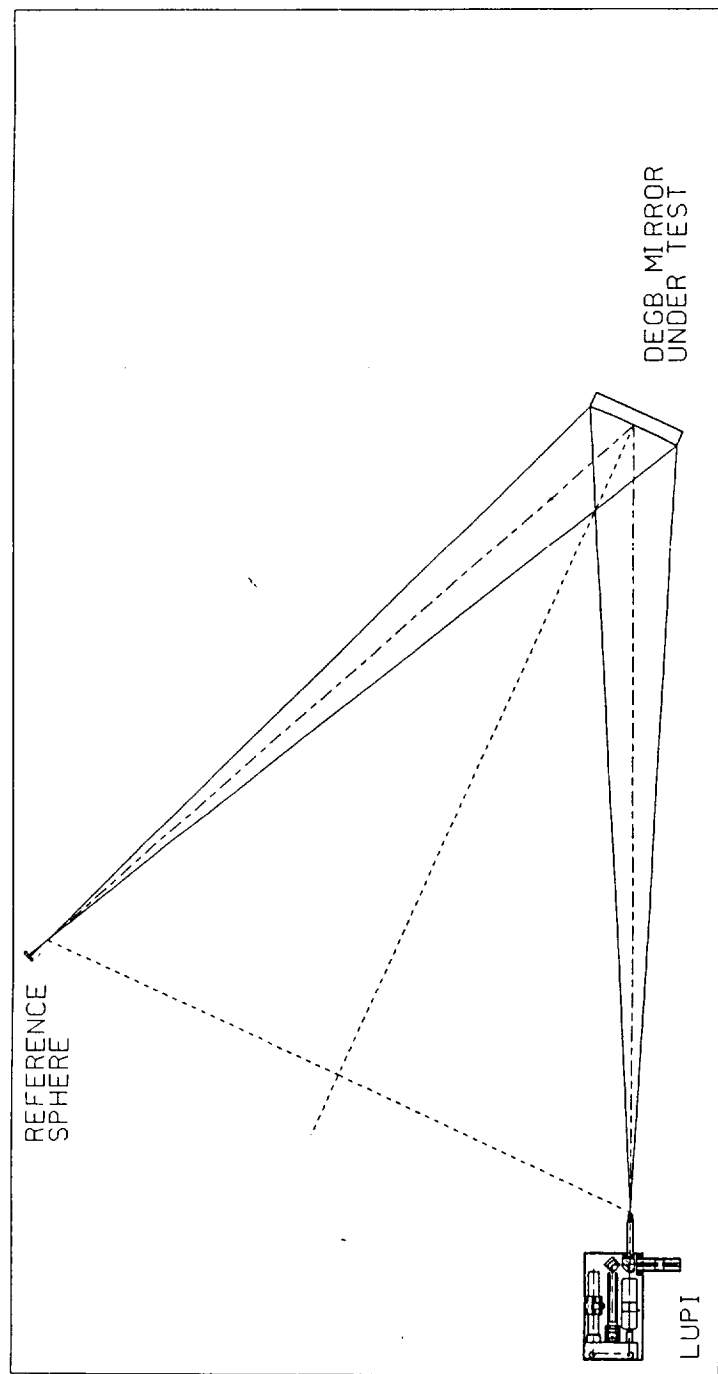
1. ALL DIMENSIONS ARE IN MM
2. TOLERANCES PER RFP5-32E16/235 DATED 10/29/90

© OUT OF PAPER
 LAYOUT
 SCALE: 1:20

63 SURFACE ROUGHNESS UNLESS SPECIFIED		APPROVALS	DATE	SORL SPACE OPTICS RESEARCH LABS DIVISION OF INTERGRAPH 7 STUART ROAD, CHELSEA, MA, 01824
STANDARD TOLERANCES FITS : : H7 ANGLES : : 30° UNLESS OTHERWISE SPECIFIED ALL DIMENSIONS ARE PRELIMINARY AND APPLY AFTER FINISH. DO NOT SCALE DRAWING.		DRAWN J. PERRY CHECKED APPROVED A. DeCew	5. 9. 91	
MATERIAL ZERODUR		THE INFORMATION CONTAINED HEREIN IS THE PROPERTY OF INTERGRAPH AND IS UNAUTHORIZED FOR REPRODUCTION OR FOR THE USE OF OTHER THAN THE ORGANIZATION TO WHICH IT IS HEREBY PROHIBITED.		TITLE DEFORMED ELLIPSOIDAL DIFFRACTION GRATING BLANK SIZE FSCMNC. B 2D543 DWG NO. 31815 SCALE 1:2
PART DASH NO.	NEXT FINAL QTY PER ASSY	NEXT ASSY	USED ON	REV A
THIRD ANGLE PROJECTION			SHEET 1 OF 2	

Form 31015 Rev. 2-78

REVISIONS		DATE	APPROVED
ZONE	REV		
	A	15 Nov 91	ACD
DESCRIPTION			
INITIAL RELEASE			



TEST TABLE (60 X 120 INCH MIN)

TEST LAYOUT

 THIRD ANGLE PROJECTION		PART DASH NO. NEXT FINAL QTY RECD PER ASSY NEXT ASSY USED ON APPLICATION	63 <input checked="" type="checkbox"/> SURFACE ROUGHNESS UNLESS SPECIFIED STANDARD TOLERANCES XX ANGLES :: 10:1 MATERIAL --- FINISH --- UNLESS OTHERWISE SPECIFIED ALL DIMENSIONS ARE TO BE TAKEN TO THE FINISH. DO NOT SCALE DRAWING.	DRAWN J. PERRY CHECKED APPROVED A DeCaro	DATE 5. 9. 91	SORL SPACE OPTICS RESEARCH LABS A DIVISION OF INTERGRAPH 7 STUART ROAD, CHELSEA, MA., 01824	
				TITLE DEFORMED ELLIPSOIDAL DIFFRACTION GRATING BLANK SIZE FSCH NO. DWG NO. 31815 A B12D543			SCALE 1:10 SHEET 2 OF 2

The Manufacturing/Test Plan

1M) PROCURING THE BLANKS

The Zerodur will be procured from Schott. The diameter of 8" leaves sufficient polishing area beyond the clear aperture. The blank will be ordered 8" Diameter with 33.4mm thickness. The thickness will provide for a 30mm vertex thickness after the figure is obtained.

2M) GENERATING THE STARTING CONFIGURATION

SORL will edge and generate the Zerodur blanks into the starting configuration. The generated blanks will then be a positive/negative spherical pair. The radius will be the shorter $R_x = 59.964"$.

3M) GRINDING THE TORIC SHAPE

The spherical blanks will be formed into a toric pair using loose abrasive grinding. The parts are ground together using 40 micron Aluminum Oxide grit.

3T) TESTING THE TORIC SHAPE

SORL has a computer controlled 3 axis measurement machine which will be used to monitor the progress of the toric grinding. This will provide the information to the optician about the actual toric radii.

4M) POLISHING THE TORIC SHAPE

Having verified the basic toric radii, the next step is to polish the surface so interferometry can be used to test the surface. This begins with working down through the grit sizes from 40 to 30 to 15 to 10 and finally 5 micron.

The fine ground surface is then polished with a full size pitch lap and Cerium Oxide polishing compound. Both sides of the test plate pair are polished.

4T) OPTICALLY TESTING THE TORIC

The polished surfaces of the test plate pair allow the viewing of interference fringes between the surfaces. This is an accurate test of the toric surface since the test plates can be translated and flipped end for end. The optician uses this method to insure the smooth toric shape.

The concave toric is then tested in the interferometric configuration shown in SORL DWG # 31815 Sheet 2 of 2. This test preparation is not performed by the optician. A member of the test engineering staff is always involved in preparing all new test set-ups. The difference between the toric and a perfectly imaging ellipsoid is very small, less than 1/5 wave. The toric is, therefore, an ideal starting point to use to verify the operation of the holographic interferometer.

5M) FIGURING THE TORIC INTO AN ELLIPSOID

The ellipsoid which will provide a perfect null test in the focus to focus configuration can be figured from the toroid by the removal of only 5 microinches of material. Using local polishing techniques, the optician will hand figure the toric into the ellipsoid.

5T) PREPARING THE HOLOGRAPHIC INTERFEROMETER

The holographic interferometer comes with a system hologram which nulls out any residual aberrations of the instrument. This can be readily checked against our reference sphere. Using this configuration, the figure of the toric can be measured. The starting point will show irregular fringes which identify high points corresponding to the difference between the toric and the ellipse. The polishing will continue until the fringe pattern in the interferometer shows straight fringes.

At this point, the hologram for nulling the effects of the deformation coefficients will be inserted into the interferometer. After alignment, the fringe pattern should match the calculated interferogram presented in the proposal as figure 1. This will not verify the hologram to 1/10 wave accuracy, but it will verify that no significant calculation or transcription error has occurred.

6M) FIGURING THE ELLIPSE INTO THE DEFORMED ELLIPSE

The figuring of the deformed ellipse requires the removal of as much as 8 microns of material. This is more than 30 times what was removed to change the toric to an ellipse. It is, however, still a small correction, and will be polished into the ellipse. The optician will again be using small laps and monitor the progress by viewing the straightness of the fringes in the interferometer.

6T) TESTING THE DEFORMED ELLIPSE

The holographic interferometer will be used throughout the manufacturing process to evaluate the progress of the figuring. The optician does not require additional engineering of test support until the part is felt to be ready. Hardcopy of the interferograms are then taken and reduced by the test engineering department. Meeting the 1/10 wave surface accuracy completes the requirements of Phase II.

7M) CREATING A 2.0nm RMS ROUGHNESS SURFACE

This step runs concurrently with the figuring. The optician, knowing that a smooth surface is a requirement, will approach the final figuring with a controlled polishing technique. As the final figure is approached, the stroking becomes lighter and the randomness of the direction of stroking is carefully maintained.

7T) TESTING THE RMS SURFACE ROUGHNESS

SORL does not have a profilometer capable of measuring surface roughness to this level. The part will be sent to an outside vendor for measuring. The data will be obtained from a Wyko or Chapman profilometer.

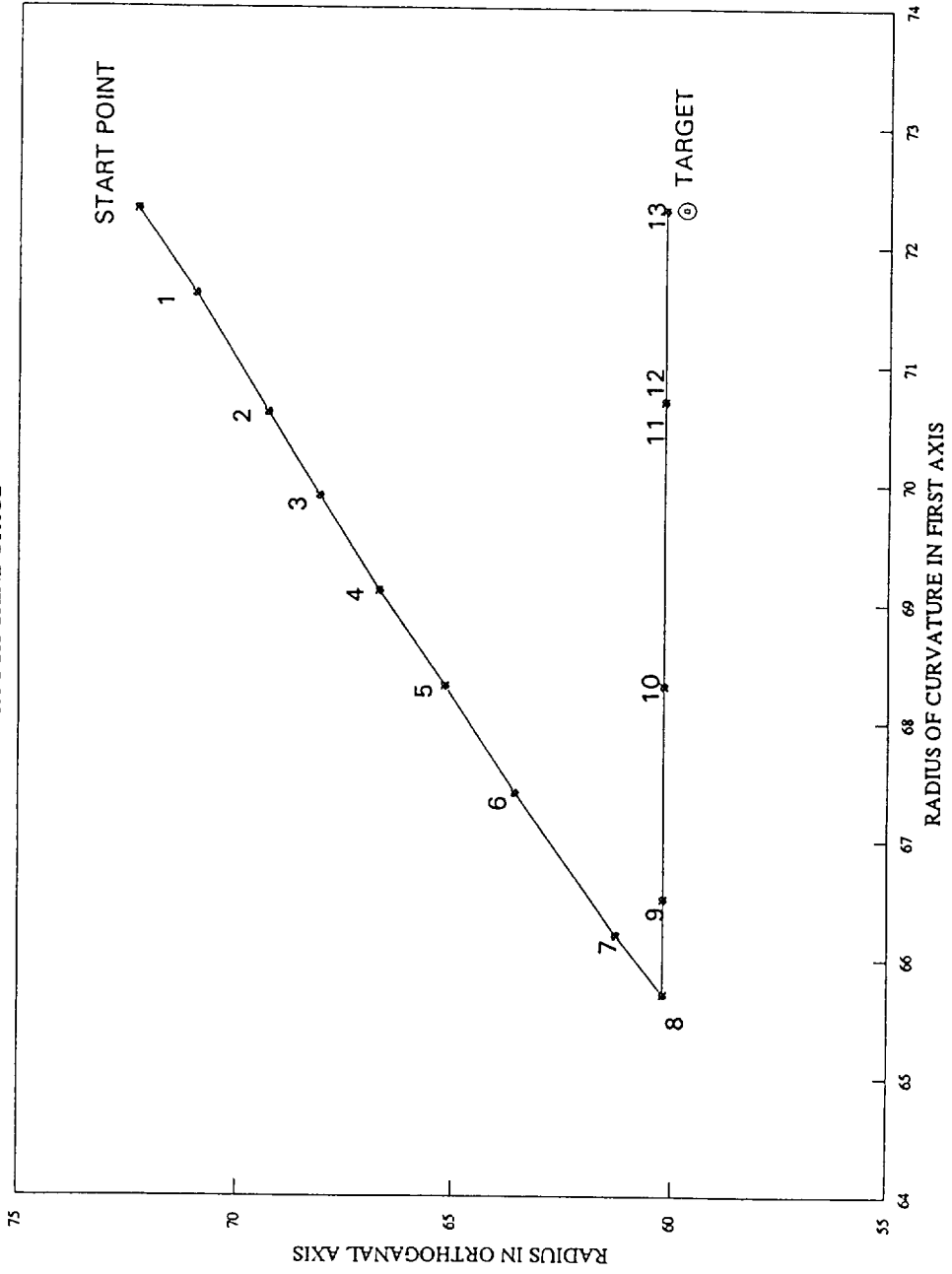
APPENDIX C

FIGURING CYCLES TO FABRICATE DEGB

- 1) Cycles required to take the generated spherical shape to the torrus which best approximates the ellipse.
- 2) Progress of the figure polishing of the deformation into the final DEGB configuration.

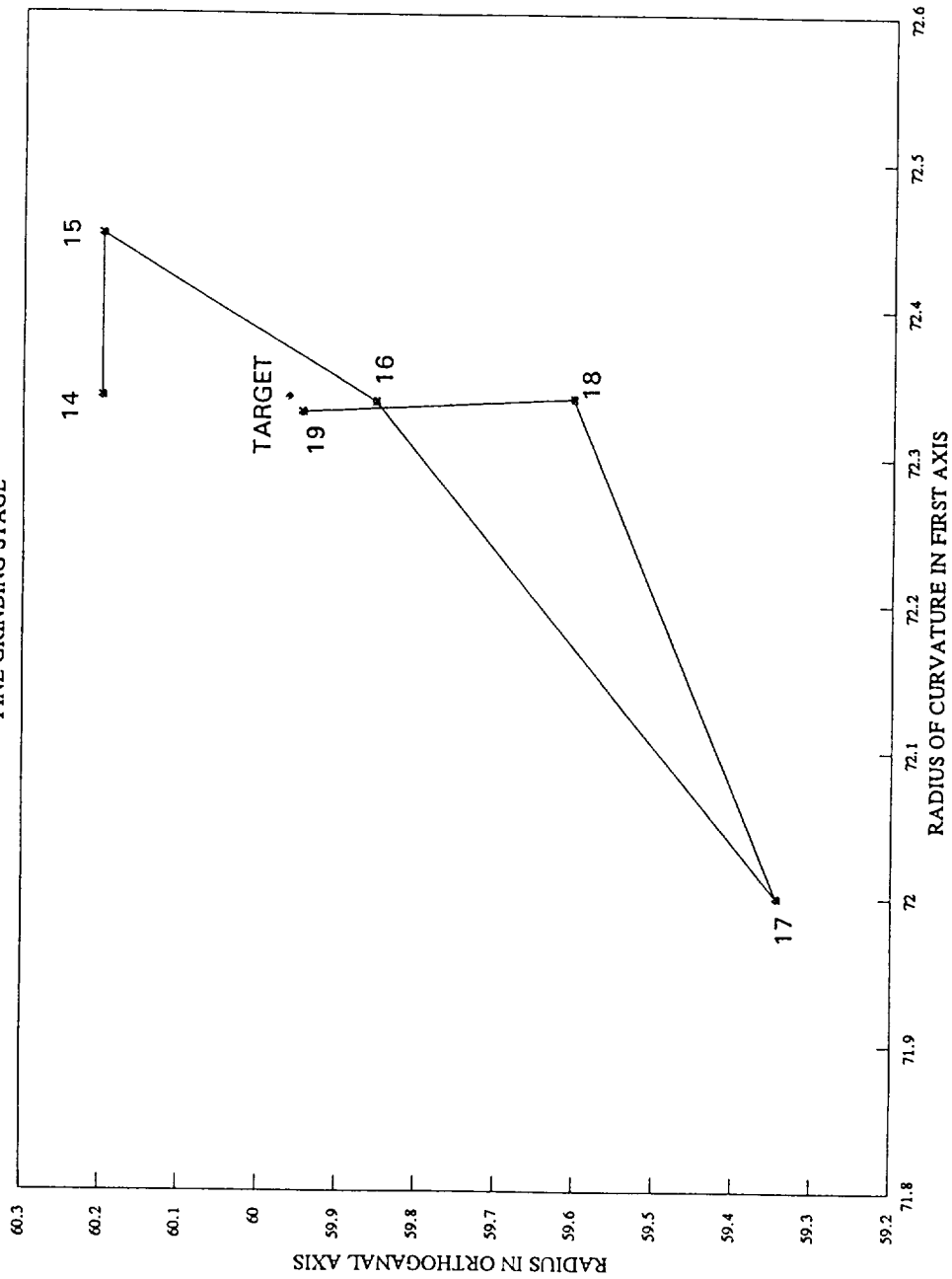
DEGB FIGURING CYCLES

ROUGH GRIND STAGE



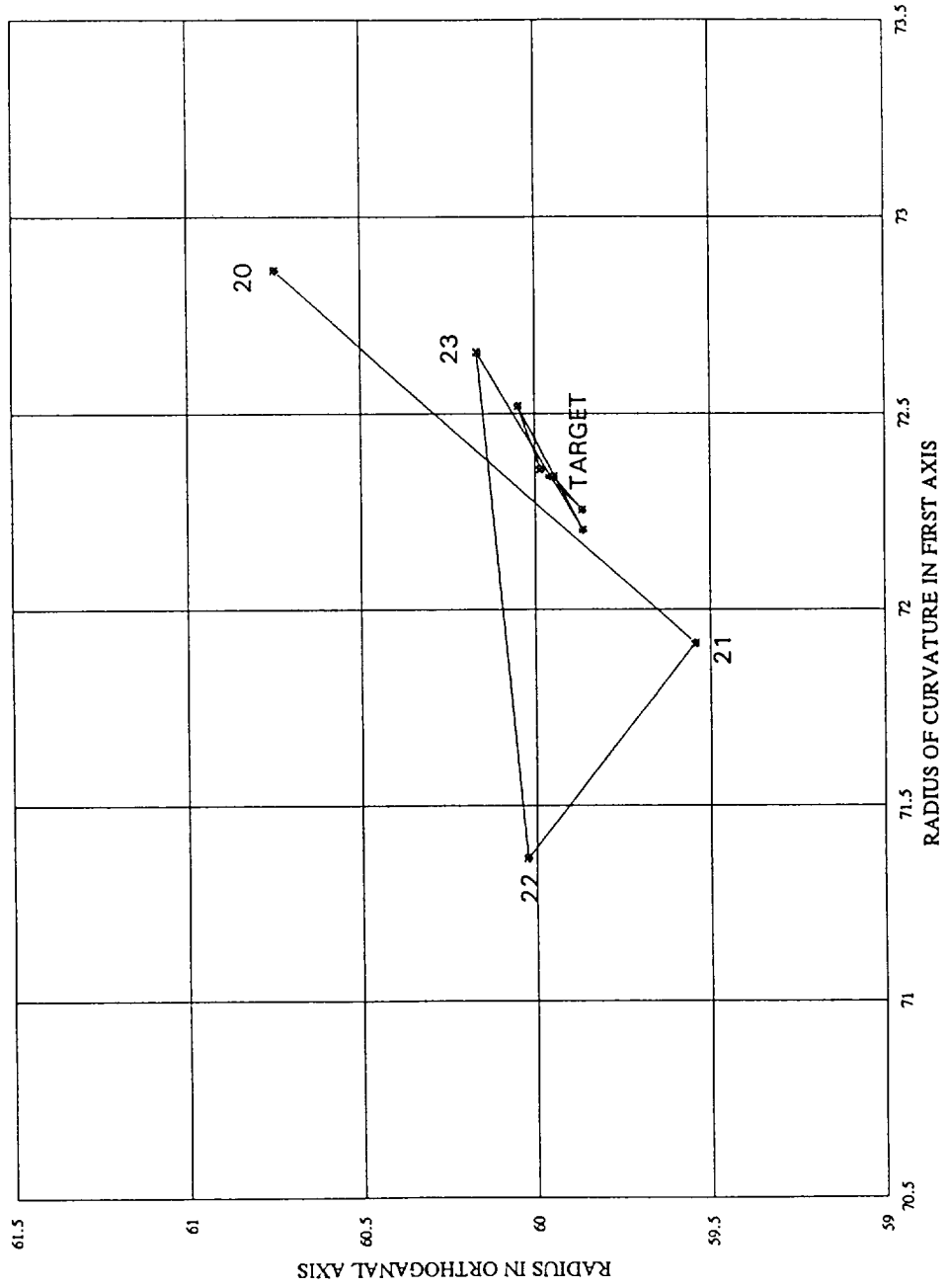
DEGB FIGURING CYCLES

FINE GRINDING STAGE



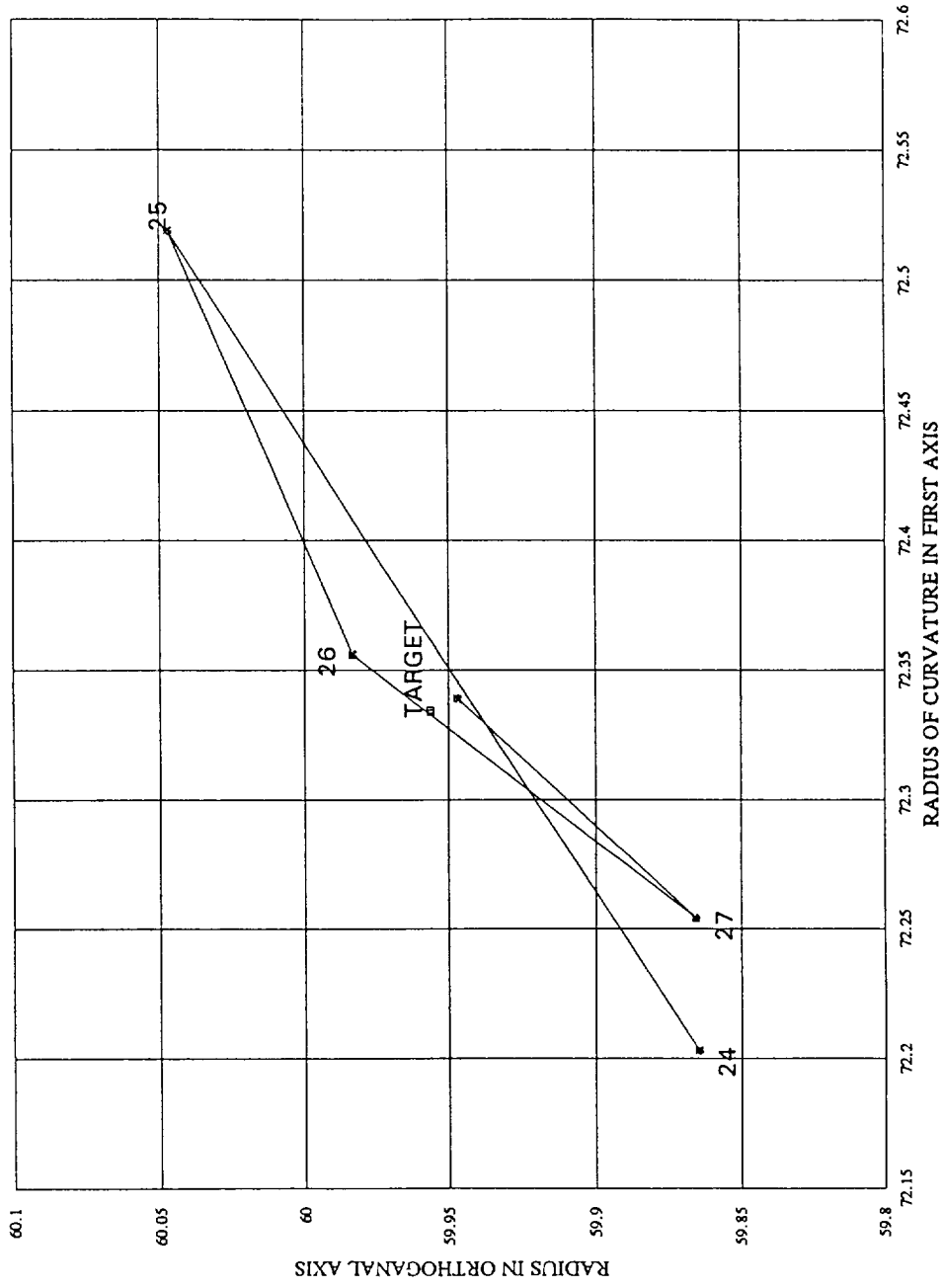
DEGB FIGURING CYCLES

POLISH STAGE



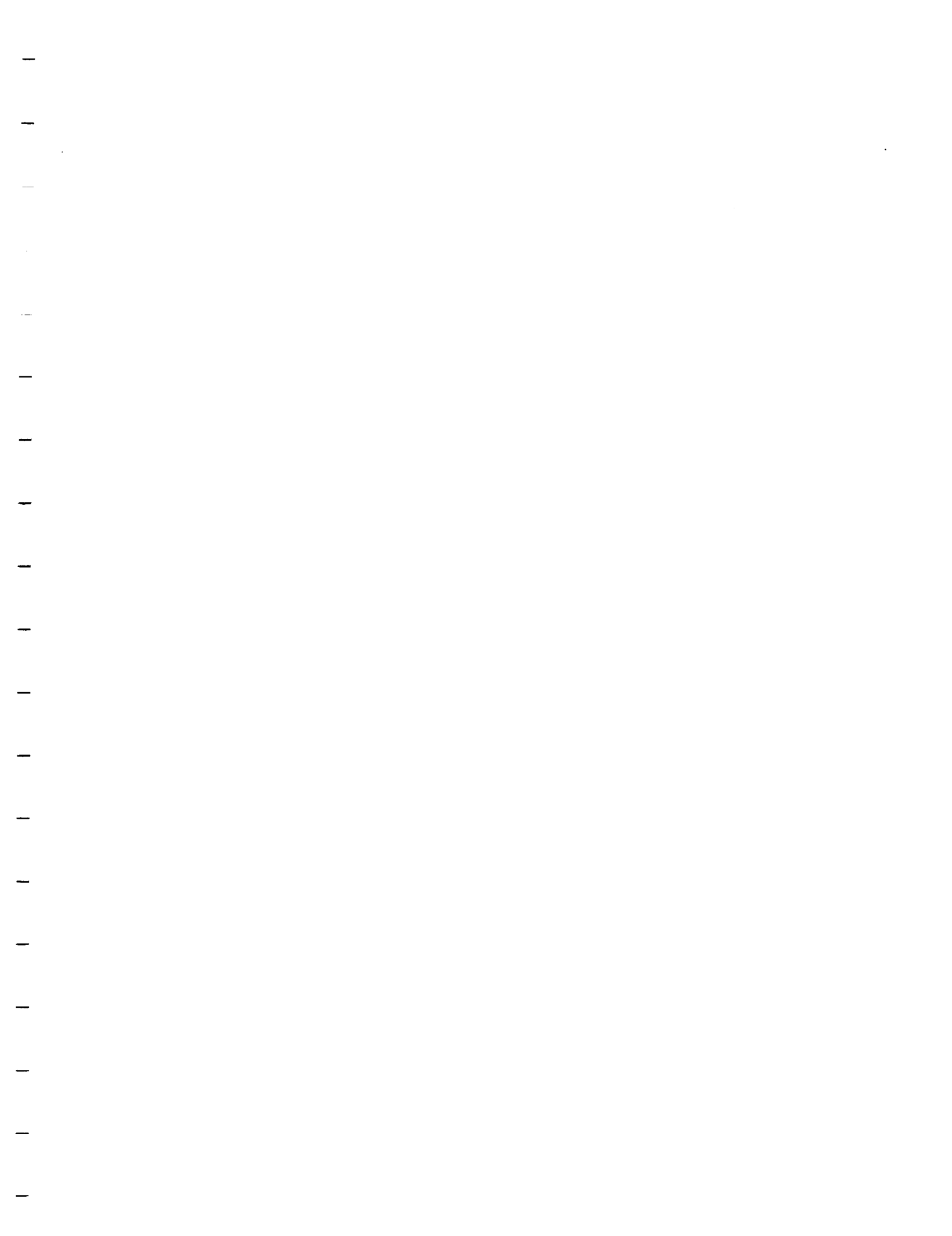
DEGB FIGURING CYCLES

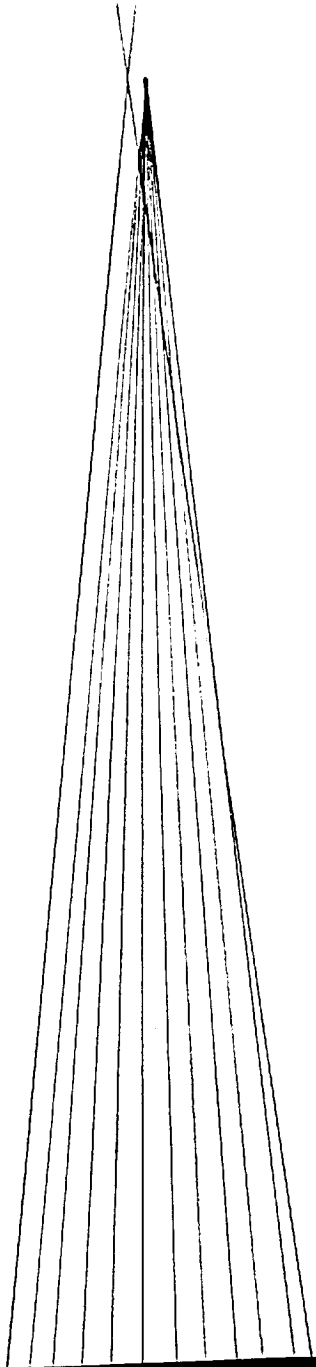
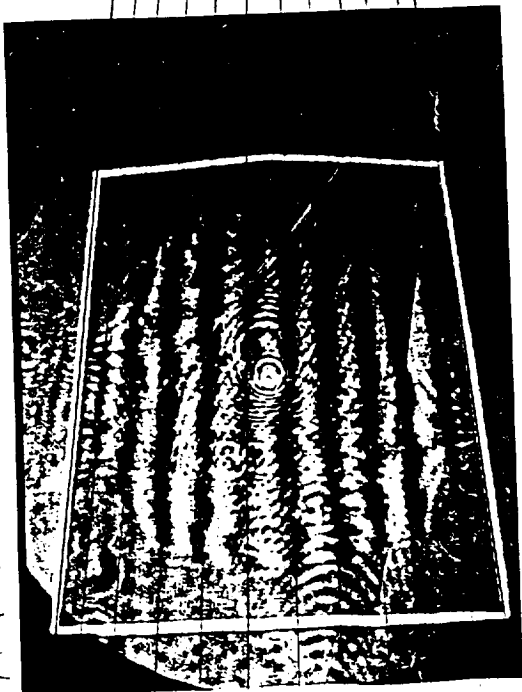
POLISHING STAGE



Raw data used for figuring cycle graphs

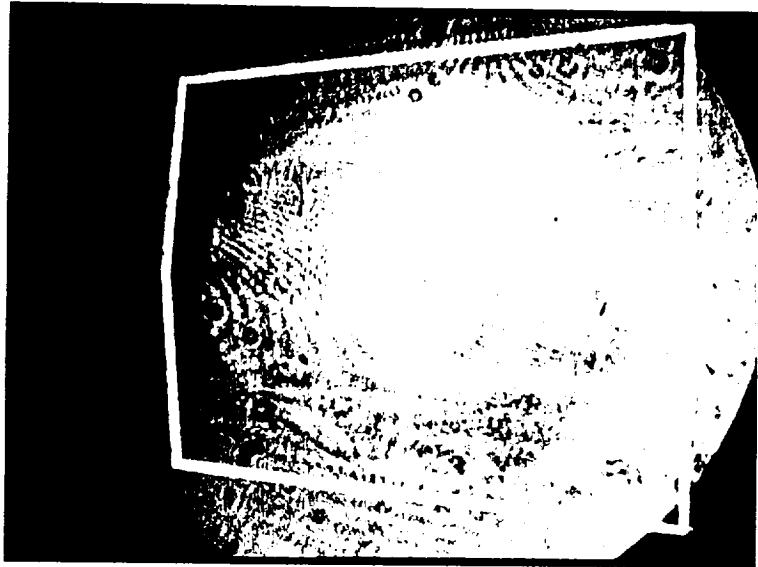
0	1	2	3	4	5	6	7	8	9	10	11	12	13
72.3	71.6	70.6	69.9	69.1	68.3	67.4	66.2	65.7	66.5	68.3	70.7	70.7	72.3
72.3	70.98	69.3	68.1	66.7	65.2	63.6	61.3	60.2	60.2	60.2	60.2	60.2	60.2
14	15	16	17	18	19								
72.34	72.45	72.337	72	72.339	72.33								
60.2	60.2	59.854	59.345	59.604	59.947								
20	21	22	23	24	25	26	27	28					
72.863	71.915	71.365	72.656	72.203	72.519	72.356	72.254	72.339					
60.748	59.546	60.024	60.165	59.865	60.047	59.983	59.866	59.947					





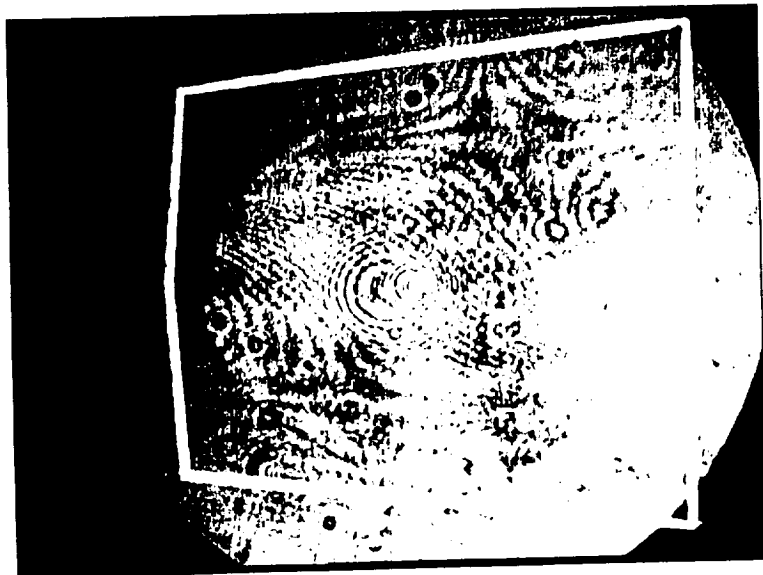
TILTED SURFACE MAKES FRINGES APPEAR TO
COME FROM A VANISHING POINT.

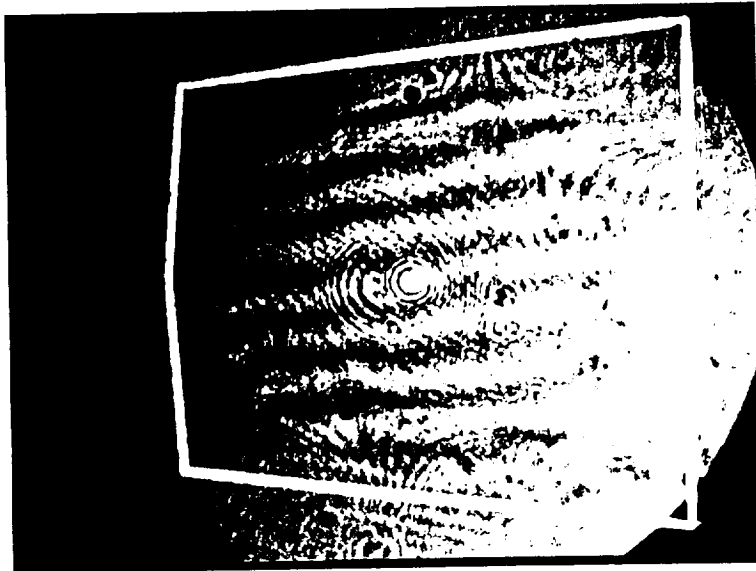
MANUAL REDUCTION METHOD FOR DEGB



NULL TEST

10-26-93





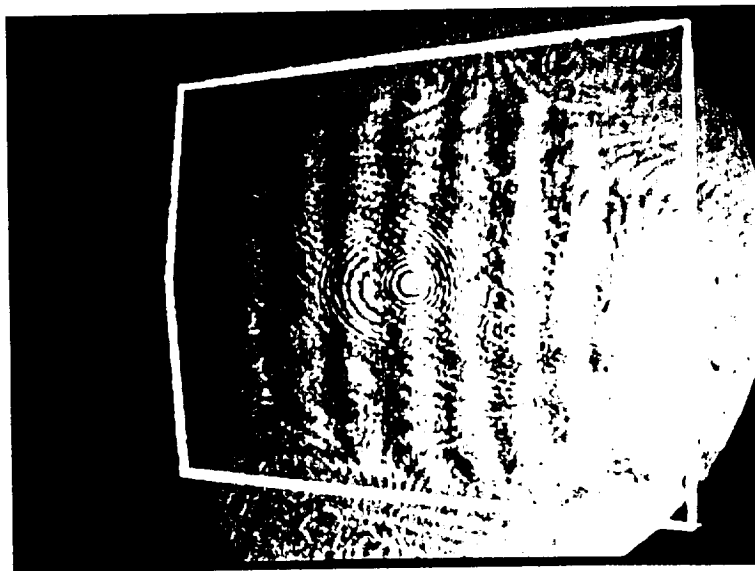
NASA DECB

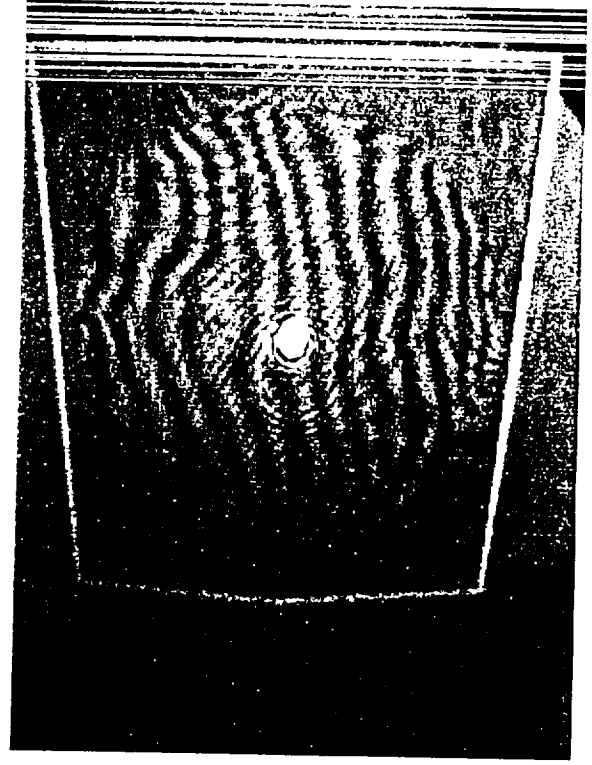
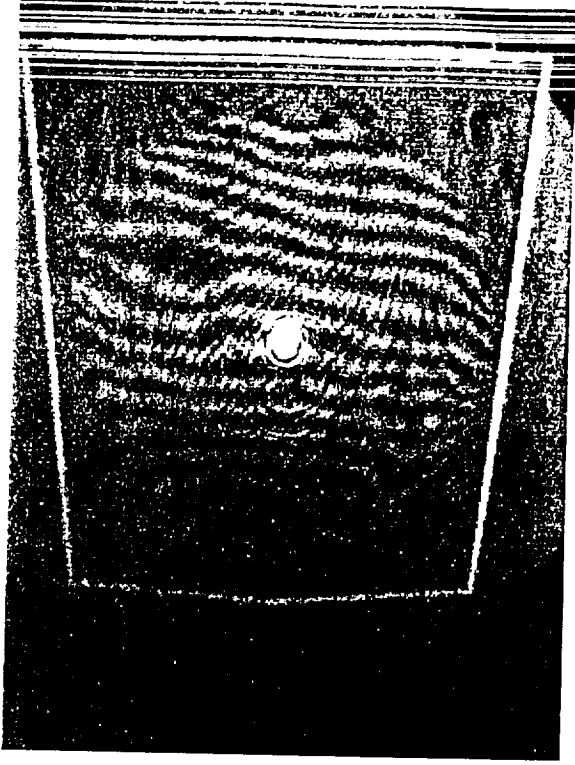
10-21-93

PV

Pain

Mashed





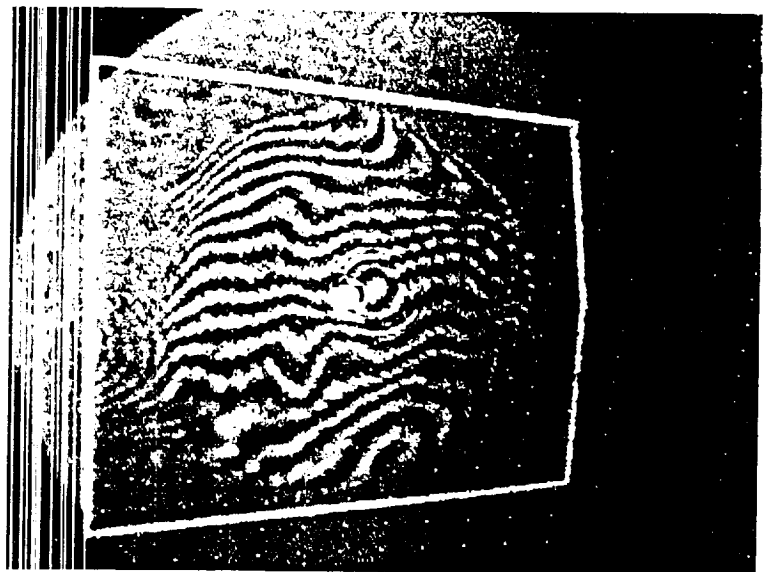
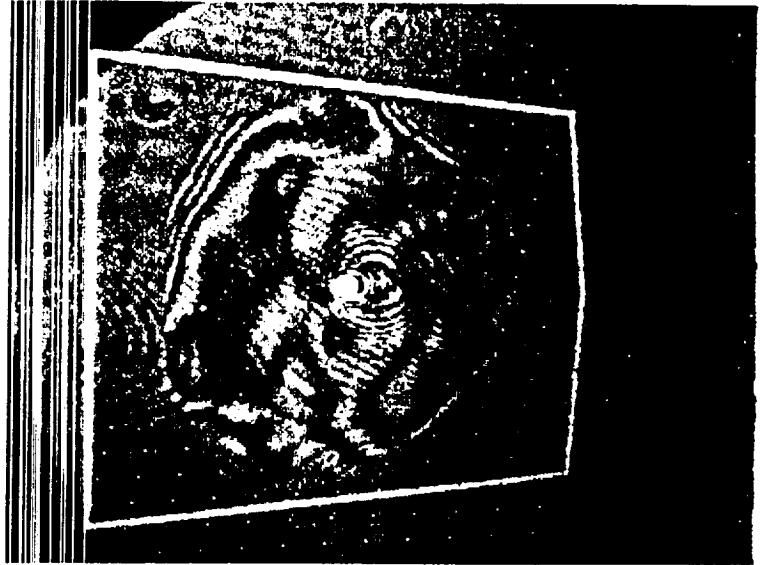
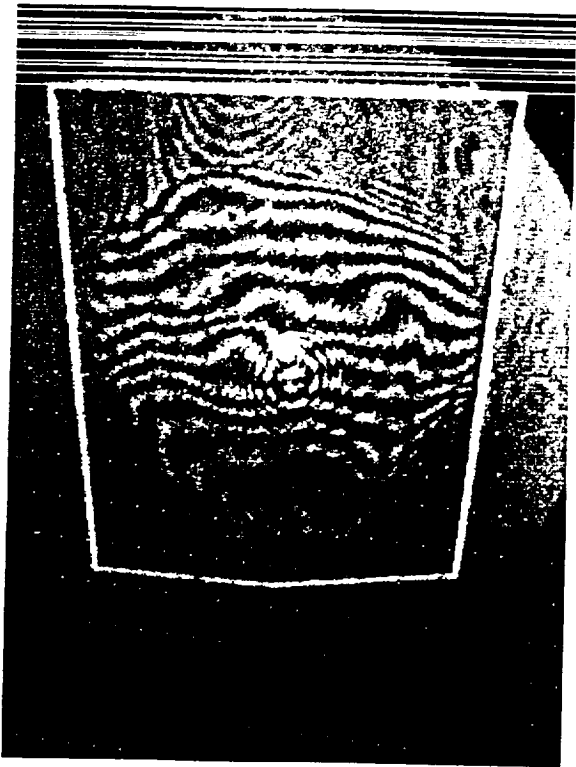
MASKED
TM 9/30/93 PM



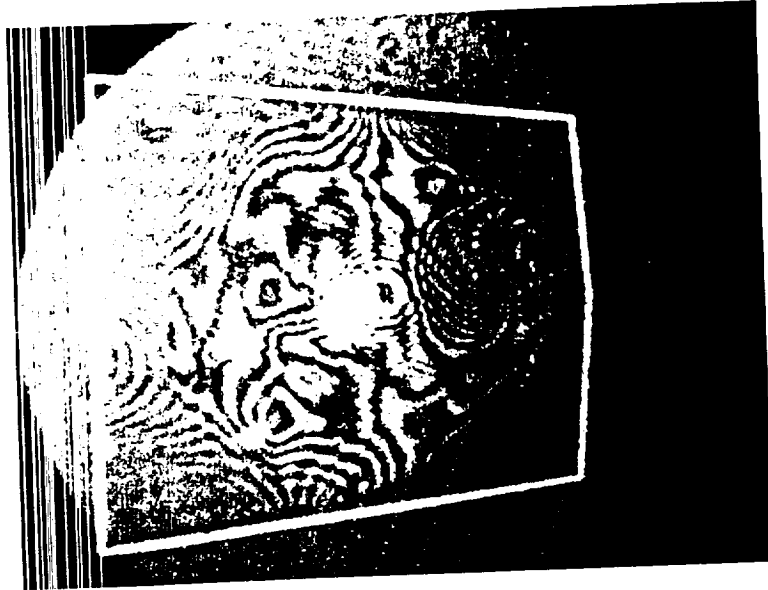
MASKED

FRI 9/24/93

11:00
AM

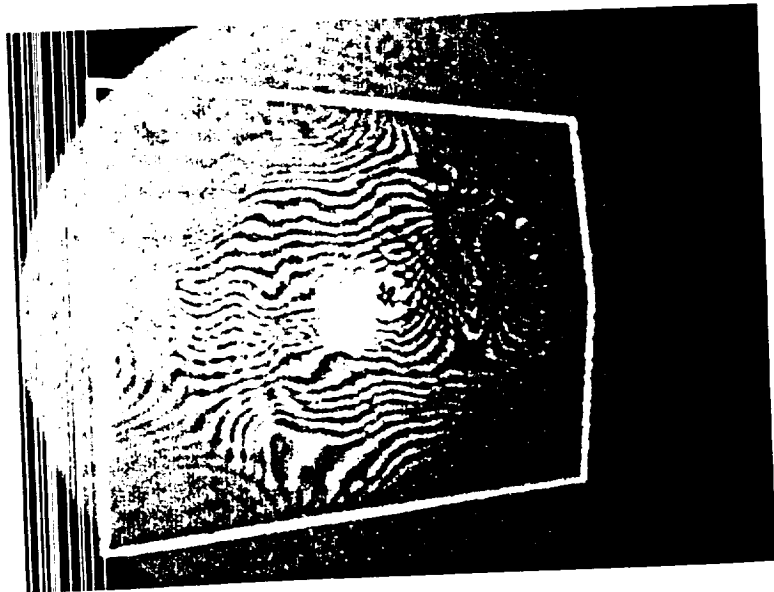


MASKED ↓



NASA DEGB

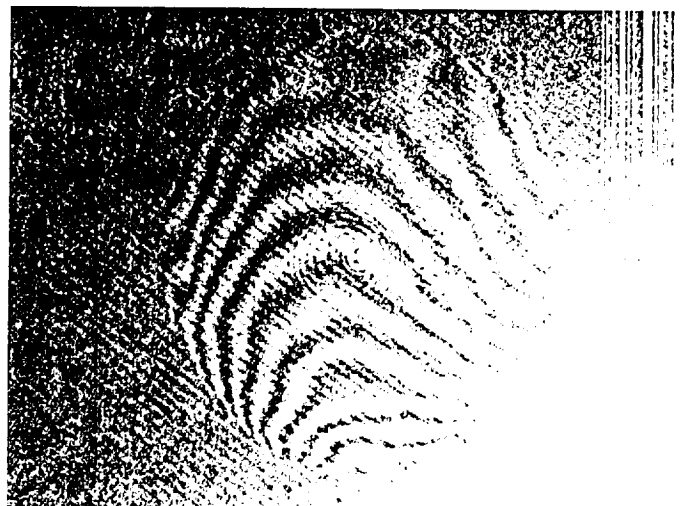
20 SEPT 93





NASA
DEGB
31 AUG 93

NASA GODDARD DEGB
or ellipse
8-31-93



APPENDIX D

INTERFEROMETER FOR ASPHERIC TESTING

- 1) Arnold, Steven M., Jain, Anil K., "*An interferometer for testing of general aspherics using computer generated holograms*", SPIE Vol 1396, 1990.
- 2) Arnold, Steven M., "*An interferometer for aspheric testing: Calibration and error compensation*", ASPE Proceedings, April 1992.
- 3) Calibration curves for IAT SN 003.

An interferometer for testing of general aspherics using computer generated holograms

Steven M. Arnold and Anil K. Jain

APA Optics Inc.
2950 N.E. 84th Lane, Minneapolis, Minnesota 55434

PREPRINT
SPIE Vol. 1396
27-28 September 1990
Chicago

ABSTRACT

An interferometer for aspheric testing (IAT) is under development at APA Optics for testing of general aspherics using inexpensive electron-beam written computer generated holograms (CGHs) as null compensators. This 152-mm aperture Twyman-Green interferometer is compatible with standard transmission spheres, fringe analysis software, and phase measuring accessories. Aspheric departures of up to several hundred waves can be measured using only standard interferometer accessories. Deeper aspheres may be tested using simple auxiliary optics. The interferometer configuration, methods of operation, and performance specifications are presented.

1. INTRODUCTION

Modern optical systems demand the use of aspheric surfaces to improve system performance and reduce the number of optical components required. Fabrication of precision aspheres is becoming less expensive because of advances in such techniques as diamond turning and automated polishing. However, these aspheric components still require testing, and optical methods are preferred. Stylus methods are slow, usually require physical contact, and cannot test for index inhomogeneities or assembly errors. The standard interferometric method of testing an aspheric surface (or lens) is to use a Fizeau interferometer with auxiliary optics to produce a wavefront matching the (ideal) aspheric surface being tested. The problem with these refractive or reflective null compensators is that they are expensive, they require a long lead time, and a separate compensator must be made for each asphere design tested.

Much has been written on the use of CGHs as aspheric null compensators. A recent paper by the author reviews this work¹. With the addition of a beamsplitter between the mainframe and transmission sphere, a commercial Fizeau-type interferometer can be adapted to test aspheres using CGHs². Depicted in Figure 1, this testing technique has several limitations: convex test surfaces cannot be imaged onto the CGH, a necessary condition for strong aspheric wavefronts; the on-axis Moiré-type fringe pattern is difficult to interpret for complicated wavefronts where the slope reverses sign; and the technique does not lend itself to phase measuring. Off-axis CGHs have been used in the test arm of a Twyman-Green or laser unequal path (LUPI) interferometer. This offers the advantage of a spatially filtered (non-Moiré) interferogram but does not solve the pupil imaging limitation and requires an expensive high diffraction efficiency CGH on a high quality substrate.

Figure 2 depicts a preferred configuration: a Twyman-Green interferometer with a CGH in the viewing arm. Key features include imaging of the test surface onto the CGH, placement of the CGH in collimated test and reference beams so that both pass similarly through the substrate, and spatial filtering of diffracted orders. Although several interferometers of this general configuration have been built, none are currently available commercially.

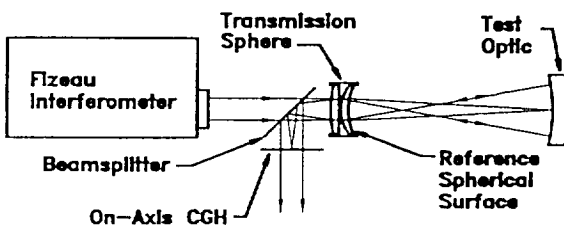


Figure 1. Aspheric testing using a Fizeau interferometer and CGH.

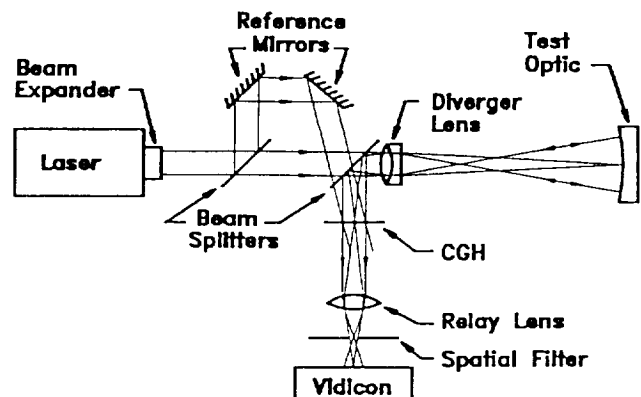


Figure 2. Twyman-Green (LUPI) interferometer with CGH in viewing arm.

2. REQUIREMENTS AND DESIGN GOALS

Our goal is a commercial instrument which can provide routine and economical interferometric testing of aspheric optics. To minimize the need for expensive null lenses, the instrument must be capable of testing aspheres which are much deeper than the few tens of fringes possible with currently available phase-measuring interferometers. Other design goals include $\lambda/10$ system accuracy, multi-aperture capability, pupil imaging of both concave and convex aspheres, ease of use, phase measuring capability, and compatibility with industry standard accessories and interferogram analysis software.

Our approach makes maximum use of inexpensive e-beam written CGHs to null the test aspheres, to ease manufacturing tolerances by compensating known instrument imperfections, and to serve as alignment and calibration tools. The interferometer design therefore begins at the CGH. For unwanted diffraction orders to be blocked by spatial filtering, a CGH must include an off-axis carrier such that the minimum spatial frequency is more than half the maximum spatial frequency. Since the diffracted reference beam matches the test beam (or vice versa), test and reference beam ray slopes, θ_t and θ_r , are related to the local spatial frequency, $1/\Lambda$, through the grating equation

$$\sin \theta_t = \sin \theta_r - \lambda/\Lambda = \lambda/\Lambda_0 - \lambda/\Lambda. \quad (1)$$

Table 1 lists CGH bandwidths, linewidths ($\Lambda/2$), ray slopes, and wavefront accuracies ($\lambda/2 = 1$ fringe) achievable with standard (*i.e.* mask shop) e-beam resolutions. The collimated test or reference beam diameter will define the maximum CGH aperture. Other apertures in the system will depend on the CGH bandwidth (ray slopes) and pathlengths. We decided on a 20-mm CGH aperture and 38-mm cube beamsplitters as a reasonable compromise between functionality and cost. These choices will accommodate ray slopes of 100 to 150 lpmm (the practical limit of e-beam lithography) and allow a one-dimensional CGH space-bandwidth product of 2000 to 3000. This is adequate for testing of aspheric deformations (less tilt and focus) as large as several hundred fringes without the use of additional null optics.

3. OPTICAL SCHEMATIC

Figure 3 depicts the overall configuration of the APA Optics interferometer for aspheric testing (IAT). Its construction is modular, consisting of a Twyman-Green or LUPI mainframe of 20-mm beam diameter, detachable beam expanding telescopes (152-mm aperture shown), and a selection of accessory optics.

3.1 Interferometer Mainframe

The interferometer mainframe uses two polarizing beamsplitter cubes with attached $\lambda/4$ plates to establish separate paths for orthogonally polarized test and reference beams. This approach is shared by an earlier holographic interferometer familiar to the author³. The He-Ne laser beam, after being spatially filtered and expanded to 20 mm diameter, is divided by the first cube into a transmitted reference beam and a reflected test beam. The test beam, which is circularly polarized as it exits the cube through a $\lambda/4$ plate, is converted to the orthogonal linear polarization upon its return from the test arm and is therefore transmitted through the cube to the pupil relay arm. After being focused, retroreflected and recollimated by the pupil relay, the test beam is transformed back to its original state of linear polarization and is thus reflected by the beamsplitter cube to rejoin the reference beam. Test and reference beams then copropagate to the second cube with opposite linear polarizations; the reference beam is collimated whereas the test beam will have acquired up to several hundred waves of aberration from the test asphere.

On entering the second polarizing beamsplitter cube, the test beam is transmitted whereas the reference beam is diverted to a pair of reference mirrors which control its tilt and decentration. (For graphic purposes, both cubes are shown as oriented similarly; the second cube and its reference mirrors must be rotated 90 degrees about the optic axis in order that the test beam and not the reference beam be transmitted.)

Table 1. Capabilities of e-beam written CGH photomasks.

CGH bandwidth (lpmm)	Minimum linewidth (μm)	Ray slopes (degrees)	Accuracy (waves) vs. e-beam resolution			
			1.0 μm	0.5 μm	0.25 μm	0.1 μm
30 \pm 10	12.5	± 0.363	$\lambda/50$	$\lambda/100$	$\lambda/200$	$\lambda/500$
75 \pm 25	5.0	± 0.906	$\lambda/20$	$\lambda/40$	$\lambda/80$	$\lambda/200$
150 \pm 50	2.5	± 1.813	—	$\lambda/20$	$\lambda/40$	$\lambda/100$
300 \pm 100	1.25	± 3.628	—	—	$\lambda/20$	$\lambda/50$
375 \pm 125	1.0	± 4.537	—	—	—	$\lambda/40$
450 \pm 150	0.83	± 5.447	—	—	—	$\lambda/33$

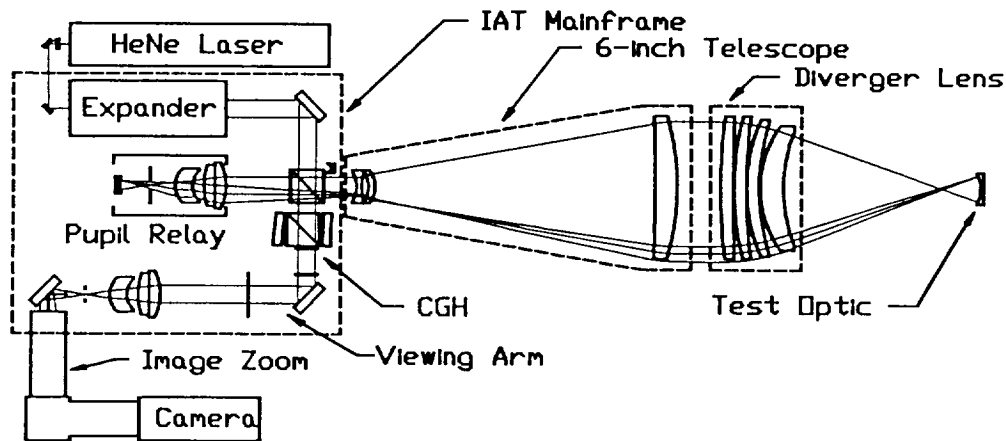


Figure 3. Overall configuration of proposed interferometer for aspheric testing (IAT) with attached 152-mm telescope and $f/1.5$ diverger lens.

On exiting the second beamsplitter cube, the test and reference beams would form an off-axis interferogram were it not for their opposite linear polarizations. Instead, the test and reference paths are raytraced from the expanded, collimated source to determine this expected interferogram which is then encoded as an e-beam written computer generated hologram. The CGH diffracts the reference beam, adding aberrations to match those expected in the test beam while simultaneously removing the reference beam tilt. The diffracted reference beam, in combination with the undiffracted (zero order) test beam, forms a nominally null interferogram. The viewing arm optics relay this interferogram to the video camera while also spatially filtering unwanted diffraction orders and converting the two beams to a like state of linear polarization by use of a diagonally oriented linear analyzer.

Like most Twyman-Green or LUPI interferometers, the proposed IAT can also operate in Fizeau mode. This requires blocking the Twyman-Green reference path (by rotating a waveplate and analyzer) and introducing a partially reflecting Fizeau transmission flat or sphere into the test arm, thus producing an on-axis reference beam of the same polarization as the test beam. Both beams then return via the pupil relay arm to the CGH.

3.2 Pupil Relay Arm

The beam expanding telescope and diverger lens will form a first image of the test surface somewhere in the vicinity of the mainframe-telescope junction. This 20-mm diameter first image is real if it lies between the telescope and the beamsplitter cube and virtual otherwise. The required image location will vary depending on the choice of diverger optics, the test surface radius, and whether the test surface is concave or convex. For concave (beyond focus) test surfaces, the first pupil image may lie outside the telescope, moving closer to and eventually into the telescope for larger test surface radii. For convex test surfaces, the image lies inside the telescope—further inside for smaller test surface radii. A generous range of image locations centered about the telescope/mainframe junction accommodates all but very small radius concave and convex parts.

The pupil relay arm transfers the first pupil image to the CGH. The relay optics consist of a multi-element focusing lens and a confocal spherical mirror for retroreflection. Both are mounted on a mechanical slide providing 150 mm of travel. From a pupil imaging standpoint, the spherical mirror acts as a field lens. The relay optics were designed by raytracing the test beam (backwards) from the CGH, through the beamsplitter cubes, out the relay arm, and back through the first cube to five different first pupil image locations, using the position of the mechanical slide as a zoom parameter. Three of the five zoom positions and their associated image locations are shown in Figure 4. An aperture stop at the CGH restricted design ray slopes to ± 3.63 degrees (± 100 lpmm). In order to make the multi-element focusing lens separately testable, we required that it form a near perfect focus when presented with a 20-mm on-axis collimated beam. This required a sixth zoom configuration. The relay optics design did not attempt to compensate aberrations of the test arm optics (which were not included in the raytrace).

The focusing lens is a cemented pair of plano-convex elements plus a thick meniscus corrector lens. The pupil imaging performance of the relay optics design is better than 5λ for all five zoom positions and ray slopes up to ± 100 lpmm. The double pass de-collimation (*i.e.* zero ray slope performance) is better than $\lambda/20$. The approximate range of first pupil image locations is from 80 mm inside to 200 mm outside the test arm face of the first beamsplitter cube.

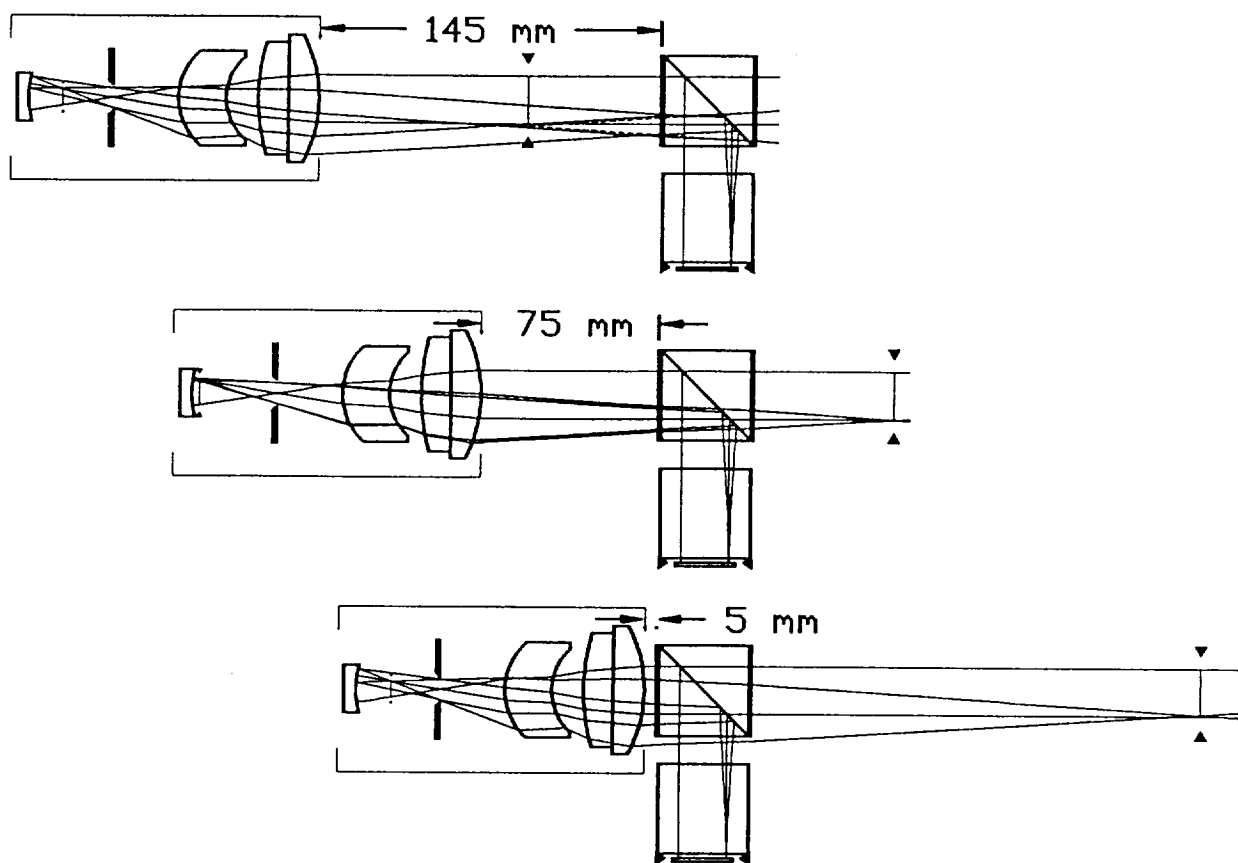


Figure 4. Pupil relay optics for three locations of first pupil image.

3.3 Test Arm

Test arm magnification should match the required test aperture. Excess magnification reduces the scale of the CGH, increasing its cost and/or forcing a reduction in space-bandwidth. The mainframe's unexpanded 20-mm beam, together with a diverger lens of suitable $f/\#$, is adequate for testing most concave or small convex parts. A telescope is required only for testing of larger convex surfaces or for compatibility with standard Fizeau accessories.

We have designed or are designing test arm optics for a range of apertures and $f/\#$'s. One completed design is for an $f/3$ Galilean telescope to expand the test beam from 20 mm to 152 mm. This telescope is atypical in that the negative lens aperture must be large enough to accommodate a returning aspheric wavefront. The design seeks to minimize coma for locations of the first pupil image which lie within the focus range of the pupil relay optics (cf. Figure 4). A desire to minimize vignetting without increasing the aperture of the objective lens beyond 152 mm drives the design to low $f/\#$. The apertures of the two smaller lenses are sized to pass all such rays which are not vignetted by the 152-mm aperture objective. The expander requirement is for 7.5X beam expansion and $\lambda/10$ collimation. The competing pupil imaging requirements can be expressed as a 20-mm field of view for a 280-mm range of image locations with an $f/8$ aperture stop at the image.

3.4 Reference Path

The function of the second beamsplitter cube and reference mirrors is to tilt the reference beam without decentration at the CGH plane. Figure 5 shows the ray paths and mirror configuration for selected CGH carrier frequencies. Note that the diffracted reference beam acquires aberrations to match those expected in the zero order (undiffracted) test beam. The 38-mm cube is decentered by 4 mm to accommodate larger reference path tilts without vignetting. The first reference mirror includes one axis of coarse tilt adjustment and a piezo transducer for phase measuring. The second reference mirror, which tilts in both axes, is used to fine adjust the number and orientation of interferogram fringes. When operating in Fizeau mode, an on-axis reference beam is provided by the final surface of a transmission sphere or flat and the orthogonally polarized Twyman-Green reference beam is blocked.

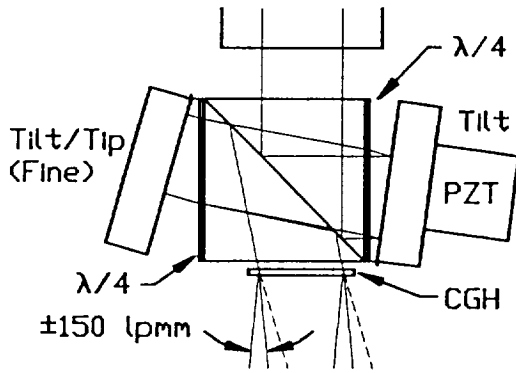


Figure 5. Reference path for CGH of 450 ± 150 lp/mm.

3.5 Viewing Arm

The viewing arm optics, shown in Figure 6, relay the 20-mm diameter interferogram at the CGH onto the 11-mm diagonal video camera while also spatially filtering unwanted diffraction orders and converting the two beams to a like polarization state by use of a diagonally oriented linear analyzer. The imaging requirements of the relay lens are rather unusual in that it must cover a full field of view with low distortion and no vignetting for an aperture stop located at the object (CGH). Because only two rays of interest (zero-order test and first-order reference) come simultaneously from any point on the CGH, and these rays are nominally copropagating, resolution is relevant only in the sense of an aperture dependence of distortion. Somewhat coincidentally, these requirements are well met by the multi-element lens previously designed for the pupil imaging relay. In Fizeau mode, an on-axis CGH collimates the first-order test beam to match the zero-order reference beam. A small aperture then blocks most light of other (spurious) diffraction orders.

Figure 3 included zoom optics between the first spatially filtered image and the camera. It appears that 5:1 image zooming can be provided by commercially available optics and a field lens, although this option has not been verified.

4. USER INTERFACE

Although the Aspheric Interferometer is of greater optical complexity than the usual Fizeau interferometer, the user interface is similar in most respects. The primary differences relate to the CGH.

4.1 Test Arm Configuration and CGH Design

Planning begins with the specification of a test arm configuration to minimize ray slopes at the CGH. Typically this will involve selecting a combination of diverger lens and/or beam expander to produce a best-fit spherical wavefront. A partial null lens will be required for very deep aspheres. However, with a CGH to accommodate the higher order aberrations, a singlet can often suffice, both as diverger lens and to null the lower order aberrations.^{4,5}

For each variety of asphere to be tested, a CGH must be designed and fabricated. The CGH design is performed using commercially available optical design software, most likely the same package as was used to design the asphere. The CGH is defined by its phase function which represents the expected optical path difference between the test and

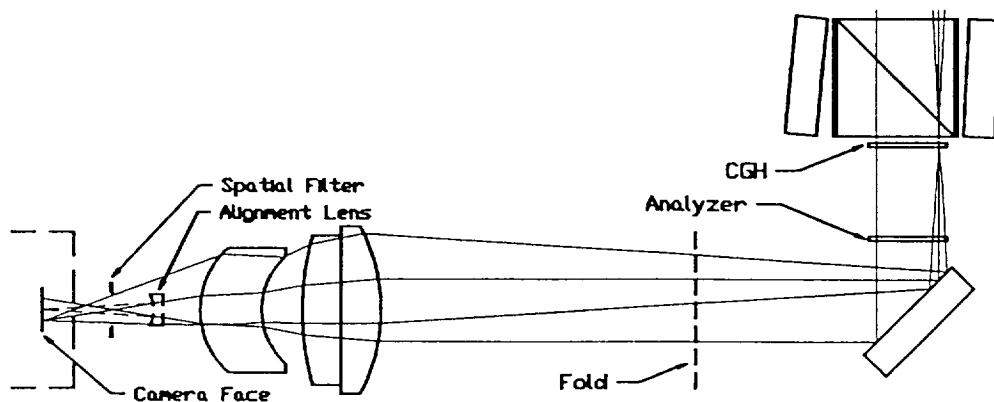


Figure 6. Viewing arm optics showing removable alignment lens.

reference beams as measured at the CGH plane. Design of the CGH requires a complete description of the interferometer and test arm optics. The raytrace begins with the 20-mm diameter collimated laser beam entering the first beamsplitter cube and ends at the CGH. The source arm and viewing arm optics need not be raytraced as they are common to both beams. The CGH design process includes specifying a test arm configuration to minimize ray slopes at the CGH and choosing a position for the relay arm slide to provide acceptable pupil imaging.

Although initial setup of the raytrace model and CGH merit function is quite complicated, modification for subsequent asphere testing should be routine. Since the reference path varies only in the mirror tilts which are uniquely determined by the CGH carrier frequency, it is not necessary to explicitly raytrace this path for each CGH design; OPD maps for various carrier frequencies are instead included as part of the interferometer documentation and subtracted from CGH designs. Similarly, the Fizeau mode reference path can be documented for each beam expander and transmission sphere configuration. Given the baseline raytrace model for each expander/transmission sphere configuration, the designer need only modify the test optic description and, for very deep aspheres, insert a refractive null compensator.

The test arm is configured in accordance with the CGH design. Aspheric test surfaces will require 5-axis or 6-axis positioning. Similarly, since the test wavefront on returning through the diverger lens has acquired the aspheric aberrations of the test surface, it is necessary that the diverger lens be coaxial with the interferometer. These alignment complexities are characteristic of any interferometric testing of aspheres and have been addressed elsewhere⁶.

4.2 Interferometer Operation

Figure 7 identifies those parts of the interferometer which are available for manipulation by the user. The CGH is then inserted and positioned so its alignment fiducials match a corresponding pattern on the exit face of the second beamsplitter cube when viewed on the video monitor. The pupil relay slide and reference mirrors are set to values specified by the the CGH design. These settings are inscribed onto the CGH and readable on the video monitor. The aperture turret is rotated to bring the negative alignment lens into the viewing path, thus focusing the test and reference beams onto the camera face. The test surface and second reference mirror are tilted to bring both focused spots to the center of the camera field. A small corner cube can be moved into the test arm path, providing a third focused spot to define the center. This corner cube is also available to verify collimation of the pupil relay optics which is adjustable via a focus screw on the retro-mirror.

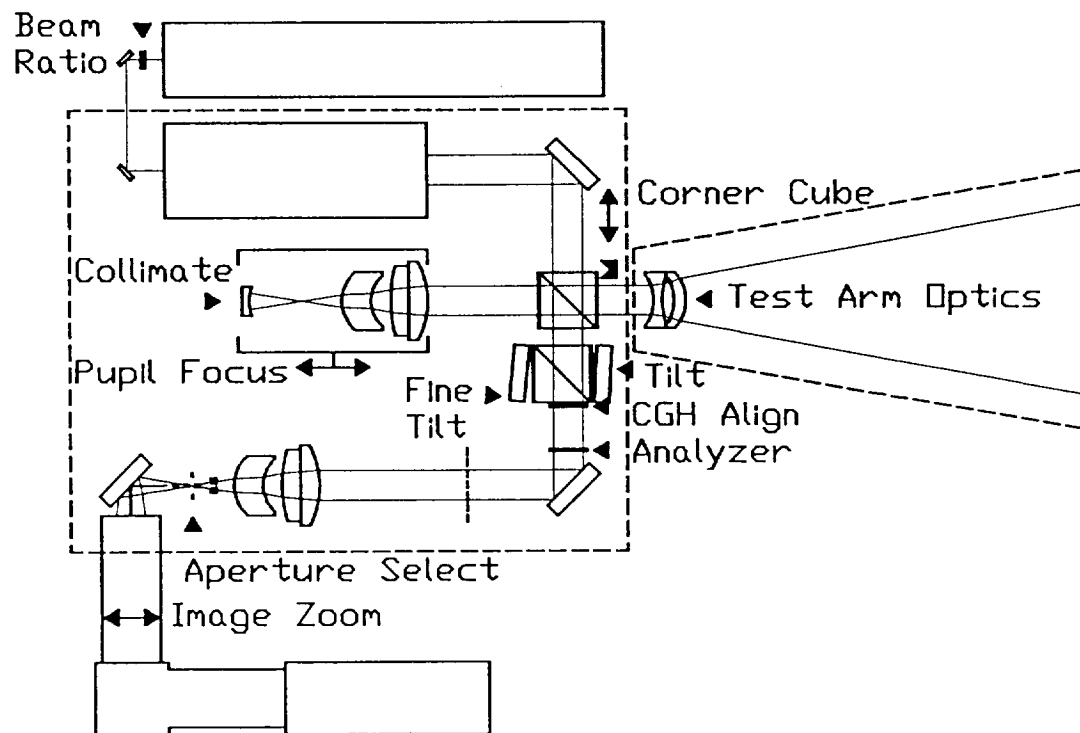


Figure 7. IAT user interface.

The corner cube is removed and the aperture turret is rotated to display the interferogram on the monitor. The smallest aperture which passes the entire interferogram is selected, blocking any unwanted diffraction orders. The apertures are labeled ± 150 , ± 100 , etc. denoting the CGH bandwidth in lp/mm. A $\lambda/2$ plate prior to the beam expander adjusts the intensity ratio of the orthogonally polarized test and reference beams while the analyzer in the viewing arm determines the fraction of each beam which will reach the camera. By rotation of the waveplate and analyzer, the user can manipulate both the intensity and contrast of the interferogram to suit any test surface reflectivity.

If the test surface includes alignment fiducials which are visible on the monitor, then it is translated and/or rotated to bring these fiducials into coincidence with corresponding marks on the CGH. It is then a matter of further manipulating the test surface to achieve straight, equally spaced fringes. For interferogram recording and analysis, both the video signal (RS-170) and the phase-shifting piezo transducer are plug compatible with commercially available fringe analysis and phase measuring attachments.

Flat surfaces can be tested in Twyman-Green mode with a generic CGH serving only to compensate aberrations of the interferometer optics. Flat or spherical surfaces (or shallow aspheres) can also be tested in Fizeau mode without the use of a CGH. One simply attaches the appropriate Fizeau transmission flat or sphere to produce a test arm reference beam and rotates the viewing arm analyzer to block the orthogonally polarized Twyman-Green reference beam.

5. TOLERANCING AND MANUFACTURABILITY

A complete sensitivity and tolerance analysis has been performed using methods similar to those outlined by Ginsberg⁷. The analysis clearly shows that the instrument cannot be economically built to provide $\lambda/10$ testing capability without a high degree of software compensation. This should come as no surprise considering the optical complexity of the Aspheric Interferometer and that most components are unique to either the test or the reference path. The ability of a CGH to provide this compensation while also nulling the test asphere is what makes the Aspheric Interferometer a viable instrument for routine aspheric testing. Each CGH design is based on a full raytrace of the interferometer from expanded laser beam to CGH. Therefore, a precise interferometer is not necessarily required—providing we have a sufficiently precise optical description in a format acceptable to the optical design software.

Lens thicknesses, spacings, surface radii, and glass refractive indices can all be measured to much better accuracy than they can be manufactured. We therefore place fairly loose manufacturing tolerances on these parameters. If surface irregularities are describable by low order Zernike polynomials, they can be characterized to $\lambda/50$ or better using phase measuring interferometry and modeled by several optical design codes. We therefore place fairly tight ($\lambda/10$) tolerances on surface figures and further require that irregularities be well behaved. Since only the central zone of each element is ever used in double pass, we can double the tolerances for the larger aperture. In designing for fairly sturdy lens thicknesses and loose thickness tolerances, we reduce the difficulty of achieving these required irregularity tolerances.

Because refractive index inhomogeneities are difficult to characterize or model, they will be a major source of residual error. Several methods are used to minimize these error contributions. First, we specify Schlieren grades of glass wherever justified. Second, the beamsplitter cubes, pupil relay lens, and telescope are all designed as individually testable afocal subassemblies. This permits localization of residual errors and insertion of compensating dummy surfaces into the raytrace model. Third, by designing with identical components in both critical and non-critical locations, we have a better inventory of components from which to select.

This brief paper cannot detail the considerable opto-mechanical design involved in the aspheric interferometer. Primary mechanical considerations are component centration and thermal stability. A defocus of 26 microns in the pupil relay or 18 microns in the 152-mm telescope will produce 1 fringe of aberration at the interferogram. Both subassemblies are therefore designed for thermal stability through initial glass and metal choices and finally by fine-tuning the mount geometries. Manual focus adjustment of the pupil relay and telescope allow compensation of defocus errors due to humidity or barometric pressure. Plans are to assemble components using a transfer-spindle technique in which individual mechanical cells are elastomerically mounted to their centered optical components and final machining is performed without remounting. Subassembly tilt and decenter tolerances are therefore limited not by any mechanical tolerances but rather by our ability to optically detect tilt and decentration. Final assembly of the interferometer involves extensive self-testing using specific CGHs to bootstrap first the beam expander and viewing arm, then the beamsplitter cubes and reference mirrors, the pupil relay arm, and finally the telescope and other attachments.

We note that the 5-dimensional space of CGH pupil coordinates x and y (test pupil), sagittal and tangential ray slopes at the CGH (asphericity), and pupil relay slide position (test optic radius) includes all possible test beam ray paths through the interferometer. Consequently, the adequacy of the raytrace model in describing the interferometer

optics to within the desired system accuracy of $\lambda/10$ can be verified by designing CGHs to test a flat mirror at selected tilt angles of up to 2.7 degrees (150 lpmm) and at various pupil relay slide positions. If sufficient accuracy does not result, the raytrace model must be improved. This will involve using the test interferograms to deduce mechanical misalignments and/or to insert dummy phase surfaces at key locations within the interferometer to compensate residual surface irregularities or glass inhomogeneities. By sufficient application of this test and calibration procedure, we can refine the raytrace model to reduce system errors to the limits imposed by interferogram measurability ($< \lambda/50$), system stability, and the capabilities of the commercial raytrace software. We are confident that the interferometer stability and existing raytrace software (e.g. Code V[®], Super Oslo[®] or GENII[®]) will be adequate to achieve the desired $\lambda/10$ system accuracy.

6. SUMMARY

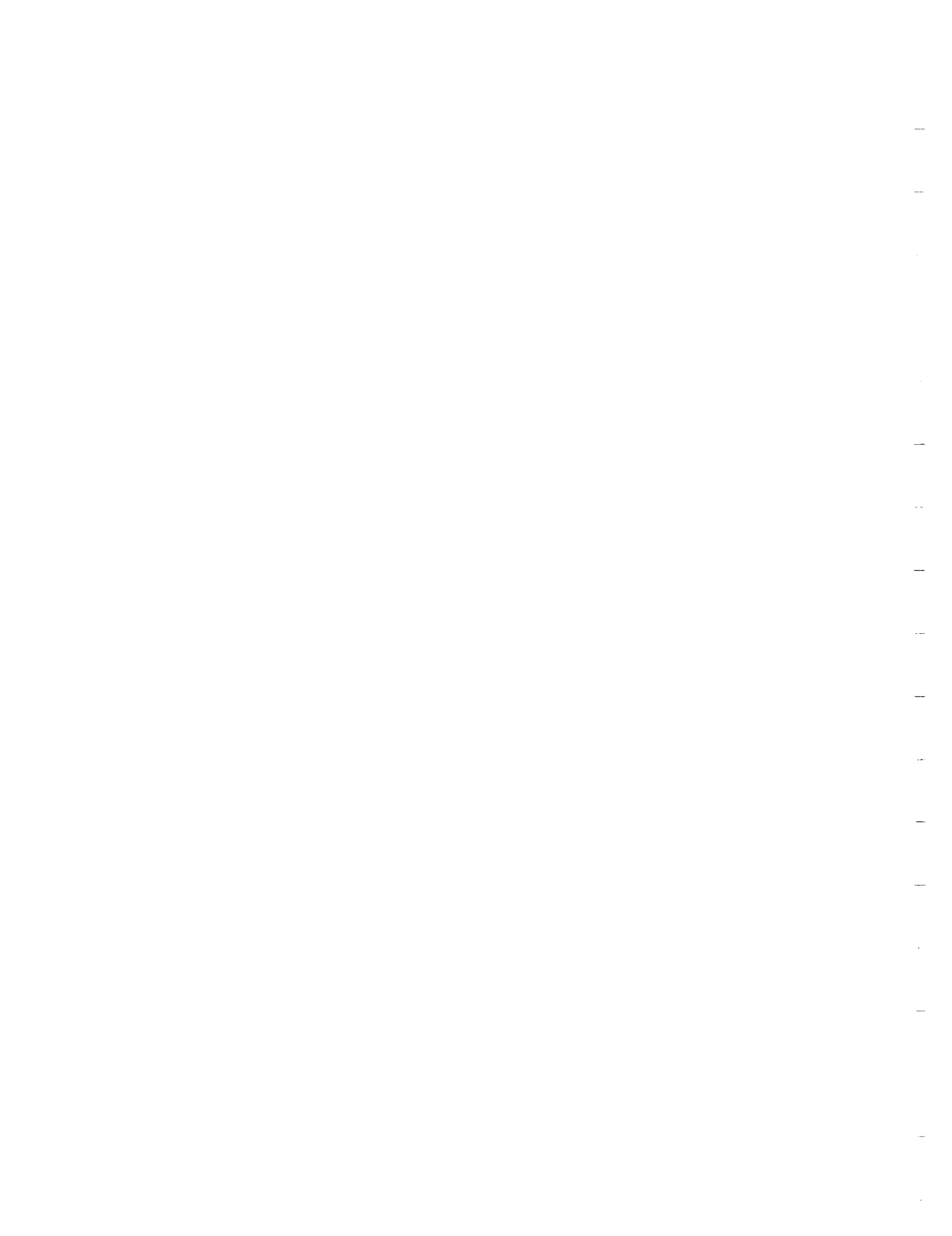
A laser unequal path interferometer (LUPI) is under development at APA Optics for testing of general aspherics. The interferometer design makes maximum use of inexpensive e-beam written CGHs to null test surface asphericity, to ease manufacturing tolerances by compensating known instrument imperfections, and to serve as alignment and calibration tools. The Interferometer for Aspheric Testing (IAT) is expected to be capable of testing aspheric departures (from base sphere) of several hundred waves with an accuracy of $\lambda/10$ using only standard auxiliary optics. Deeper aspheres will be testable using simple optics as partial null compensators.

7. ACKNOWLEDGEMENT

The authors acknowledge the capable help of Mr. Lubomir Koudelka in accomplishing the opto-mechanical design and addressing the manufacturability of the aspheric interferometer.

8. REFERENCES

1. S.M. Arnold, "How to test an asphere with a computer generated hologram", in *Holographic Optics: Optically and Computer Generated*, SPIE Vol. 1052, 191-197 (1989).
2. E.J. Danielewicz and D. Selman, "Computer-generated holograms test aspheric optics", in *Laser Focus World*, pp143-146 (April 1990).
3. K.M. Leung, S.M. Arnold and J.C. Lindquist, "Using e-beam written computer-generated holograms to test deep aspheric wavefronts", in *Contemporary Methods of Optical Fabrication*, SPIE Vol. 306, 161-167 (1981).
4. D.C. Smith, "Testing diamond turned aspheric optics using computer-generated holographic (CGH) interferometry", in *Contemporary Methods of Optical Fabrication*, SPIE Vol. 306, 112-121 (1981).
5. P.L. Ruben, "Refractive null correctors for aspheric surfaces", *Applied Optics* 15(12), 3080-3083 (1976).
6. B. Dörband and Hans J. Tiziani, "Testing aspheric surfaces with computer-generated holograms: analysis of adjustment and shape errors", *Applied Optics* 24(16), 2604-2611 (1985).
7. R.H. Ginsberg, "Outline of tolerancing (from performance specification to toleranced drawings)", *Optical Engineering* 20(2), 175-180 (1981).



AN INTERFEROMETER FOR ASPHERIC TESTING: CALIBRATION AND ERROR COMPENSATION

Steven M. Arnold

APA Optics, Inc.

2950 N.E. 84th Lane, Minneapolis, Minnesota 55434

PREPRINT

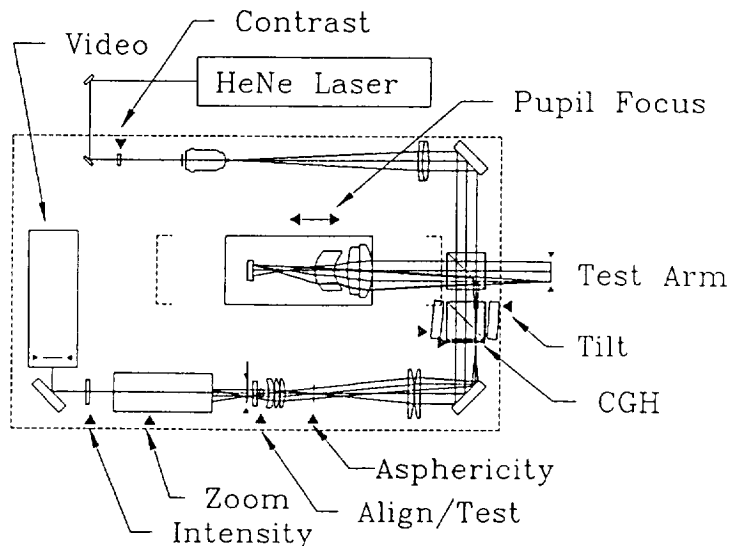
ASPE Spring Topical Meeting
April 7-9, 1992, Tucson, AZ

EXTENDED ABSTRACT

APA Optics has developed a phase measuring interferometer for testing of general aspherics using electron-beam written computer generated holograms as null compensators. Aspheric departures of up to several hundred waves are measured using only standard accessories; deeper aspheres may be tested using simple auxiliary optics.

The interferometer configuration is depicted in the figure below and has been described more completely elsewhere [1]. It is a Twyman-Green interferometer which uses polarization optics to separate the test and reference paths. The test beam is reflected by a first beamsplitter cube, enters the test arm, and returns through a 150-mm travel afocal telecentric relay system which images the test optic onto a 20-mm diameter computer generated hologram (CGH) located just after the second beamsplitter cube. Meanwhile, the collimated reference beam is transmitted by the first beamsplitter cube and undergoes four reflections by the second beamsplitter cube and the two reference mirrors before striking the CGH at an off-axis angle. The test beam and the diffracted reference beam form a nominally null interferogram which is spatially filtered and reimaged onto a diffuser glass by an afocal telescope. The image on the diffuser is then viewed by a video camera and zoom optics.

Because of 8 reflections and 8 double-pass air-glass interfaces unique to either the test or reference paths, the interferometer is not expected to achieve diffraction-limited performance without error compensation. Our approach has been to incorporate the system error compensation into the design of each CGH null compensator. In this manner, we can compensate known imperfections of the interferometer and accessory optics while presenting the user with a nominally null interferogram.

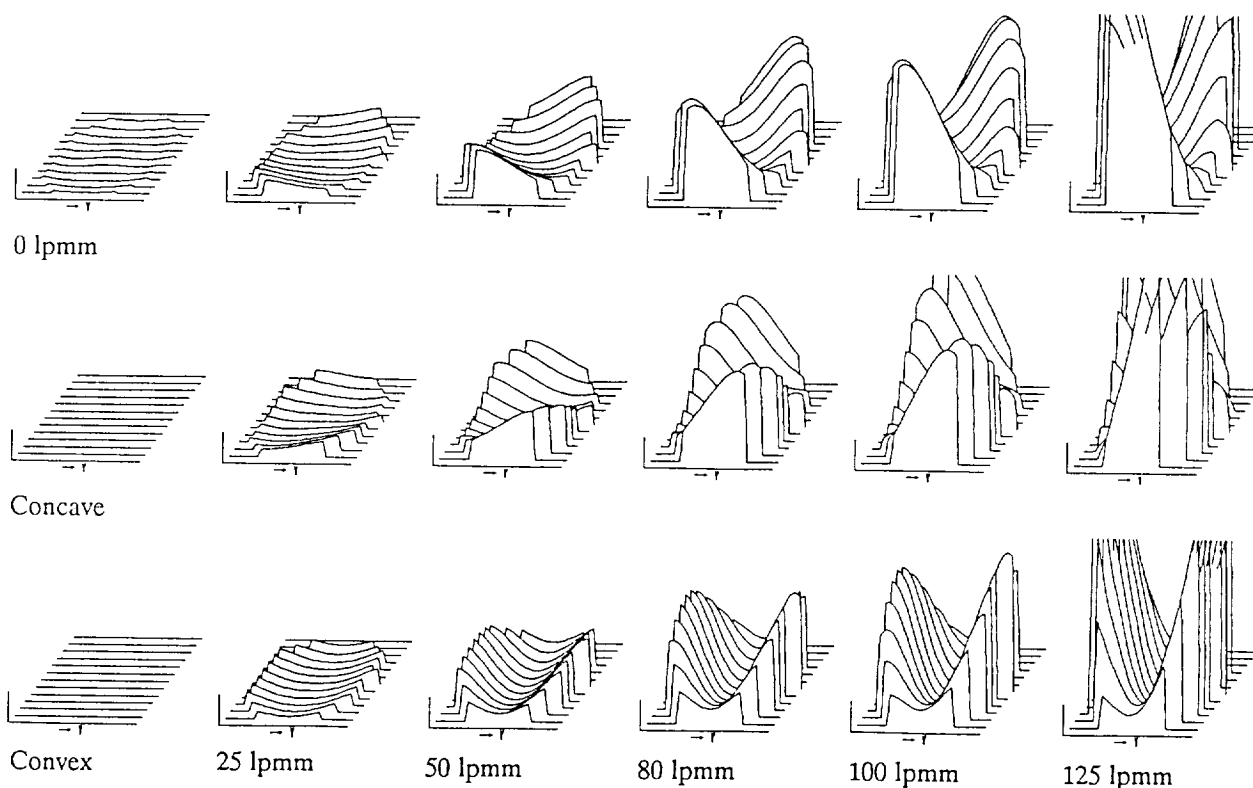


Several measures have been taken to assure that the interferometer alignment remains invariant from source arm pinhole to CGH. The front of the interferometer includes a kinematic bayonet mount for the attachment of various accessories. The removable CGH null compensator is also mounted kinematically. The laser collimator and the pupil relay optics are both designed to remain focused through a range of temperature. The positions of the pupil relay slide and the reference mirror tilt are displayed to the user and are to be set per the CGH design data. The optics following the CGH are common to both test and reference paths and therefore do not influence a null interferogram.

Calibration of the instrument is accomplished by attaching test fixtures to the accessory bayonet mount and inserting corresponding CGHs. The three test fixtures consist of a 500 mm radius concave mirror, a 500 mm radius convex mirror, and a variable tilt plano mirror. We find it useful to express the tilt angle of the plano mirror as an interferogram spatial frequency at the CGH ($\text{lpmm} = 2 \lambda^{-1} \sin \theta$). Each fixture can be mounted to the bayonet in three orientations differing by 120 degree increments. The plano fixture alone samples the entire range of possible rayslopes over the full CGH aperture. The concave and convex fixtures provide a sensitive measure of centration and some redundancy.

The 13 calibration CGHs are of three types. The concave and convex configurations use off-axis CGHs with a carrier frequency of 300 lpmm. The tilted plano configurations use triple crossed binary gratings comprised of equilateral triangles. These CGHs work for all three bayonet orientations and no off-axis carrier is required since the test beam is itself tilted. A third CGH group consists of 7 linear gratings used to map the reference beam path with the untilted plano fixture in the test beam.

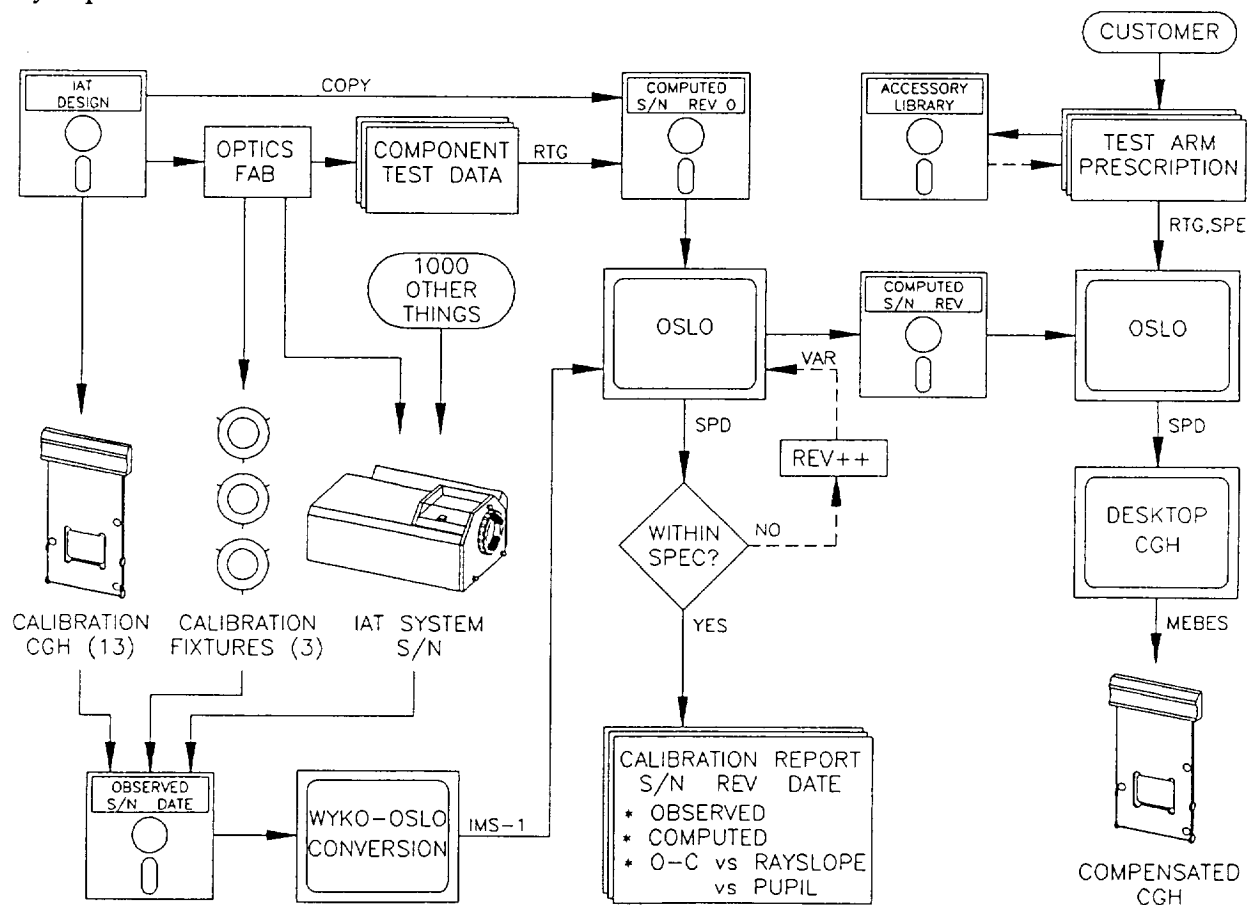
The figure below shows the expected interferograms resulting from the 18 test arm configurations. The leftmost column includes the concave, convex, and untilted plano



configurations. Additional columns represent increasing plano tilts of 25, 50, 80, 100 and 125 lpmm with each row being a different bayonet orientation (0, 120 and 240 degrees). The vertical scale is indicated by a bar representing two waves of OPD. The hardware calibration process consists of recording these 18 + 7 phase measured interferograms along with the system serial number and a date stamp. The process is simple enough to be performed in the field.

The flowchart diagram outlines the complete hardware and software calibration processes. After the 18 + 7 calibration interferograms are recorded to floppy disk, the data is ported to the OSLO raytrace program so that reverse optimization may be used to deduce the imperfections in the actual interferometer.

The WYKO DOS/RTI[®] software package is used to fit the interferogram data with 36 Zernike polynomials and a stand-alone program then converts the Zernike coefficients to an OSLO[®] diffractive surface (type DFX) described by a polynomial in x and y. This multi-configuration diffractive surface, located just after and coincident with the CGH phase function, acts to collimate the observed interferogram wavefronts. Separate raytrace models are maintained for the test and reference paths. With the Zernike representation, we have effectively $18 \times 36 = 648$ optimization targets for the test path model and $7 \times 36 = 252$ optimization targets for the reference path model. Orthogonal Zernike polynomials are well suited to describing the expected decentering, tilting, focusing, and radius errors [2]. A 6-ring and 6-spoke rayset is now used, although we expect to identify a better rayset over which the Zernike polynomials are orthogonal [3]. The optimization operands then consist of OPD maps for each test configuration. Operands are inversely weighted by rayslope.



A question could be raised as to which optimization variables are legitimate. Clearly the 5 discrete tilt settings of the plano calibration fixture are valid optimization variables. Other key variables include the relative orientations of the bayonet, the test arm relay, and the CGH mount with respect to the optical axis (18 variables). Collimator and test relay focus are 2 additional variables. Decenter of the smaller half of the test relay doublet and tilt, decenter and airspace of the meniscus add another 7 variables. We therefore have at least 32 legitimate parameters. Some parameters will act as compensators for others, so the solution obtained may not be unique.

Another modeling approach is to sidestep questions of what constitutes a legitimate parameter and instead use whatever ad-hoc model best reproduces the observed interferogram data with a reasonable number of free parameters. This is what we have done with the reference path which has only a one-dimensional space of accessible configurations (*i.e.* tilt). For the test path, we have thus far opted for a strictly physical raytrace model in order to better understand the hardware. However, we would claim that the test arm space is sufficiently sampled by the 18 test configurations to justify the insertion of one or more fictitious phase surfaces if these are found to significantly reduce the residuals.

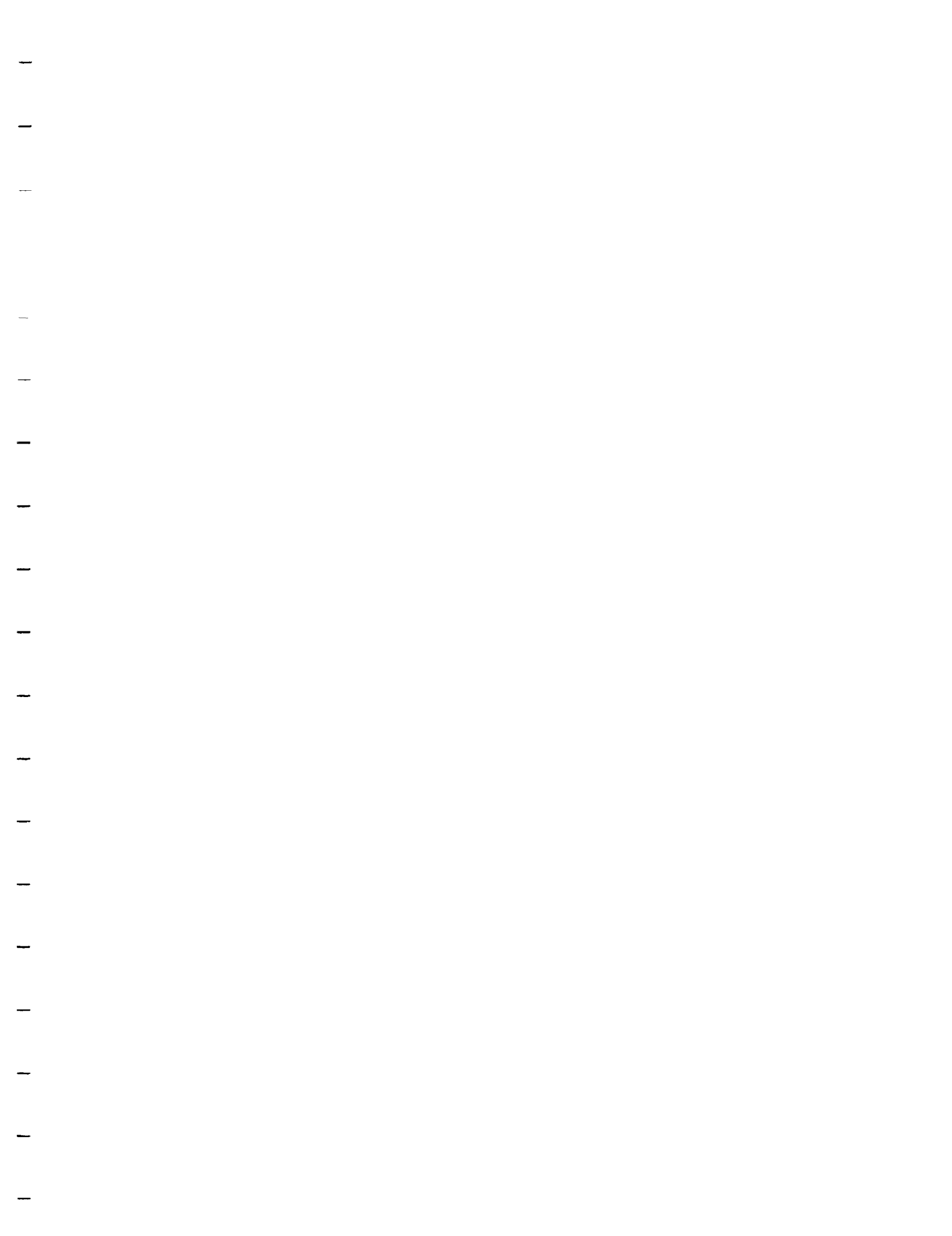
Accessory optics such as diverger lenses and an afocal beam expanding telescope are similarly modeled by recording their double-pass interferograms versus field angle. This requires no special CGHs or fixturing and can be accomplished using a conventional Fizeau interferometer.

Two principle outcomes of the interferometer calibration process are: 1) a report detailing the residual system error versus pupil coordinate and versus rayslope, and 2) a raytrace model which can be used in designing CGH null compensators.

We plan to present initial calibration data from one of our interferometers.

REFERENCES

1. S.M. Arnold and A.K. Jain, "An interferometer for testing of general aspherics using computer generated holograms", SPIE Vol. 1396 (1990).
2. B. Dörband and H. J. Tiziani, "Testing aspheric surfaces with computer-generated holograms: analysis of adjustment and shape errors", Appl. Opt. 24(16), 2604-2611 (1985).
3. D. Malacara, J.M. Carpio-Valadéz and J.J. Sánchez-Modragón, "Wavefront fitting with discrete orthogonal polynomials in a unit radius circle", Optical Engineering 29(6), 672-675 (1990).

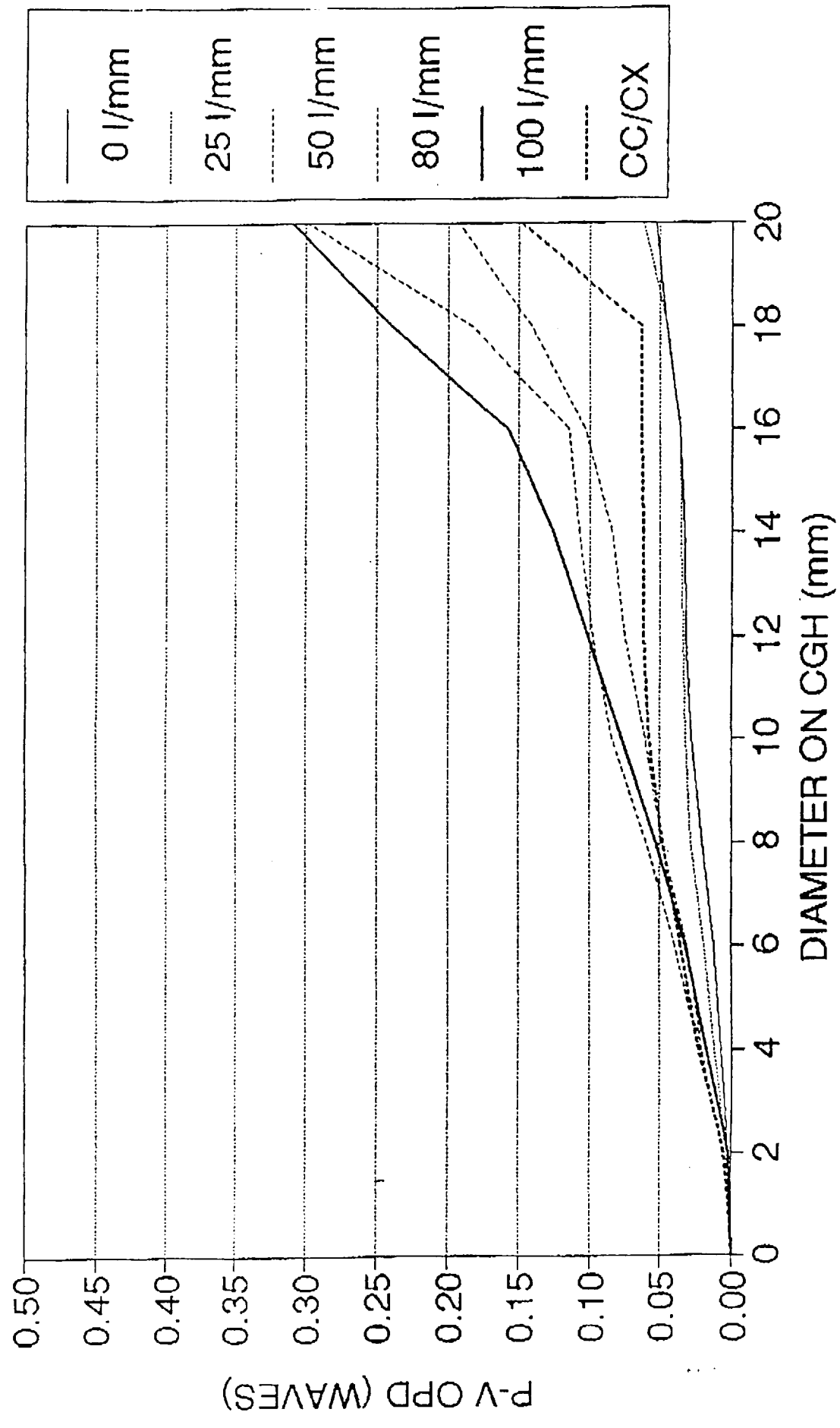


Post-It™ brand fax transmittal memo 761-1-11

To	Dr. Alan De Cew	From	ANIL JAIN
Co.	SOXL	Co.	APA OPTICS, INC
Dept.		Phone	(612) 784-4995
Phone	(508) 250 8681	Fax #	(612) 784-2038
Fax #	(508) 256 5605		

MF01DEC3

IAT COMPENSATION ACCURACY



APPENDIX E

OPTICAL TEST SET UP CONFIGURATION

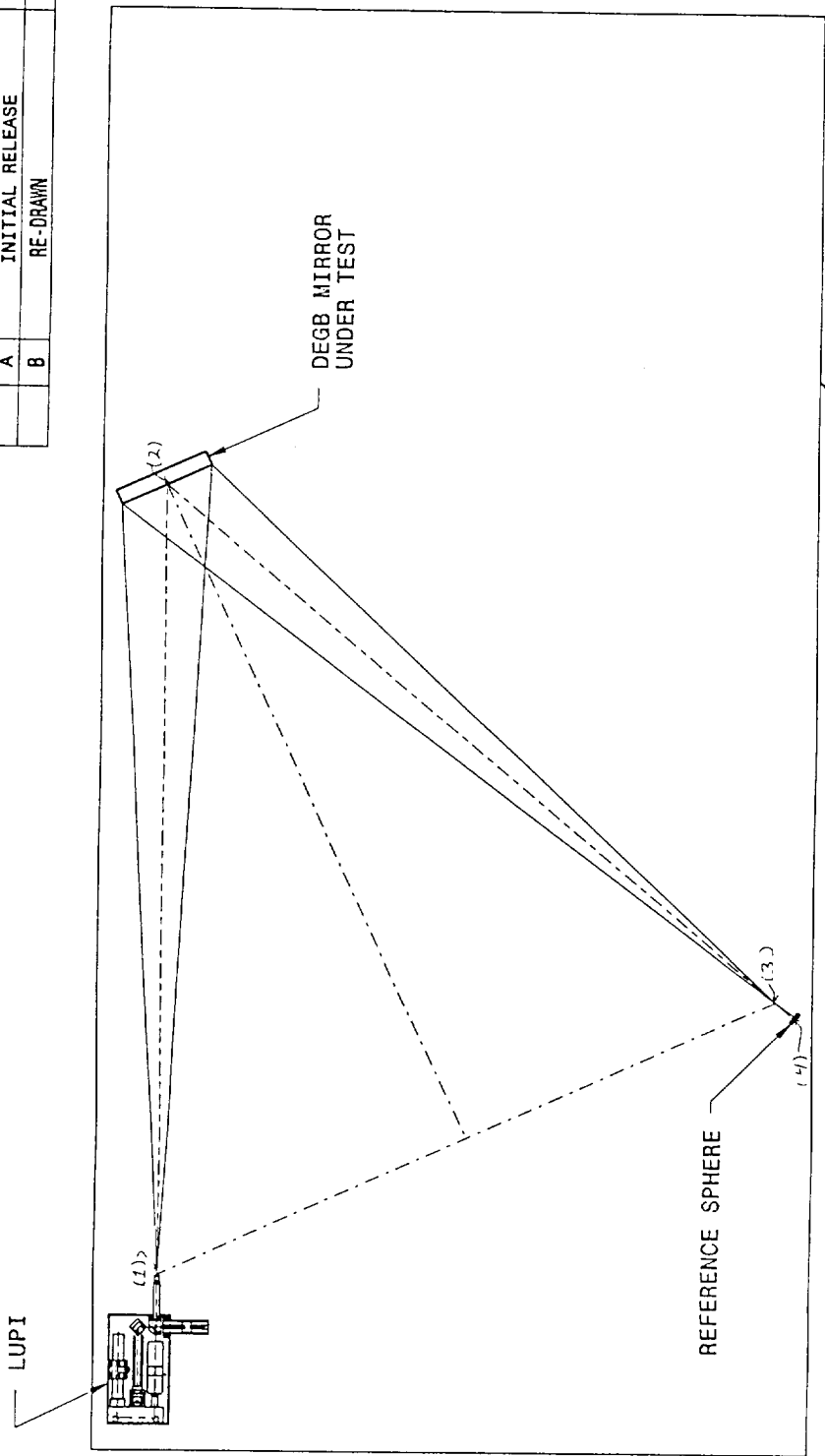
DRG No. 31815

REV 1

REV B

REVISIONS		
ZONE	REV	DESCRIPTION
	A	INITIAL RELEASE
	B	RE-DRAWN

DATE	APPROVED
15 NOV 91	A. DeCEW



TEST LAYOUT
TEST TABLE (60 X 120 INCH MIN)

THE INFORMATION CONTAINED HEREIN IS THE PROPERTY OF SPACE OPTICS RESEARCH LABS. DISSEMINATION OR OTHER USE OF THIS INFORMATION IS HEREBY PROHIBITED.		THIRD ANGLE PROJECTION	
PART DASH No.		NEXT QTY PER ASSY	
NEXT FINAL		NEXT ASSY USED ON	
APPLICATION		USED ON	
63 SURFACE ROUGHNESS UNLESS SPECIFIED		APPROVALS	
STANDARD TOLERANCES .XX : .01 .XXX : .005 ANGLES : 0° 30'		DRAWN J. PERRY CHECKED ENGINEER OPTICAL	
MATERIAL FINISH		DATE 5.9.91	
UNLESS OTHERWISE SPECIFIED ALL DIMENSIONS ARE IN INCHES AND APPLY AFTER FINISH. DO NOT SCALE DRAWING.		TEST APPROVED A. DeCEW	
TITLE DEFORMED ELLIPSOIDAL DIFFRACTION GRATING BLANK		DRG No. 31815	
SIZE FSC# No. B12D543		SCALE 1/20	
SPACE OPTICS RESEARCH LABS A DIVISION OF INTERGRAPH 7 STUART ROAD, CHELMSFORD, MA, 01824		SHEET 1 OF 1	

Designated locations in Hologram design program:

- (1) LUPI-II focus { 0, 0 }
- (2) DEGB Vertex { 0, 1672.918 }
- (3) Ellipsoid focus { 1260.067, 572.512 }
- (4) Ref Sphere Vertex { 1448.371, 408.069 }

Distances:

- (1) - (2) 1672.918mm or 65.863 in
- (2) - (3) 1672.918mm or 65.863 in
- (1) - (3) 1384.030mm or 54.489 in
- (3) - (4) 250.063mm or 9.845 in

SET-UP PROCEDURE

1. Set up components in rough positions. Place a refocusing sphere 0.125"R at the focus of the IAT. Locate center of DEGB with mask.
2. Using a radius rod position the center of the DEGB to be 65.863". Actual reading of radius rod should be 65.488 after taking into account the refocusing sphere radius and the diameter of the tangent balls on the radius rod ends.
3. Using same radius rod. set up second ball on the arc of the second focus.
4. With second radius rod, relocate second ball on both the arc from the DEGB vertex and the arc from the interferometer focus measuring 54.489".
5. Extend radius rod from DEGB vertex to 75.708", and position the concave spherical return mirror.

APPENDIX F

AN ALTERNATE TEST METHOD

TECHNICAL REPORT

CGH NULL TEST OF DEFORMED ELLIPSOIDAL GRATING BLANK

4 November 1993

Submitted to:

Alan DeCew, General Manager
Space Optics Research Labs
7 Stuart Road
Chelmsford, MA 01824

Prepared by:

Steven M. Arnold
Diffraction International
11345 Hwy 7, #421
Minneapolis, Minnesota 55305
Tel: (612) 945-9912
Fax: (612) 945-9912



Diffraction International

CGH & BINARY OPTICS - ASPHERIC METROLOGY - DESIGN ENGINEERING

Diffraction International has recently developed a CGH null adapter to allow testing of highly aspheric optics using a conventional Fizeau or Twyman-Green interferometer. Based on this invention, we have designed and analyzed a null test for the Deformed Ellipsoidal Grating Blank (DEGB).

Null Test Configuration

The test configuration is shown in Figure 1 below. The DEGB is tested from its center of curvature using a conventional interferometer such as SORL's LUPI-II. A CGH null positioned in the test beam between the focus and the DEGB transforms the spherical test beam into a highly astigmatic aspheric wavefront which is everywhere perpendicular to the DEGB surface. Peripheral portions of the CGH aperture, not required for the DEGB null, are devoted to a return sphere grating for aligning the CGH with respect to the interferometer. The proposed CGH is depicted schematically in Figure 2.

The CGH null must be positioned outside the caustic so that there will be a one-to-one correspondence between points on the CGH and points on the DEGB. Since CGH alignment tolerances, required resolution and aperture each scale with distance from test beam focus, the CGH should be located as far as practical from the focal position. For fabrication by e-beam lithography, the CGH aperture must be less than 150 mm. I have selected a CGH location 400 mm from the test beam focus as a reasonable compromise between performance and cost. Furthermore, to balance the x-axis and y-axis resolution requirements of the CGH, I have located the DEGB vertex 1670 mm from the test beam focus. The required CGH aperture for the DEGB null is then 62 x 28 mm.

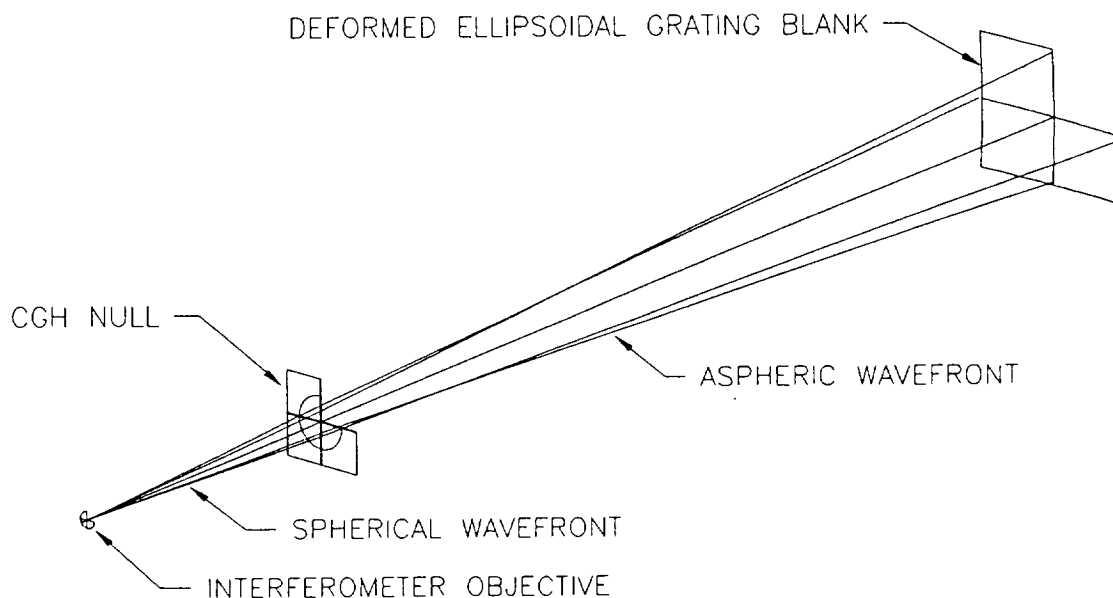


Figure 1 CGH null test of Deformed Ellipsoidal Grating Blank (DEGB).

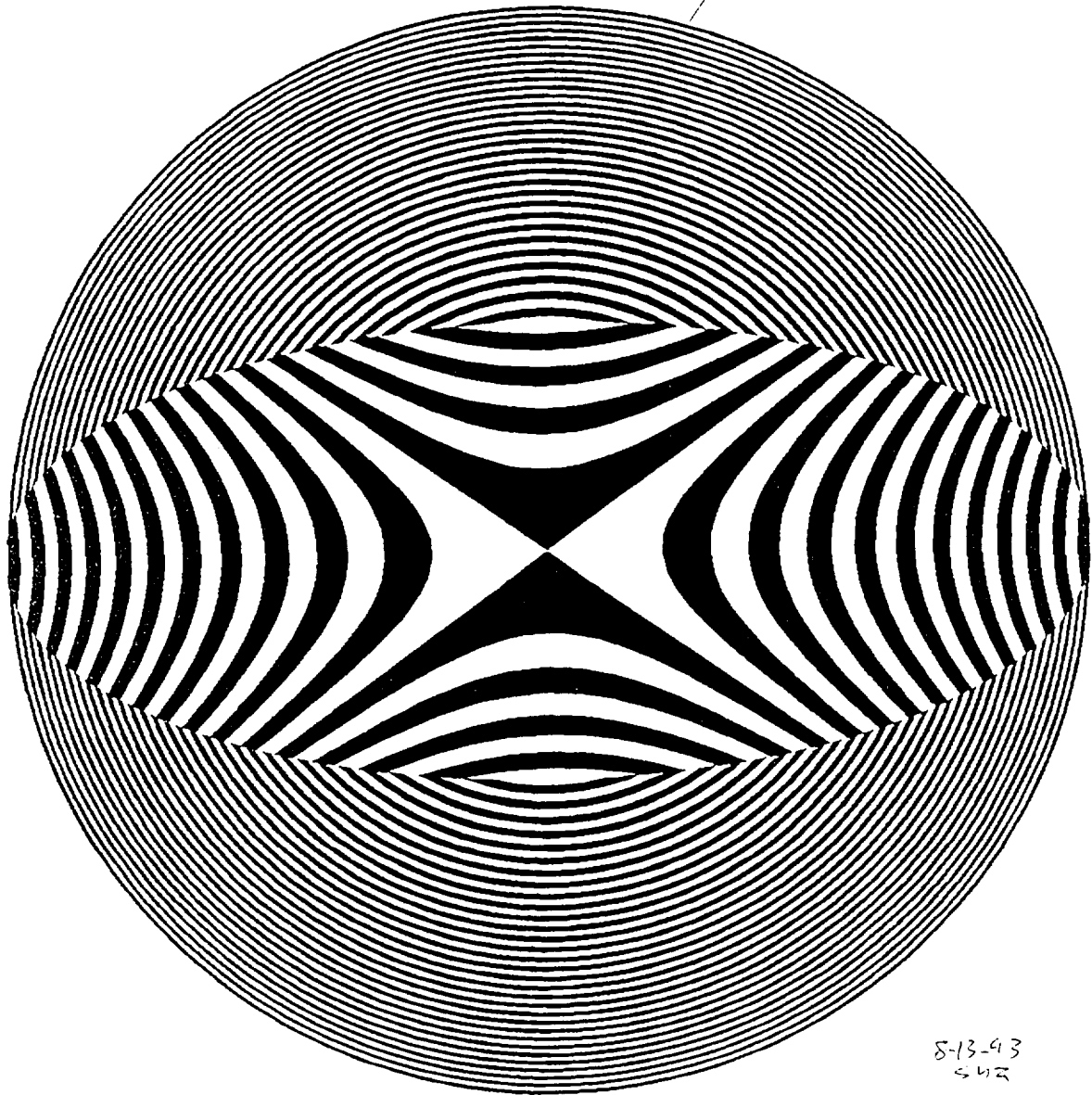


Figure 2 Proposed CGH including astigmatic DEGB null (center) and axisymmetric return sphere alignment grating. Optional fiducial projecting alignment gratings are not shown. The fringe spacing has been increased for purposes of illustration. Actual CGH diameter is 62 mm.

Alignment

Since the DEGB lacks rotational symmetry, the proposed test requires 9 alignment degrees of freedom. Alignment of either the CGH null or the DEGB to the spherical test beam establishes an axis and consumes 3 degrees of freedom—1 of focus and 2 of tilt or decenter. Alignment of the remaining component (CGH or DEGB) then requires a full 6 degrees of freedom.

The alignment procedure is somewhat more intuitive if the test optic (DEGB) has 6 degrees of freedom, and the CGH null only 3. This is appropriate for an acceptance test. During the figuring process, however, the CGH will be aligned only once while the DEGB will be repeatedly removed and replaced. In this case, it is easier to use a 6-axis mount for the CGH and a simple tilt-tip-focus mount for the test optic. Mechanical repositioning of the test optic can be sufficiently repeatable that no decenter or clock adjustments are needed.

Locating the CGH null outside the region of the caustic results in a quite elliptical working aperture. This is perhaps fortunate as it leaves a large portion of the physical aperture available for alignment features. In particular, a reflection CGH is proposed for purposes of aligning the CGH to the spherical test beam. The reflection CGH will act like a 400 mm radius concave sphere and can be optically aligned by nulling its interferogram. It is also possible, as an aid in aligning the decenter and clock degrees of freedom, to incorporate various transmission CGHs which focus otherwise unused portions of the test beam onto two or more fiducial locations on the DEGB.

Optical Prescription

The optical prescriptions of the DEGB surface and the CGH null have been approximated to a high degree of accuracy by cartesian polynomials. A raytrace model was constructed using Oslo Series 2 optical design software. The CGH wavefront coefficients were optimized to produce a null test to within 0.0002 fringe P-V and 0.00004 fringe RMS. The raytrace data is attached as Appendix A.

I do not know what tolerances have been assigned to the DEGB vertex radius and eccentricity. In testing from center of curvature with a null, the test wavefront is a good (deformed) ellipsoid only for the prescribed axial distance (vertex radius). This is not a problem for fabrication testing since the DEGB would be figured to match the null wavefront. However, for acceptance testing of an already completed DEGB, the vertex radius and eccentricity must be known with sufficient accuracy to assure a near null test.

Tolerance Analysis

Error sources include CGH fabrication errors, interferometer errors, and alignment errors. A distinction is made between manufacturing tolerances and measurement tolerances. Errors which can be well measured and characterized may be removed during the test results analysis or compensated in the CGH design. Nonetheless, it is best to minimize dependence on data analysis for error compensation, as the optician's job is much easier if the observed interferogram accurately represents only test optic errors.

The various error contributions are listed in the following table and discussed in the following paragraphs.

Parameter	Tolerance	Error (waves)	Compensation Method	Compensated Error (waves)
Interferometer	0.05-0.10 wave	0.100	Characterize	0.020
CGH Encoding	± 0.01 wave	0.020	None	0.020
CGH Digitization	± 0.125 micron	0.009	None	0.009
CGH Registration	0.15 micron	0.005	None	0.005
CGH Substrate	0.1 wave	0.100	Characterize	0.020
CGH Focus	25 micron	0.048	Phase Measure	0.005
CGH Tilt	1 μ rad	0.000	None	0.000
DEGB Focus	0.6 mm	2.750	System Alignment	0.007
Total (worst case)		3.032		0.086
Total (quadrature)		2.754		0.037
DEGB Error Budget		N/A		0.125

Interferometer Errors

Interferometer system error depends on the focusing optics and test aperture and are typically 0.05 to 0.1 wave. System error is characterized and compensated by the standard technique of testing a return sphere in two clock orientations plus the cats-eye configuration. Compensation accuracy depends on the the test environment, but is typically better than 0.02 wave.

CGH Fabrication Errors

CGH errors are comprised of pattern errors (encoding, digitization, registration) and substrate errors. Appendix B discusses these error sources in general terms.

The minimum fringe spacing of the proposed DEGB null is 28.3 microns, so pattern errors will be quite small in terms of phase. It is proposed that the CGH be encoded with an algorithm precision of ± 0.01 wave and a data grid (pixel size) of 0.25 microns. The guaranteed mean plus 3σ registration accuracy of the MEBES e-beam system is 0.15 microns. Together, these error sources yield a CGH pattern error of 0.04 wave P-V. This could be reduced to 0.02 wave or less by tightening the algorithm precision and using a smaller pixel size.

Diffraction International offers photomask substrates with transmitted wavefront distortion of better than $\lambda/10$ P-V. This error is measured and characterized interferometrically and may be verified by the end user.

CGH Alignment Errors

By incorporating a 400 mm radius reflection CGH, the CGH null can be aligned with respect to the spherical test wavefront to better than 25 micron focus and 1 μ rad tilt (equivalently 1 μ m decenter). These values each correspond to 1/4 fringe in the alignment interferogram. A 25 micron CGH focus error contributes a significant 0.048 wave to the DEGB interferogram. In a good test environment, phase measuring interferometry can reduce this error by a factor of 10. The CGH tilt error of 1 μ rad is entirely negligible, contributing only 0.0001 fringe to the DEGB interferogram.

Test Optic Alignment Errors

Assuming a null test is achieved, focus is the only DEGB degree of freedom which contributes to a surface figure error (*i.e.* vertex radius). The wavefront shape produced by the CGH null and the axial distance of the DEGB from the CGH completely define the DEGB surface figure. If a portion of the CGH peripheral aperture is allotted to a transmission CGH which focuses onto the DEGB vertex, then the DEGB vertex radius can be optically determined to an accuracy of about 0.6 mm (1/2 fringe). This corresponds to a P-V figure error of 2.75 waves, but is it significant? Since it is almost entirely power and astigmatism, this figure error can be mostly compensated during final system alignment. To determine what fraction of the figure error caused by an incorrect CGH to DEGB spacing is but a minor change in vertex radius and eccentricity and what fraction is higher order aberrations, the x^2 and y^2 terms of the DEGB polynomial surface description were varied. It was found that only 0.007 wave is higher order aberrations.

The other 5 degrees of freedom are required only to establish that the backside of the blank is perpendicular to the optic axis to within ± 15 arc seconds and that the alignment fiducials coincide with the ellipsoid major and minor axes. Depending on how the available CGH aperture is partitioned, the size of fiducial spots focused onto the DEGB will be 20-50 microns. This should be sufficient to meet the DEGB mechanical centration specifications.

Pupil Distortion and Diffraction Effects

There is significant pupil distortion in mapping the 200 x 160 mm DEGB aperture onto the 62 x 28 mm CGH aperture. Pupil distortion is of no consequence for a perfect null test, but must be considered when interpreting interferograms which depart from null.

Because the DEGB is not imaged onto the CGH null, there will be diffraction effects from the edges of the CGH aperture(s). For this reason, the proposed aperture of the DEGB null is made somewhat oversized so that the DEGB will act as the limiting aperture.

Implementation

The proposed CGH null would be fabricated by e-beam lithography as a chrome pattern on a standard size 4-inch photomask blank. Figure 3 shows the expected fringe visibility for both chrome and phase CGH nulls when used in a Fizeau configuration. Visibility with a chrome CGH is adequate for visual inspection. For maximum accuracy with phase measuring Fizeau interferometry, the photomask should be ion etched to produce a phase-only CGH. It would be necessary to mask the alignment reflection CGH from the chrome etch. Alternatively, fringe visibility can be increased by reducing the reflectivity of the reference mirror of SORL's LUPI-II interferometer.

Diffraction International has recently developed a kinematic 3-axis mount for 4-inch photomask CGHs. The only additional hardware required to perform the proposed null test is a 6-axis mount for the DEGB.

Interferogram Visibility

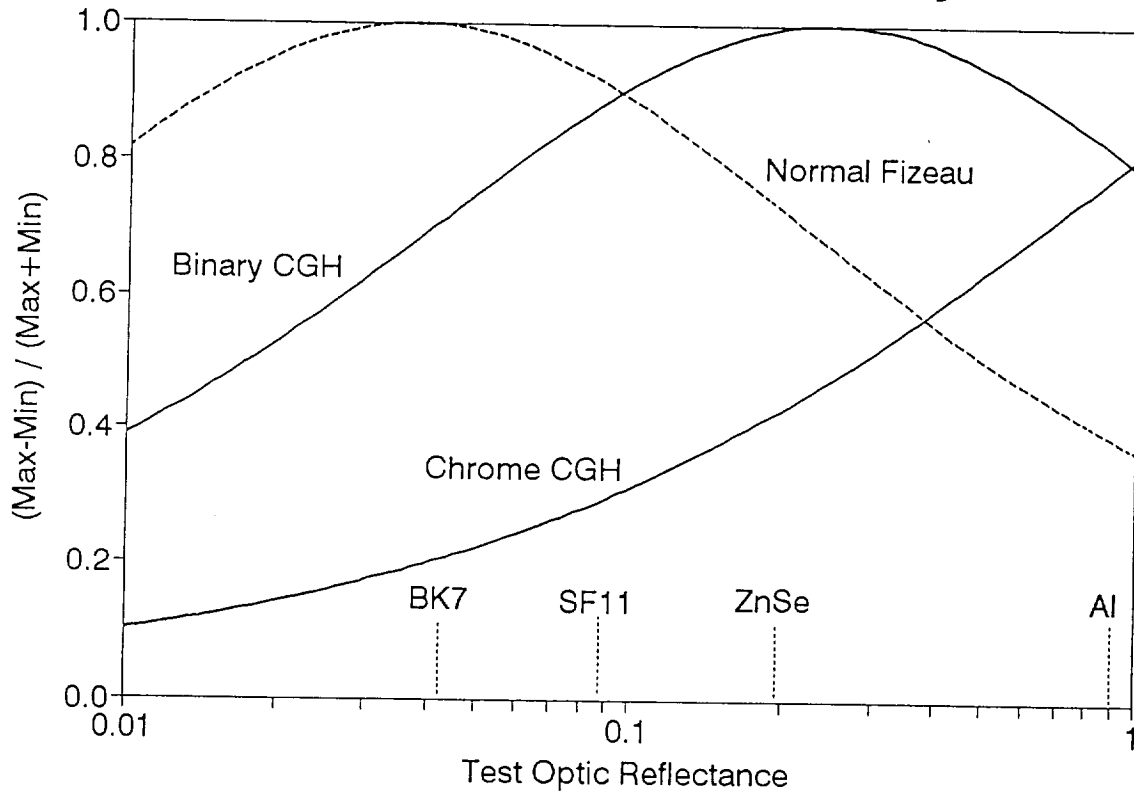


Figure 3 Fizeau interferogram visibility with chrome and phase CGH nulls.

Conclusion

When combined with phase measuring interferometry to establish the correct interferometer to CGH spacing, the proposed CGH null test will measure the DEGB figure error to an expected accuracy of better than $\lambda/20$ and the DEGB power to about 3λ . The accuracy of the observed interferogram, before software compensation to correct interferometer system and CGH substrate errors, is about 0.15 waves.

_LEN NEW "SORL DEGB CGH NULL TEST"
AST 2
RFS 11
EPR 0.4
_OBY -0.001
THO -10
DES "sma"
_IDN 44
WW 1 0 0 0 0 0
WV 0.63282 0.48613 0.65627 0.43584 0.70652 0.40466
GTO 1
_GTO 2
GLA BK7
RD 10
_AP 1
NOT "Micro-Objective"
GTO 3
_PK CV 2
TH 410
PK AP 2
NOT "Micro-Objective"
_GTO 4
NOT "Design CGH Face"
GTO 5
_GLA SILICA
AP 31
NOT "Actual CGH Face"
_GTO 6
_GLA SILICA
TH 2.286
PK AP 5
_PDT PDR 2
SDT DFX 10
S3 -3.700544119884E-04
_S5 7.200710687056E-04
S8 1.313929814807E-06
S10 1.725699643609E-09
S12 1.561993743483E-09
_S14 -5.379144915847E-09
S17 -7.523552078414E-12
S19 -3.387904665471E-11
_S21 -6.397123329599E-15
S23 -7.42107296602E-15
S25 4.745158907399E-14
_S27 3.616767921395E-14
NOT "CGH Phase Function"
GTO 7
TH -2.286
_PK THM 6
SDT SAP
_APT 2
_Y1 -50
AY2 50
_X1 -50
_X2 50
_NOT "CGH Backside"
GTO 8
PK THM 4
_PKP SDM 5
NOT "Restore Design CGH"

-GTO 9
TH 1270
NOT "Nominal Test Optic "
GTO 10
-NOT "Test Optic Align"
GTO 11
RFL
-PK THM 10
PDT PDX 6
P3 -2.72108859282E-04
P5 -3.282819711021E-04
-P8 -1.1283E-08
P10 -2.430705791785E-11
P12 -5.861123049922E-11
-P14 -3.537863699515E-11
P21 -4.342622773699E-18
P23 -2.041886399956E-17
-P25 -2.766986059897E-17
P27 -7.625444379005E-18
SDT SAP
APT 2
-AY1 -80
AY2 80
AX1 -100
-AX2 100
NOT "DEGB"
GTO 12
_TH -1270
PK THM 9
PKP SDM 10
NOT "Restore Design Axis"
-GTO 13
PK TH 4
NOT "Design CGH Face"
_GTO 14
TH 2.286
PK TH 6
PK AP 5
-PKP SD 5
NOT "Actual CGH Face"
GTO 15
-PKP GLA 5
TH -2.286
PK THM 6
_PK AP 7
NOT "CGH Backside"
GTO 16
PK THM 13
-PK AP 6
PKP SD 6
NOT "CGH Phase Function"
-GTO 17
TH -400
PK THM 3 10
_PKP SDM 14
NOT "Restore Design CGH"
GTO 18
GLA BK7
AP 10
NOT "Nominal Focus"

```

-GTO 19
PK AP 18
END 19
_JAR NEW
TLA 10 0 -1 1 1 1E-05
TLB 10 0 -1 1 1 1E-05
FLC 10 0 -1 1 1 0.001
-DCX 10 0 -0.5 0.5 1 0.001
DCY 10 0 -0.5 0.5 1 0.001
PH 10 0 -5 5 1 0.01
END
OPI
F1 0 0
R1 1 0 0
R2 0 0 0.5
R3 0 0 -0.5
R4 0 0 1
-R5 0 0 -1
R6 0 0 1.5
R7 0 0 -1.5
_R8 0 0 2
R9 0 0 -2
R10 0 0.25 0
R11 0 0.25 0.5
-R12 0 0.25 -0.5
R13 0 0.25 1
R14 0 0.25 -1
-R15 0 0.25 1.5
R16 0 0.25 -1.5
R17 0 0.25 2
_R18 0 0.25 -2
-R19 0 0.5 0
R20 0 0.5 0.5
R21 0 0.5 -0.5
-R22 0 0.5 1
R23 0 0.5 -1
R24 0 0.5 1.5
_R25 0 0.5 -1.5
R26 0 0.5 2
R27 0 0.5 -2
R28 0 0.75 0
-R29 0 0.75 0.5
R30 0 0.75 -0.5
R31 0 0.75 1
-R32 0 0.75 -1
R33 0 0.75 1.5
R34 0 0.75 -1.5
_R35 0 0.75 2
-R36 0 0.75 -2
R37 0 1 0
R38 0 1 0.5
-R39 0 1 -0.5
R40 0 1 1
R41 0 1 -1
-R42 0 1 1.5
R43 0 1 -1.5
R44 0 1 2
-R45 0 1 -2
-R46 1 80 0
R47 1 -80 0

```



Diffraction International

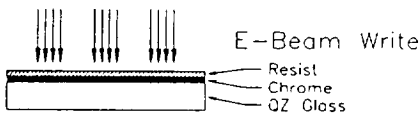
CGH & BINARY OPTICS ■ ASPHERIC METROLOGY ■ DESIGN ENGINEERING

CGH Photomasks

At Diffraction International, we specialize in diffractive optics. Our staff has over 15 years experience in CGH and binary optics technology. Our goal is to become a leading supplier of custom precision diffractive optics. As a small business, we offer flexibility, attention and fast response.

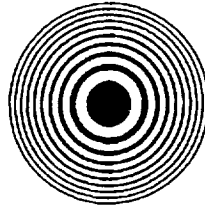
General Description

CGH Photomasks are the basis of our diffractive optic products and are also used directly as diffractive optical elements. CGH Photomasks are encoded using our HoloMask software and written using a MEBES e-beam lithography system. The MEBES is the standard photomask tool in the microelectronics industry. In resolution, accuracy and format size, it is unsurpassed for CGH writing. Unfortunately, the MEBES pattern vocabulary is limited to trapezoids. Our HoloMask software accurately encodes a diffractive optic element using a minimum number of these trapezoids.

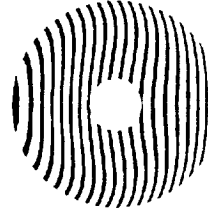


Resolution and Feature Size

Patterns are written in a raster manner. The range of address resolution, or pixel size, is 0.10 to 1.1 micron. Common address sizes are 0.50, 0.25 and 0.10 micron.



ON-AXIS



OFF-AXIS



GENERAL

$$\varphi(x,y) = \frac{Cr^2}{1 + \sqrt{1 - (\kappa+1)C^2r^2}} + \sum_i A_i r^i + \sum_j P_j x^j y^j + \sum_l Z_l U'_n(r, \theta) + custom$$

Because of exposure proximity effects, the minimum feature size should be not less than 5 pixels. This is seldom a limitation for CGH patterns since a minimum of 10 pixels per grating period (5 pixels per line or space) is required to achieve a typical recording accuracy of 0.1 fringe. Feature sizes below 0.7 microns are extremely difficult to control in processing.

Aperture

Within a rectangular data field, apertures of any shape may be encoded. Patterns may not exceed the MEBES physical reticle limit of 155x155 mm.

Optical Prescription

The optical phase function is specified by an equation. Virtually any functional form $\varphi(x,y)$ can be accommodated. Simple zone plate lenses may be specified by giving the focal length and wavelength. More general phase functions are described by radial or cartesian monomials or by Zernike polynomials. We will accept Sweatt model wavefront prescriptions. We can also write a custom wavefront evaluation subroutine or link to your code.

Most often, phase function coefficients are generated by an optical design program. Our preferred tool is Oslo Series

2, but we are also familiar with Code V and GENII-PC. If your phase function requires a large number of coefficients, we ask that you supply it on floppy disk.

Units and Dimensions

We usually design in millimeters but can accommodate any unit of measure. Wavelength is in microns or nanometers. The MEBES works in microns.

Artwork Generation

In addition to the phase function, other image elements such as fiducials, title blocks, etc. may be included. A conversion program for customer generated AutoCAD DXF files is available, or we can produce CAD layouts from your drawings. Points and zero width lines are ignored. Text is converted to a single monospace font.

Pattern Composition

Multiple images may be combined to form an overall pattern. Images may overlap and can be either positive (digitized area exposed/clear) or negative (digitized area unexposed/dark). It is difficult to add dark features within a positive pattern or clear features within a negative pattern. The MEBES writes most efficiently when patterns repeat in a rectangular array. This is often true of lenslet arrays or linear gratings.

APPENDIX G

SURFACE SCAN DATA FOR MIDFREQUENCY

- 1.) Scan data from BAUER Model 100 Noncontact profilometer
- 2.) Legendre polynomials

BAUER MODEL 100: Surface Height

DEGB - Displaced by 50 mm towards two dashed lines

Vertex Curvature (longitudinal/lateral): (5.0000D-04 / 5.0000D-04) mm⁻¹

Conic Constant (- eccentricity²): .0000

Average of 1 scan pair(s), starting w/ pair # 1; Filename: D:\BAUER\DEGB_B

Beams: Sheared; Drift analysis: 2nd order; Steering compensation: On

Scan start: -48.643 mm; Length: 97.266 mm; Pixel: .039 mm

Velocity: 3.00 mm/sec; Calibration location: .000 mm

Piece offset: .000 mm; Other-axis position: .000; Refl: .040

Beam sep: -.162 mm; Standoff (nom / extra): (10.000 / .000) mm

Relative calibration (half-width, # of pts, fit order): .000 0 3

Absolute calibration (half-width, # of pts, fit order): .200 7 3

Poly removal: 9; Boxcar: .000 mm; Measured Nov 12, 1993 9:26:42

Scan 1 - RA: 12.55; RMS: 15.58; P-V: 76.78 (Angstroms)

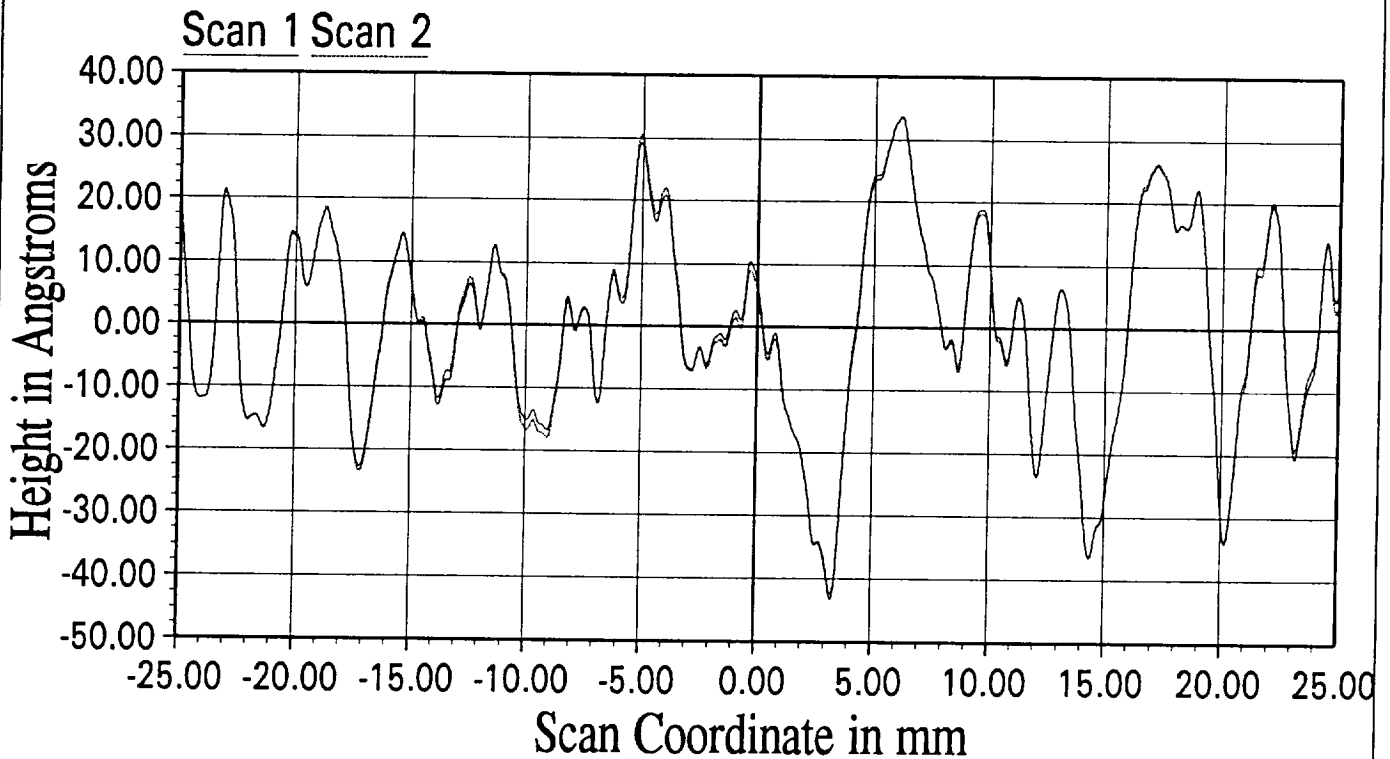
Polynomials 0-4: .00 .00 .00 .00 .00

5-9: .00 .00 .00 .00 .00

Scan 2 - RA: 12.61; RMS: 15.65; P-V: 76.18 (Angstroms)

Polynomials 0-4: .00 .00 .00 .00 .00

5-9: .00 .00 .00 .00 .00



BAUER MODEL 100: Surface Height

DEGB - Displaced by 50 mm towards two dashed lines

Vertex Curvature (longitudinal/lateral): (5.0000D-04 / 5.0000D-04) mm⁻¹

Conic Constant (- eccentricity²): .0000

Average of 1 scan pair(s), starting w/ pair # 1; Filename: D:\BAUER\DEGB_B

Beams: Sheared; Drift analysis: 2nd order; Steering compensation: On

Scan start: -48.643 mm; Length: 97.266 mm; Pixel: .039 mm

Velocity: 3.00 mm/sec; Calibration location: .000 mm

Piece offset: .000 mm; Other-axis position: .000; Refl: .040

Beam sep: -.162 mm; Standoff (nom / extra): (10.000 / .000) mm

Relative calibration (half-width, # of pts, fit order): .000 0 3

Absolute calibration (half-width, # of pts, fit order): .200 7 3

Poly removal: 8; Boxcar: .000 mm; Measured Nov 12, 1993 9:26:42

Scan 1 - RA: 12.64; RMS: 15.71; P-V: 76.24 (Angstroms)

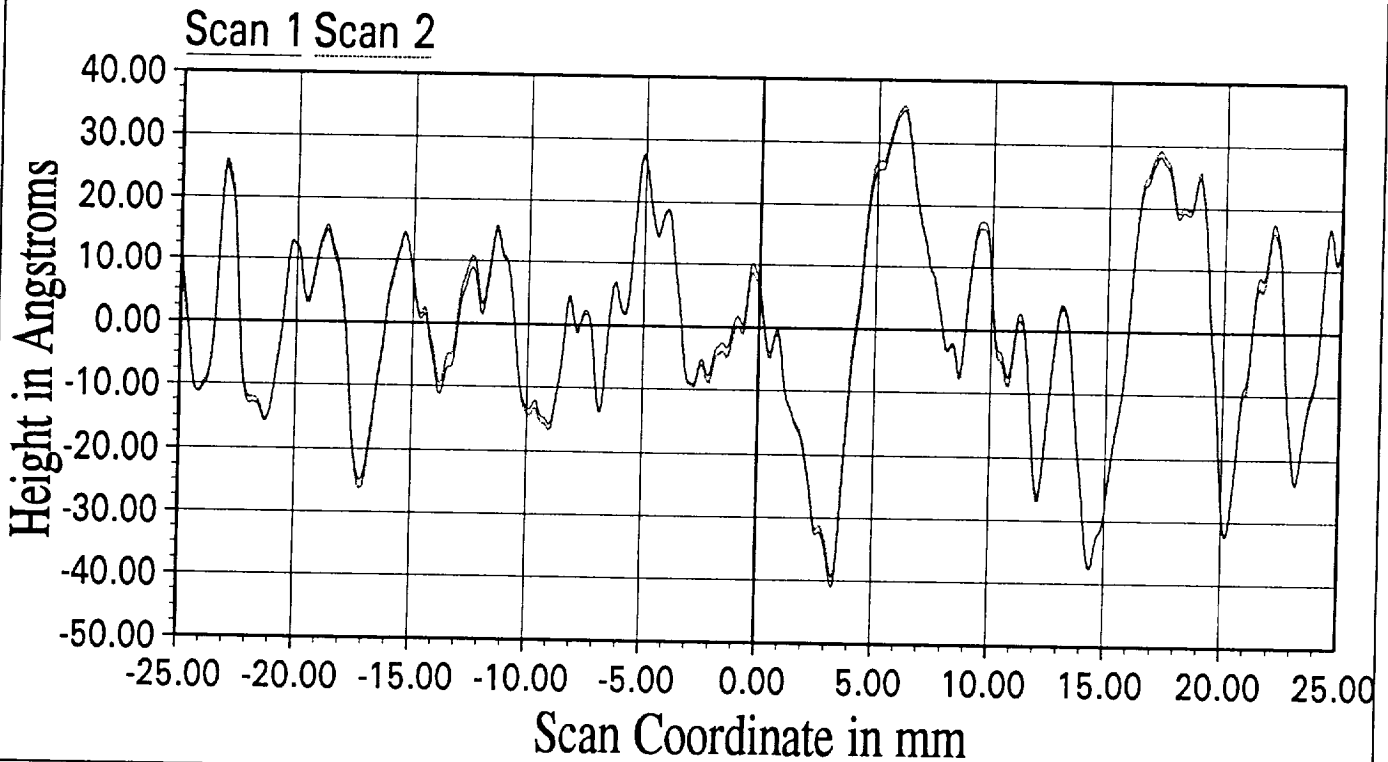
Polynomials 0-4: .00 .00 .00 .00 .00

5-9: .00 .00 .00 .00 1.99

Scan 2 - RA: 12.78; RMS: 15.88; P-V: 75.46 (Angstroms)

Polynomials 0-4: .00 .00 .00 .00 .00

5-9: .00 .00 .00 .00 2.68



BAUER MODEL 100: Surface Height

DEGB - Displaced by 50 mm towards two dashed lines

Vertex Curvature (longitudinal/lateral): (5.0000D-04 / 5.0000D-04) mm⁻¹

Conic Constant (- eccentricity²): .0000

Average of 1 scan pair(s), starting by w/ pair # 1; Filename: D:\BAUER\DEGB_B

Beams: Sheared; Drift analysis: 2nd order; Steering compensation: On

Scan start: -48.643 mm; Length: 97.266 mm; Pixel: .039 mm

Velocity: 3.00 mm/sec; Calibration location: .000 mm

Piece offset: .000 mm; Other-axis position: .000; Refl: .040

Beam sep: -.162 mm; Standoff (nom / extra): (10.000 / .000) mm

Relative calibration (half-width, # of pts, fit order): .000 0 3

Absolute calibration (half-width, # of pts, fit order): .200 7 3

Poly removal: 7; Boxcar: .000 mm; Measured Nov 12, 1993 9:26:42

Scan 1 - RA: 13.59; RMS: 17.09; P-V: 83.48 (Angstroms)

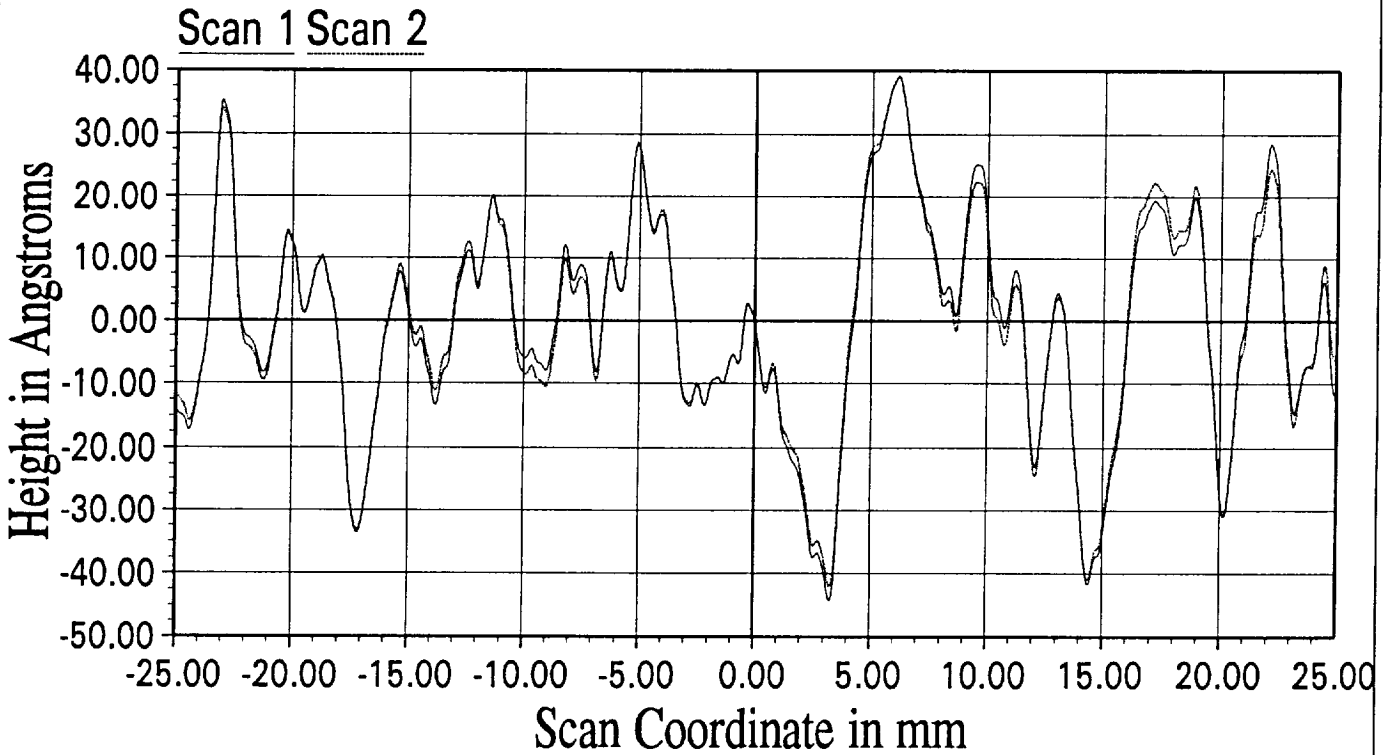
Polynomials 0-4: .00 .00 .00 .00 .00

5-9: .00 .00 .00 -6.67 1.99

Scan 2 - RA: 13.33; RMS: 16.72; P-V: 81.12 (Angstroms)

Polynomials 0-4: .00 .00 .00 .00 .00

5-9: .00 .00 .00 -5.21 2.68



BAUER MODEL 100: Surface Height

DEGB - Displaced by 50 mm towards two dashed lines

Vertex Curvature (longitudinal/lateral): (5.0000D-04 / 5.0000D-04) mm⁻¹

Conic Constant (- eccentricity²): .0000

Average of 1 scan pair(s), starting w/ pair # 1; Filename: D:\BAUER\DEGB_B

Beams: Sheared; Drift analysis: 2nd order; Steering compensation: On

Scan start: -48.643 mm; Length: 97.266 mm; Pixel: .039 mm

Velocity: 3.00 mm/sec; Calibration location: .000 mm

Piece offset: .000 mm; Other-axis position: .000; Refl: .040

Beam sep: -.162 mm; Standoff (nom / extra): (10.000 / .000) mm

Relative calibration (half-width, # of pts, fit order): .000 0 3

Absolute calibration (half-width, # of pts, fit order): .200 7 3

Poly removal: 6; Boxcar: .000 mm; Measured Nov 12, 1993 9:26:42

Scan 1 - RA: 13.60; RMS: 17.20; P-V: 85.59 (Angstroms)

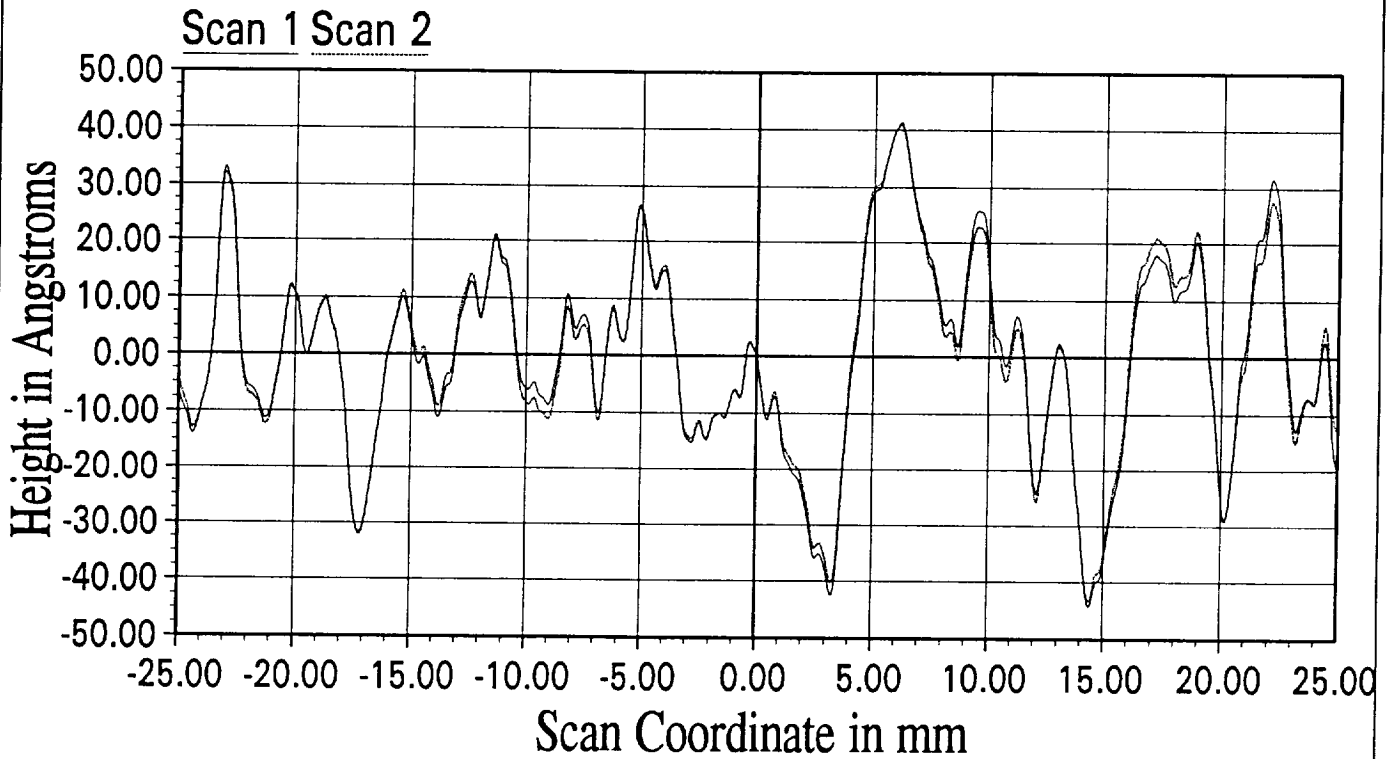
Polynomials 0-4: .00 .00 .00 .00 .00

5-9: .00 .00 -2.01 -6.67 1.99

Scan 2 - RA: 13.36; RMS: 16.82; P-V: 84.41 (Angstroms)

Polynomials 0-4: .00 .00 .00 .00 .00

5-9: .00 .00 -1.87 -5.21 2.68



BAUER MODEL 100: Surface Height

DEGB - Displaced by 50 mm towards two dashed lines

Vertex Curvature (longitudinal/lateral): (5.0000D-04 / 5.0000D-04) mm⁻¹

Conic Constant (- eccentricity²): .0000

Average of 1 scan pair(s), starting w/ pair # 1; Filename: D:\BAUER\DEGB_B

Beams: Sheared; Drift analysis: 2nd order; Steering compensation: On

Scan start: -48.643 mm; Length: 97.266 mm; Pixel: .039 mm

Velocity: 3.00 mm/sec; Calibration location: .000 mm

Piece offset: .000 mm; Other-axis position: .000; Refl: .040

Beam sep: -.162 mm; Standoff (nom / extra): (10.000 / .000) mm

Relative calibration (half-width, # of pts, fit order): .000 0 3

Absolute calibration (half-width, # of pts, fit order): .200 7 3

Poly removal: 5; Boxcar: .000 mm; Measured Nov 12, 1993 9:26:42

Scan 1 - RA: 26.53; RMS: 30.91; P-V: 151.17 (Angstroms)

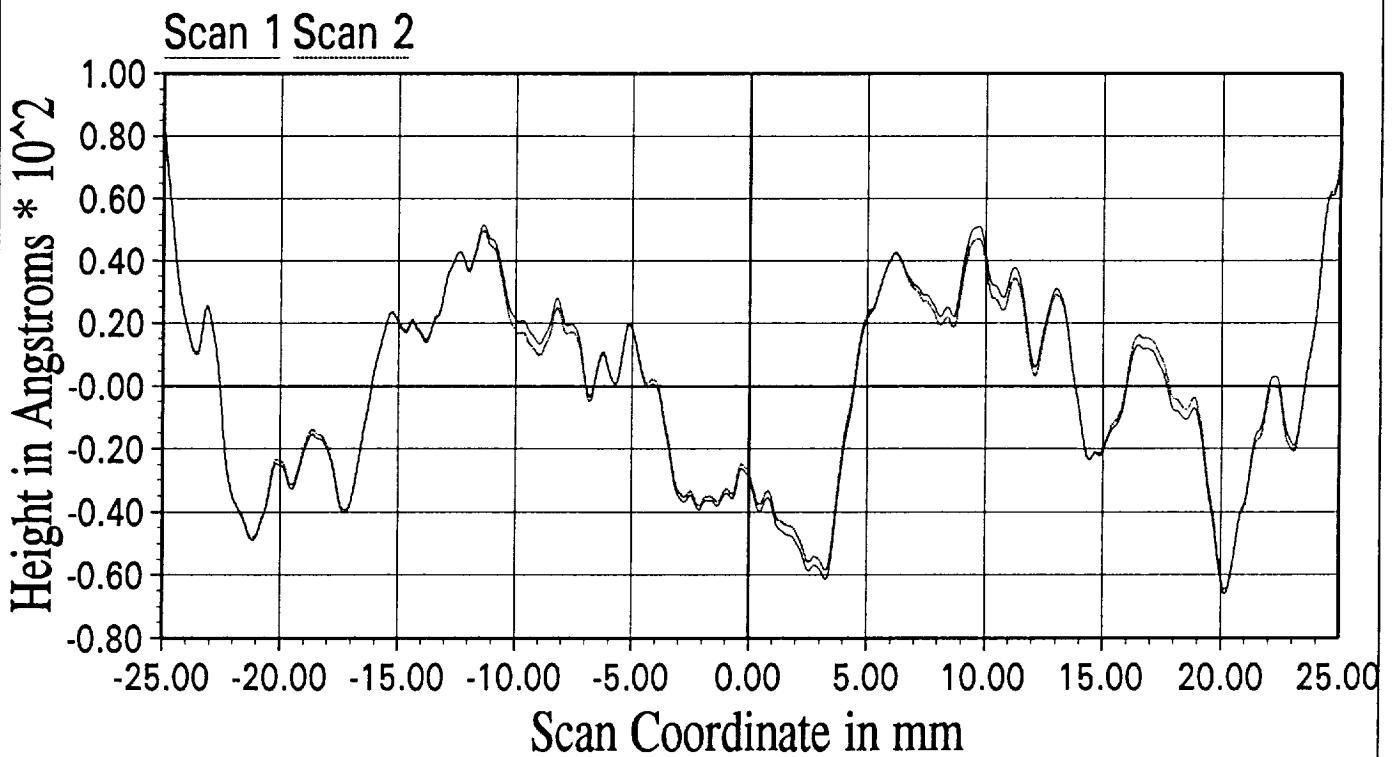
Polynomials 0-4: .00 .00 .00 .00 .00

5-9: .00 25.64 -2.01 -6.67 1.99

Scan 2 - RA: 25.44; RMS: 29.74; P-V: 147.81 (Angstroms)

Polynomials 0-4: .00 .00 .00 .00 .00

5-9: .00 24.47 -1.87 -5.21 2.68



BAUER MODEL 100: Surface Height

DEGB - Displaced by 50 mm towards two dashed lines

Vertex Curvature (longitudinal/lateral): (5.0000D-04 / 5.0000D-04) mm⁻¹

Conic Constant (- eccentricity²): .0000

Average of 1 scan pair(s), starting w/ pair # 1; Filename: D:\BAUER\DEGB_B

Beams: Sheared; Drift analysis: 2nd order; Steering compensation: On

Scan start: -48.643 mm; Length: 97.266 mm; Pixel: .039 mm

Velocity: 3.00 mm/sec; Calibration location: .000 mm

Piece offset: .000 mm; Other-axis position: .000; Refl: .040

Beam sep: -.162 mm; Standoff (nom / extra): (10.000 / .000) mm

Relative calibration (half-width, # of pts, fit order): .000 0 3

Absolute calibration (half-width, # of pts, fit order): .200 7 3

Poly removal: 4; Boxcar: .000 mm; Measured Nov 12, 1993 9:26:42

Scan 1 - RA: 28.96; RMS: 35.95; P-V: 221.25 (Angstroms)

Polynomials 0-4: .00 .00 .00 .00 .00

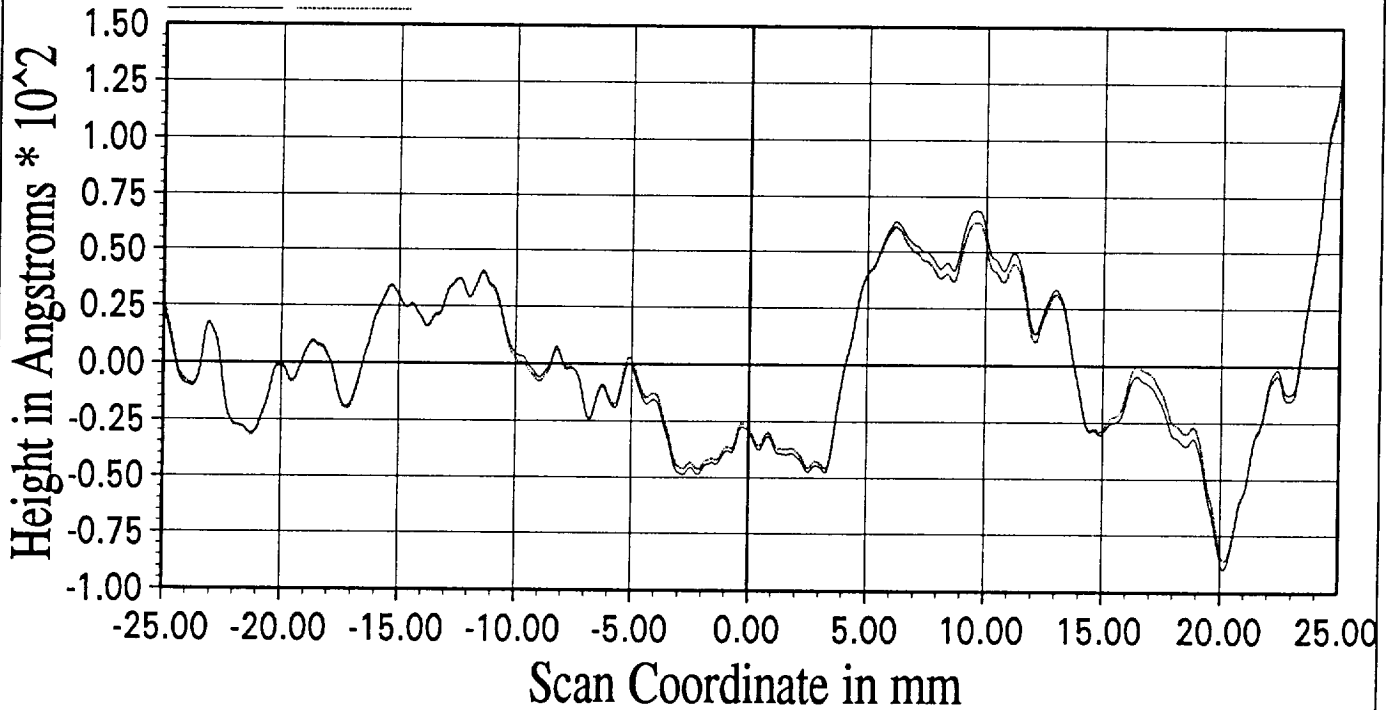
5-9: 18.27 25.64 -2.01 -6.67 1.99

Scan 2 - RA: 27.42; RMS: 34.14; P-V: 215.26 (Angstroms)

Polynomials 0-4: .00 .00 .00 .00 .00

5-9: 16.68 24.47 -1.87 -5.21 2.68

Scan 1 Scan 2



BAUER MODEL 100: Surface Height

DEGB - Displaced by 50 mm towards two dashed lines

Vertex Curvature (longitudinal/lateral): (5.0000D-04 / 5.0000D-04) mm⁻¹

Conic Constant (- eccentricity²): .0000

Average of 1 scan pair(s), starting w/ pair # 1; Filename: D:\BAUER\DEGB_B

Beams: Sheared; Drift analysis: 2nd order; Steering compensation: On

Scan start: -48.643 mm; Length: 97.266 mm; Pixel: .039 mm

Velocity: 3.00 mm/sec; Calibration location: .000 mm

Piece offset: .000 mm; Other-axis position: .000; Refl: .040

Beam sep: -.162 mm; Standoff (nom / extra): (10.000 / .000) mm

Relative calibration (half-width, # of pts, fit order): .000 0 3

Absolute calibration (half-width, # of pts, fit order): .200 7 3

Poly removal: 3; Boxcar: .000 mm; Measured Nov 12, 1993 9:26:42

Scan 1 - RA: 62.35; RMS: 70.10; P-V: 263.81 (Angstroms)

Polynomials 0-4: .00 .00 .00 .00 -60.15

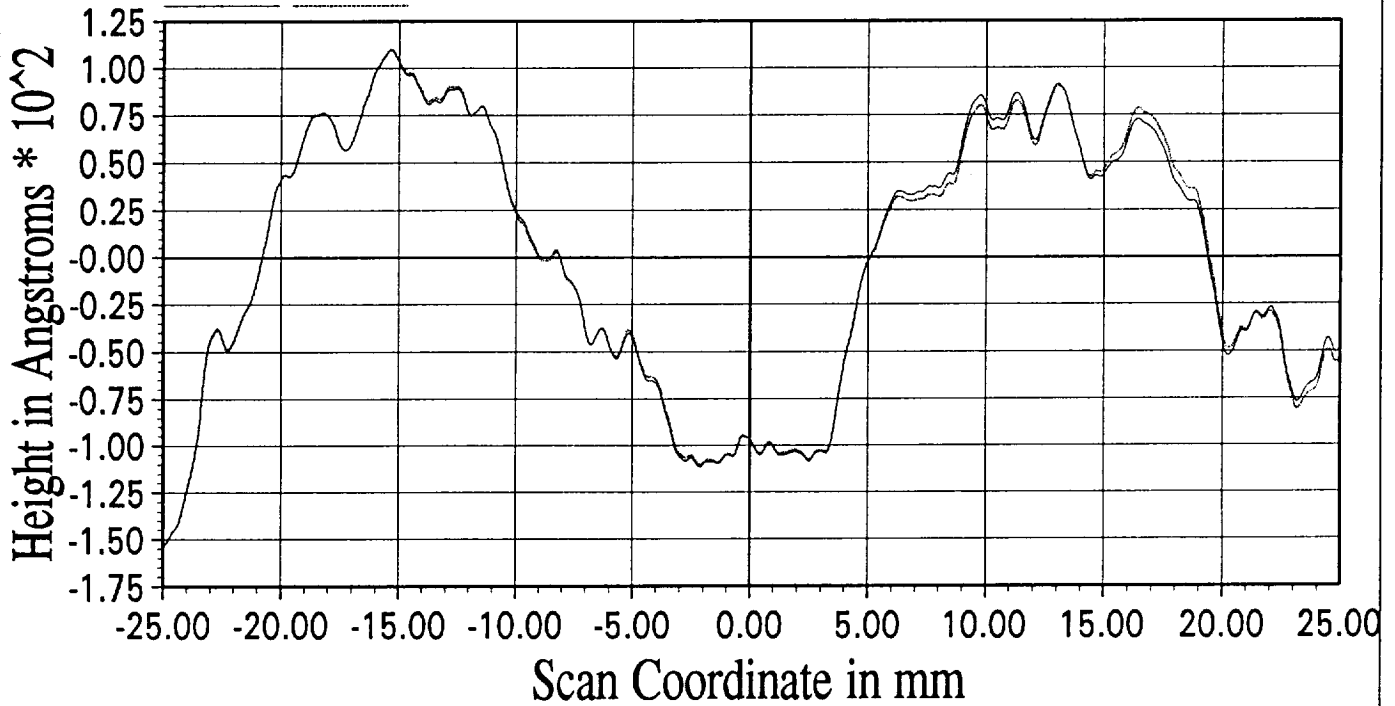
5-9: 18.27 25.64 -2.01 -6.67 1.99

Scan 2 - RA: 62.26; RMS: 69.96; P-V: 263.70 (Angstroms)

Polynomials 0-4: .00 .00 .00 .00 -61.04

5-9: 16.68 24.47 -1.87 -5.21 2.68

Scan 1 Scan 2



BAUER MODEL 100: Surface Height

DEGB - Displaced by 50 mm towards two dashed lines

Vertex Curvature (longitudinal/lateral): (5.0000D-04 / 5.0000D-04) mm⁻¹

Conic Constant (- eccentricity²): .0000

Average of 1 scan pair(s), starting w/ pair # 1; Filename: D:\BAUER\DEGB_B

Beams: Sheared; Drift analysis: 2nd order; Steering compensation: On

Scan start: -48.643 mm; Length: 97.266 mm; Pixel: .039 mm

Velocity: 3.00 mm/sec; Calibration location: .000 mm

Piece offset: .000 mm; Other-axis position: .000; Refl: .040

Beam sep: -.162 mm; Standoff (nom / extra): (10.000 / .000) mm

Relative calibration (half-width, # of pts, fit order): .000 0 3

Absolute calibration (half-width, # of pts, fit order): .200 7 3

Poly removal: 2; Boxcar: .000 mm; Measured Nov 12, 1993 9:26:42

Scan 1 - RA: 64.70; RMS: 85.64; P-V: 437.88 (Angstroms)

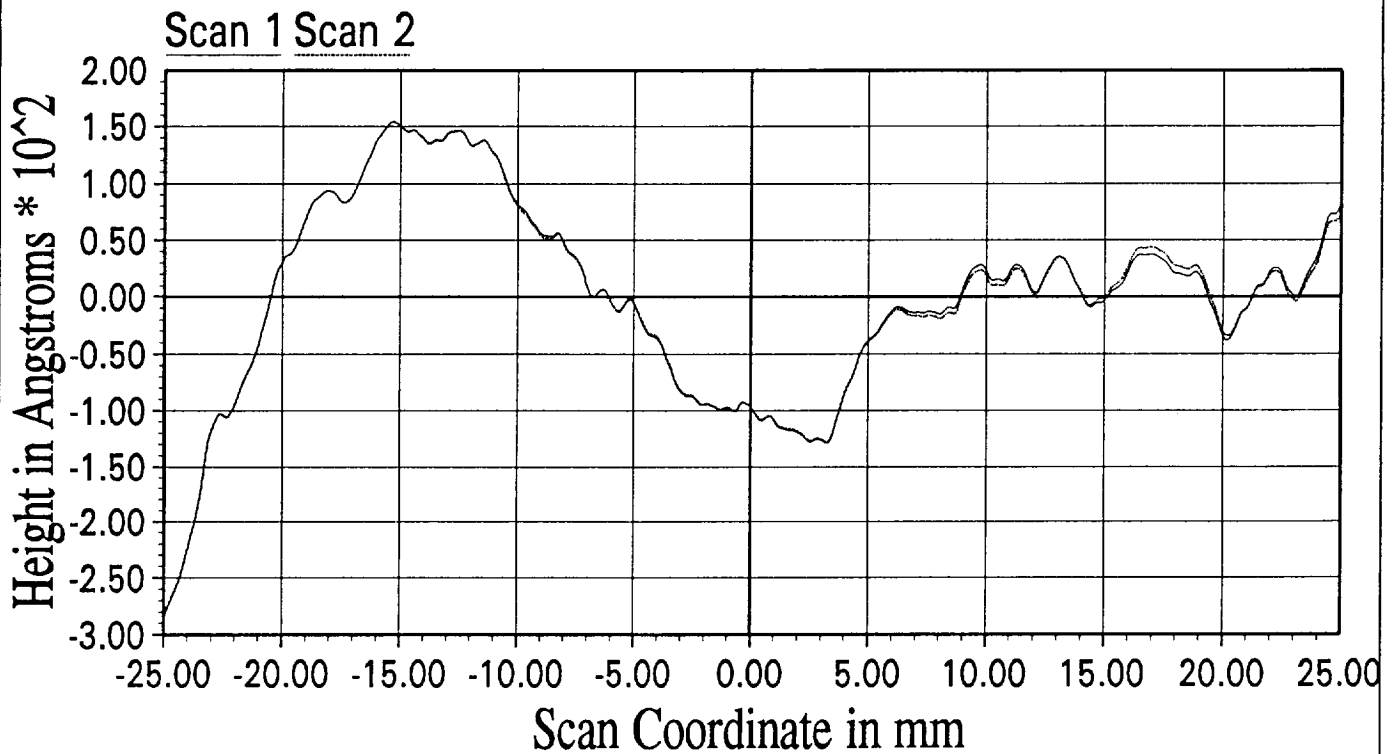
Polynomials 0-4: .00 .00 .00 48.94 -60.15

5-9: 18.27 25.64 -2.01 -6.67 1.99

Scan 2 - RA: 64.36; RMS: 85.26; P-V: 436.21 (Angstroms)

Polynomials 0-4: .00 .00 .00 48.49 -61.04

5-9: 16.68 24.47 -1.87 -5.21 2.68



BAUER MODEL 100: Surface Height

DEGB - Displaced by 50 mm towards two dashed lines

Vertex Curvature (longitudinal/lateral): (5.0000D-04 / 5.0000D-04) mm⁻¹

Conic Constant (- eccentricity²): .0000

Average of 1 scan pair(s), starting w/ pair # 1; Filename: D:\BAUER\DEGB_B

Beams: Sheared; Drift analysis: 2nd order; Steering compensation: On

Scan start: -48.643 mm; Length: 97.266 mm; Pixel: .039 mm

Velocity: 3.00 mm/sec; Calibration location: .000 mm

Piece offset: .000 mm; Other-axis position: .000; Refl: .040

Beam sep: -.162 mm; Standoff (nom / extra): (10.000 / .000) mm

Relative calibration (half-width, # of pts, fit order): .000 0 3

Absolute calibration (half-width, # of pts, fit order): .200 7 3

Poly removal: 1; Boxcar: .000 mm; Measured Nov 12, 1993 9:26:42

Scan 1 - RA: 161.85; RMS: 201.17; P-V: 904.31 (Angstroms)

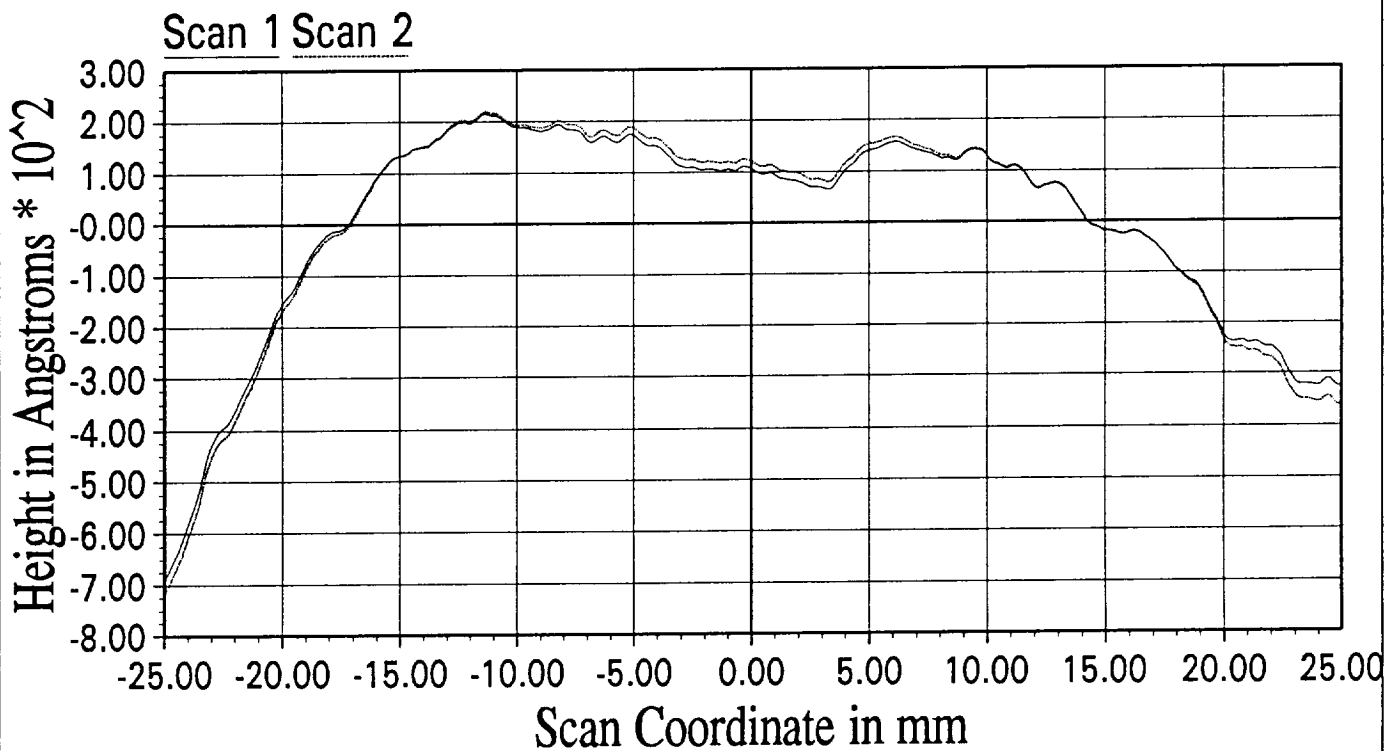
Polynomials 0-4: .00 .00 -181.54 48.94 -60.15

5-9: 18.27 25.64 -2.01 -6.67 1.99

Scan 2 - RA: 172.01; RMS: 212.90; P-V: 936.29 (Angstroms)

Polynomials 0-4: .00 .00 -194.56 48.49 -61.04

5-9: 16.68 24.47 -1.87 -5.21 2.68



BAUER MODEL 100: Surface Height

DEGB - Displaced by 50 mm towards two dashed lines

Vertex Curvature (longitudinal/lateral): (5.0000D-04 / 5.0000D-04) mm⁻¹

Conic Constant (- eccentricity²): .0000

Average of 1 scan pair(s), starting w/ pair # 1; Filename: D:\BAUER\DEGB_B

Beams: Sheared; Drift analysis: 2nd order; Steering compensation: On

Scan start: -48.643 mm; Length: 97.266 mm; Pixel: .039 mm

Velocity: 3.00 mm/sec; Calibration location: .000 mm

Piece offset: .000 mm; Other-axis position: .000; Refl: .040

Beam sep: -.162 mm; Standoff (nom / extra): (10.000 / .000) mm

Relative calibration (half-width, # of pts, fit order): .000 0 3

Absolute calibration (half-width, # of pts, fit order): .200 7 3

Poly removal: 0; Boxcar: .000 mm; Measured Nov 12, 1993 9:26:42

Scan 1 - RA: 1155.54; RMS: 1332.32; P-V: 4274.28 (Angstroms)

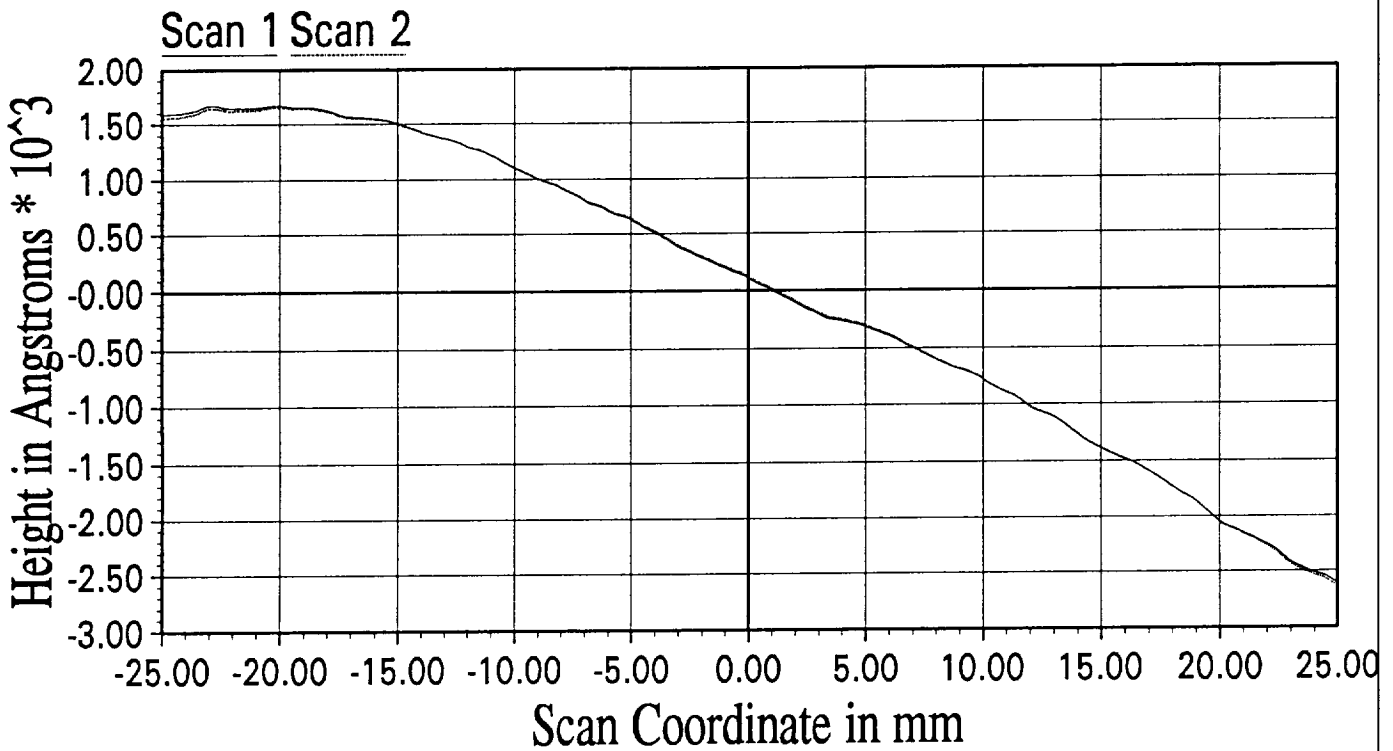
Polynomials 0-4: .00 -1316.26 -181.54 48.94 -60.15

5-9: 18.27 25.64 -2.01 -6.67 1.99

Scan 2 - RA: 1153.17; RMS: 1330.56; P-V: 4284.41 (Angstroms)

Polynomials 0-4: .00 -1312.63 -194.56 48.49 -61.04

5-9: 16.68 24.47 -1.87 -5.21 2.68



BAUER MODEL 100: Surface Height

DEGB - Displaced by 50 mm towards two dashed lines

Vertex Curvature (longitudinal/lateral): (5.0000D-04 / 5.0000D-04) mm⁻¹

Conic Constant (- eccentricity²): .0000

Average of 1 scan pair(s), starting w/ pair # 1; Filename: D:\BAUER\DEGB_B

Beams: Sheared; Drift analysis: 2nd order; Steering compensation: On

Scan start: -48.643 mm; Length: 97.266 mm; Pixel: .039 mm

Velocity: 3.00 mm/sec; Calibration location: .000 mm

Piece offset: .000 mm; Other-axis position: .000; Refl: .040

Beam sep: -.162 mm; Standoff (nom / extra): (10.000 / .000) mm

Relative calibration (half-width, # of pts, fit order): .000 0 3

Absolute calibration (half-width, # of pts, fit order): .200 7 3

No poly's rmvd; Boxcar: .000 mm; Measured Nov 12, 1993 9:26:42

Scan 1 - RA: 1155.54; RMS: 1332.32; P-V: 4274.28 (Angstroms)

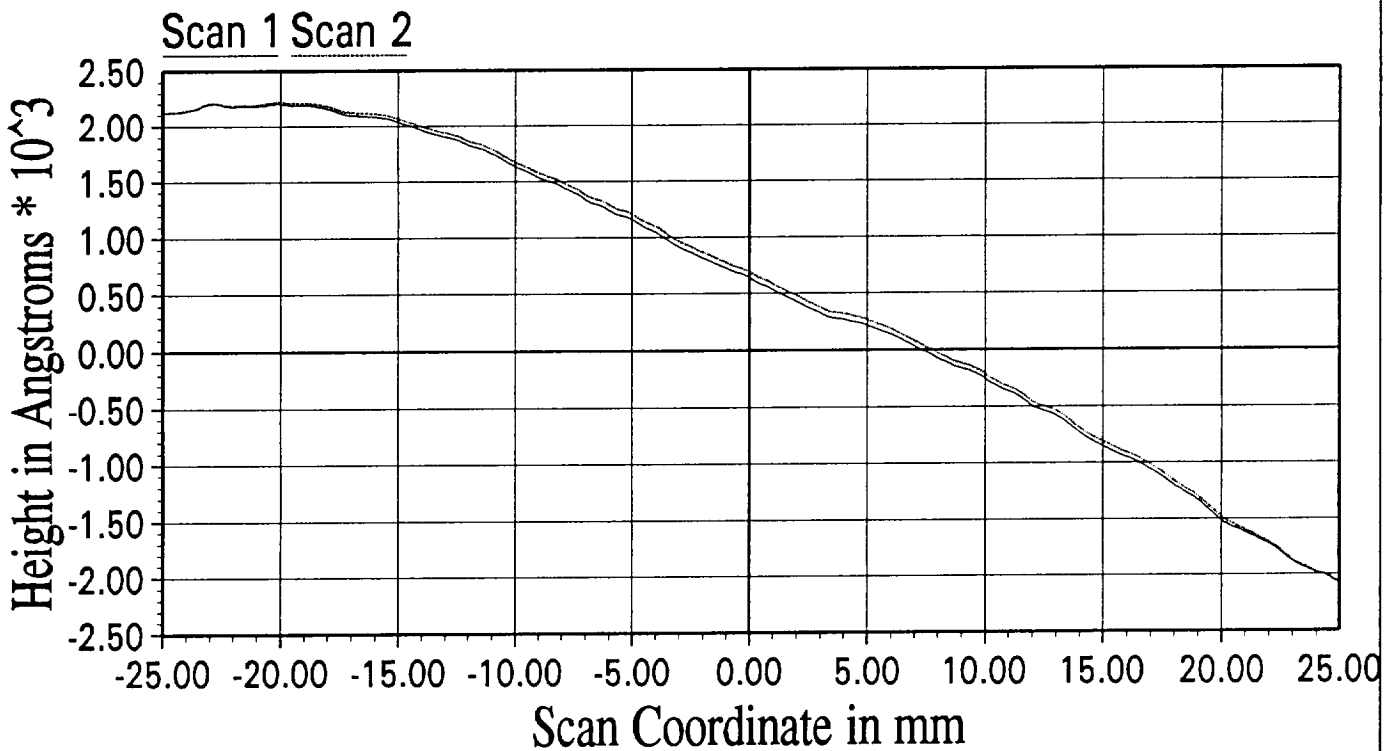
Polynomials 0-4: 531.77 -1316.26 -181.54 48.94 -60.15

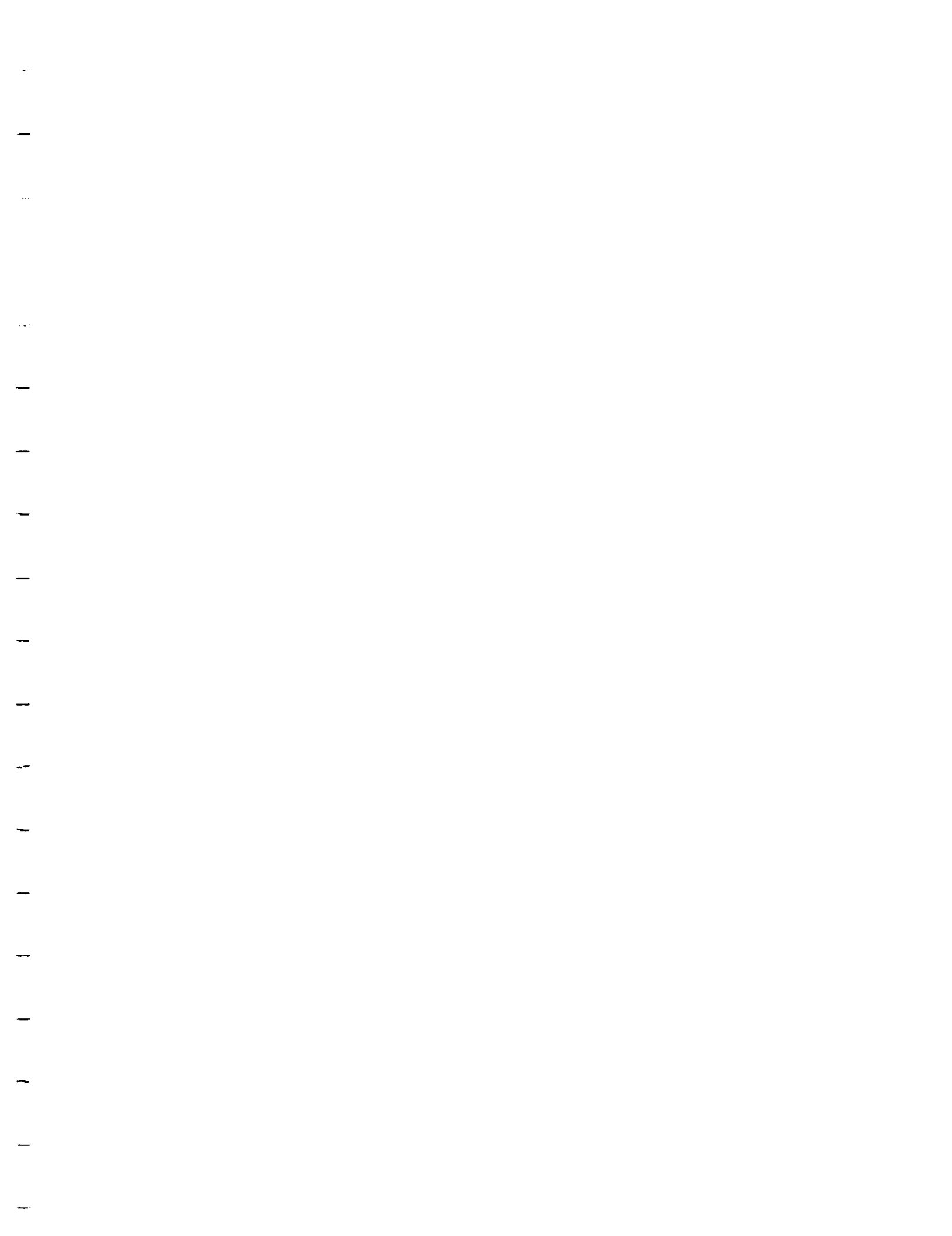
5-9: 18.27 25.64 -2.01 -6.67 1.99

Scan 2 - RA: 1153.17; RMS: 1330.56; P-V: 4284.41 (Angstroms)

Polynomials 0-4: 568.80 -1312.63 -194.56 48.49 -61.04

5-9: 16.68 24.47 -1.87 -5.21 2.68





===== VARIABLE SHEET =====

St	Input	Name	Output	Unit	Comment
0		z			
	531.77	a0			
	-1316.26	a1			
	-181.54	a2			
	48.94	a3			
	-60.15	a4			
	18.27	a5			
	25.64	a6			
	-2.01	a7			
	-6.67	a8			
	1.99	a9			
		G00	531.77		
		G10	0		
		G20	202.96789		
		G30	0		
		G40	-67.66875		
		G50	0		
		G60	-28.88948		
		G70	0		
		G80	-7.519836		
		G90	0		
		G9	630.65982		
		G8	630.65982		
		G7	638.17966		
		G6	638.17966		
		G5	667.06914		
		G4	667.06914		
		G3	734.73789		
		G2	734.73789		
		G1	531.77		
		G0	531.77		
		G09	630.65982		
		G19	98.889825		
		G29	98.889825		
		G39	-104.0781		
		G49	-104.0781		
		G59	-36.40932		
		G69	-36.40932		
		G79	-7.519836		
		G89	-7.519836		
		G99	0		

===== RULE SHEET =====

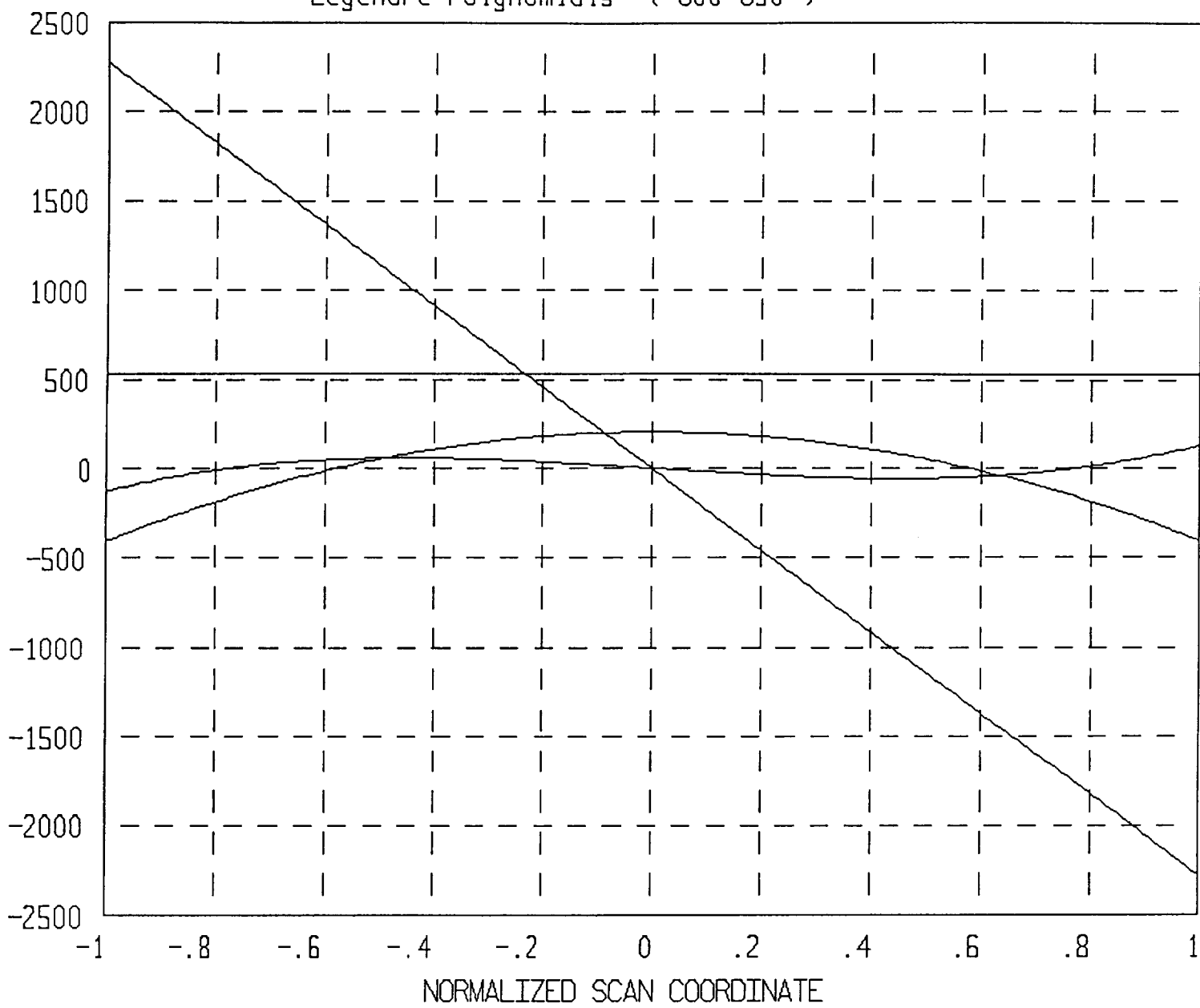
S Rule-----

- G00 = a0*1
- G10 = a1*SQRT(3)*z
- G20 = a2*SQRT(5)*(3*z^2 - 1)/2
- G30 = a3*SQRT(7)*(5*z^3 - 3*z)/2
- G40 = a4*SQRT(9)*(36*z^4 - 30*z^2 + 3)/8
- G50 = a5*SQRT(11)*(63*z^5 - 70*z^3 + 15*z)/8
- G60 = a6*SQRT(13)*(231*z^6 - 315*z^4 + 105*z^2 - 5)/16
- G70 = a7*SQRT(15)*(429*z^7 - 693*z^5 + 315*z^3 - 35*z)/16
- G80 = a8*SQRT(17)*(6435*z^8 - 12012*z^6 + 6930*z^4 - 1260*z^2 + 35)/128
- G90 = a9*SQRT(19)*(12155*z^9 - 25740*z^7 + 18018*z^5 - 4620*z^3 + 315*z)/128

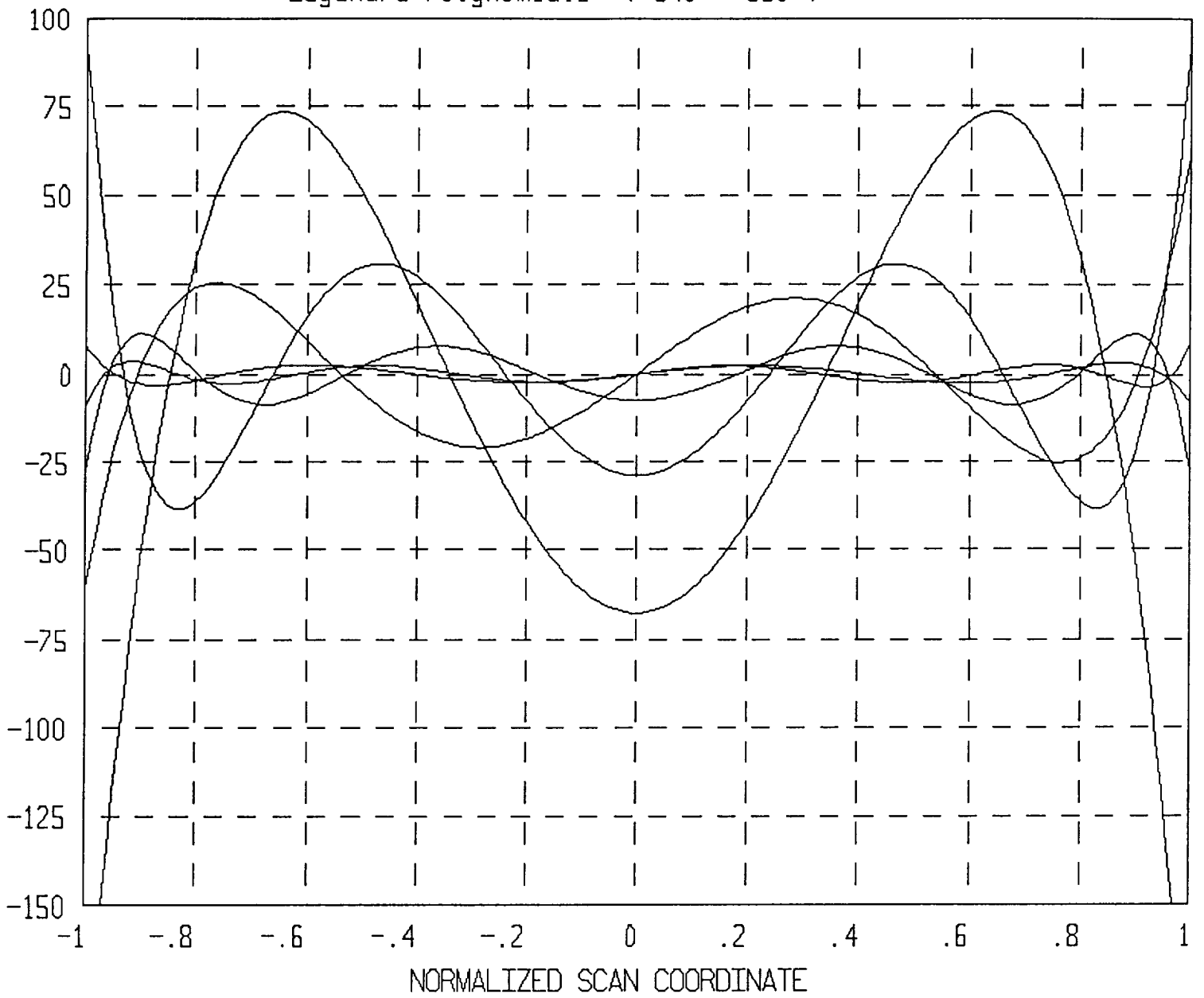
- G9 = G00+G10+G20+G30+G40+G50+G60+G70+G80+G90
- G8 = G00+G10+G20+G30+G40+G50+G60+G70+G80
- G7 = G00+G10+G20+G30+G40+G50+G60+G70
- G6 = G00+G10+G20+G30+G40+G50+G60
- G5 = G00+G10+G20+G30+G40+G50
- G4 = G00+G10+G20+G30+G40
- G3 = G00+G10+G20+G30
- G2 = G00+G10+G20
- G1 = G00+G10
- G0 = G00

- G09 = G00+G10+G20+G30+G40+G50+G60+G70+G80+G90
- G19 = G10+G20+G30+G40+G50+G60+G70+G80+G90
- G29 = G20+G30+G40+G50+G60+G70+G80+G90
- G39 = G30+G40+G50+G60+G70+G80+G90
- G49 = G40+G50+G60+G70+G80+G90
- G59 = G50+G60+G70+G80+G90
- G69 = G60+G70+G80+G90
- G79 = G70+G80+G90
- G89 = G80+G90
- G99 = G90

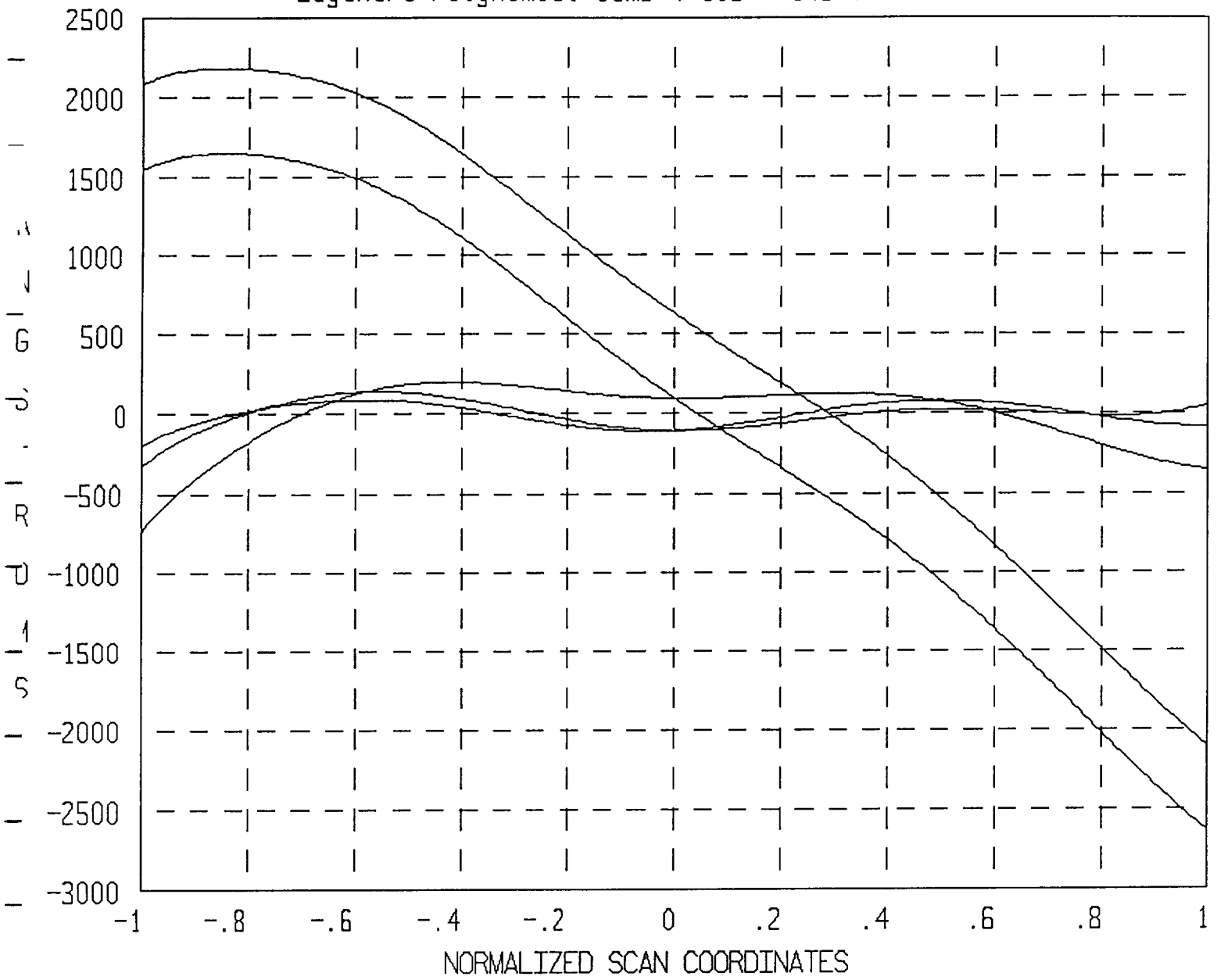
Legendre Polynomials (G00-G30)



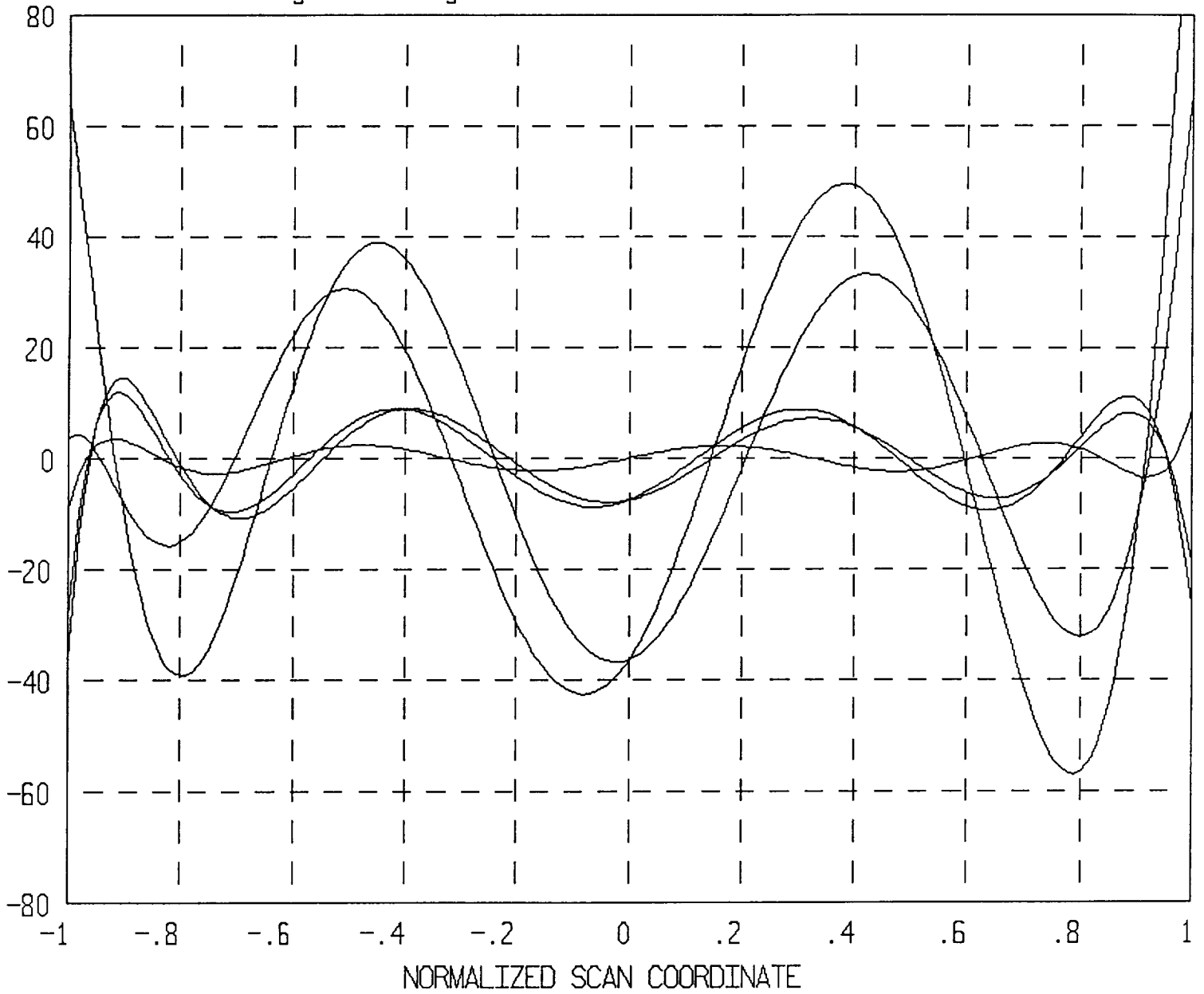
Legendre Polynomials (G40 - G90)



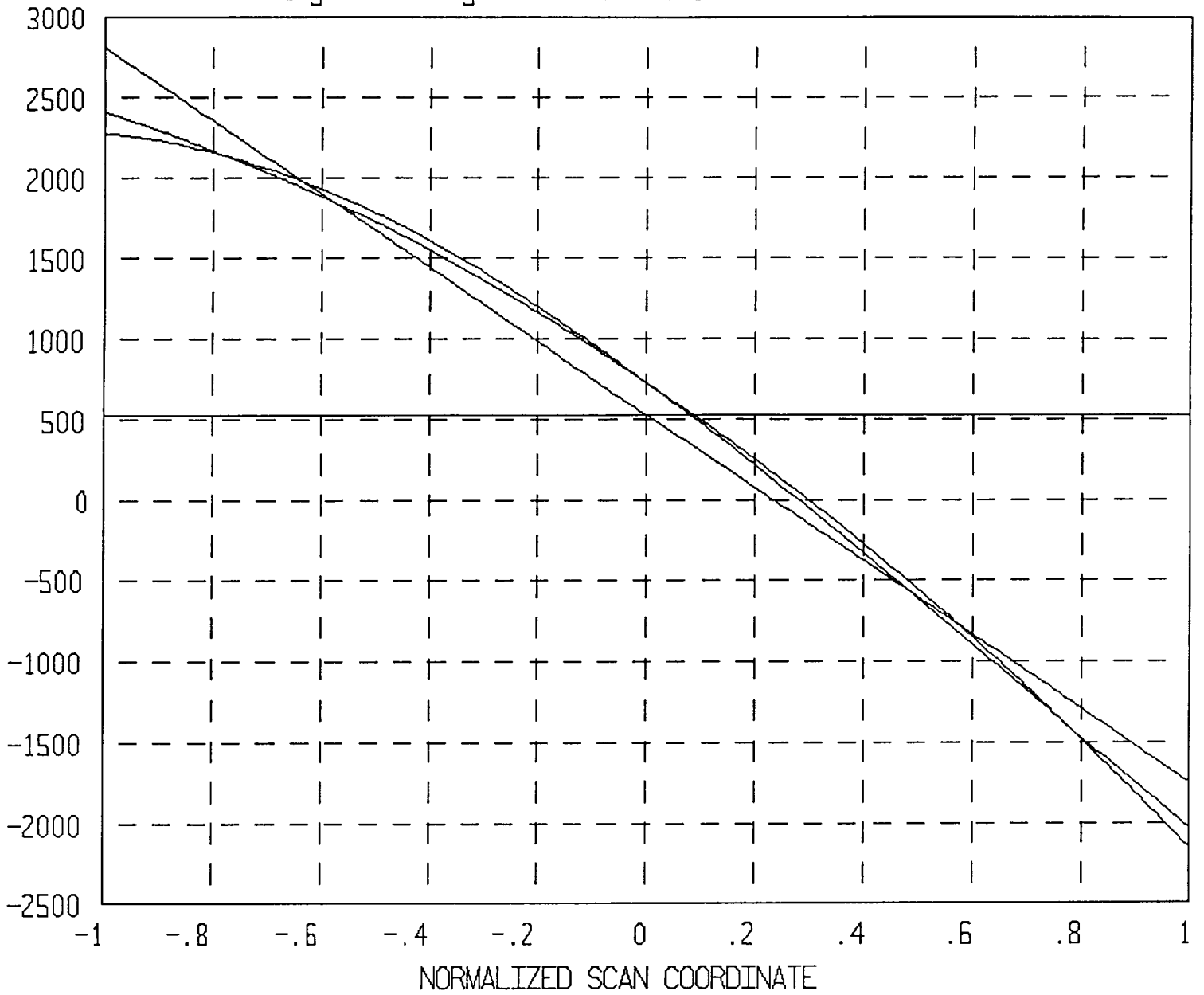
Legendre Polynomial Sums (G09 - G49)



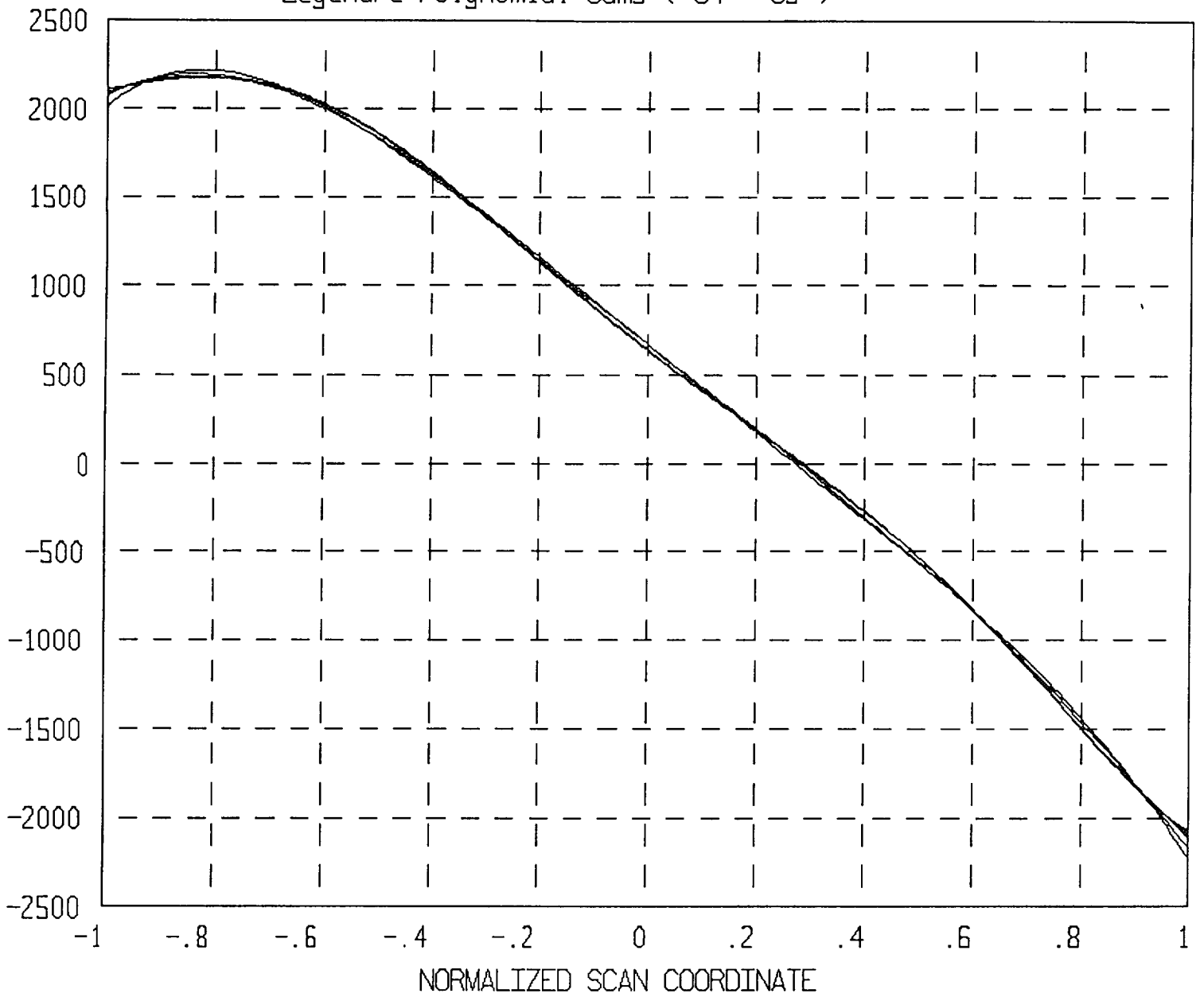
Legendre Polynomial Sums (G59 - G99)



Legendre Polynomial Sums (G0 - G3)



Legendre Polynomial Sums (G4 - G9)



APPENDIX H

CONTRACT STATEMENT OF WORK

STATEMENT OF WORK

FABRICATION AND TESTING OF A DEFORMED ELLIPSOIDAL DIFFRACTION GRATING BLANK

1.0 Introduction

The grating blank to be fabricated is intended for use, when ruled as a high line density diffraction grating, as the sole optical element in a high spectral resolving power far ultraviolet (FUV) spectrograph. The ruling of this blank is not part of the current contract. The blank is a non-symmetric asphere (as specified below), designed to minimize optical aberrations when used in first diffracted order in a specific use geometry.

The performance goal of a resolving power of 30000 when used as an FUV diffraction grating leads to tight figuring requirements. The lack of a simple null lens interferometric test of the blank makes the manufacturing process challenging.

This grating blank is intended as a technology demonstration item, and is not currently being considered for any flight mission. The successful demonstration of figuring and ruling such a grating would, however, be of strong interest to planned NASA ultraviolet spectroscopy missions.

2.0 Tasks\Specifications

This statement of work consists of three phases. Phase 1 is the fabrication planning phase, Phase 2 is the fabrication and preliminary testing phase, and Phase 3 is the final testing phase. At the end of each Phase, a written report is required.

RFP Note: Although there are several tests which shall be required on the diffraction grating blank, as listed below, a principal area of concern is that test or tests used to measure the surface figure. This may be an interferometric test, or otherwise.

2.0.1

The contractor shall be responsible not only for the figuring and polishing of the diffraction grating blank, but also for designing, preparing, verifying, and implementing the testing procedure(s) required to verify the correct figuring of the blank to the accuracy required by the specifications below. No Government materials, designs, or test equipment would be supplied to the contractor as part of this contract.

2.0.2 Coordinate system

The coordinate system used to describe the diffraction grating blank is right handed, with **x** axis normal to the piece at the vertex (oriented so as to emerge out of the illuminated face), **y** axis parallel to the width, and **z** axis parallel to the height. The diffraction rulings, when applied, would be parallel to the **z** axis. Unless stated otherwise, all coordinates are given in this coordinate system.

2.0.3 Analytic expression for the optical surface

The analytic form of the surface can be expressed as a sag from the tangent plane $x=0$, with

$$x = a(1 - \sqrt{1 - (y/b)^2 - (z/c)^2}) + \epsilon_0 yz^2$$

The ϵ_0 term is the asymmetric deformation and represents the deformation from an ellipsoid. The maximum sag over the active area as compared to the undeformed ellipsoid is ± 2.315 microns. A sag table expressing the **x** coordinate of the surface on a rectangular grid of points (**y,z**) is attached for reference.

When ruled, the diffraction grating grooves shall be aligned with the **z** axis.

The specifications are enumerated below as tasks. For convenience, they also appear in attachment 3 to this Statement of Work. In the case of a conflict, the list of tasks below shall be used.

2.1 Mechanical specifications

2.1.1 Surface Figure and shape

The surface of the diffraction grating blank shall be a deformed ellipsoid of the analytic form above in §2.0.4. The shape of the diffraction grating blank as delivered will be that of an 203.2 mm (8.00 inch) diameter circle. The thickness at the vertex shall be at least 20 mm, but no more than 30 mm. The backside of the diffraction grating blank shall be flat, with the normal to the backside aligned to the **-x** axis to within ± 15 arcseconds.

2.1.2 Active area

The active area of the diffraction grating blank shall be an ellipse with semi axes 92.5 mm (along the **y** axis) and 77.5 mm (along the **z** axis).

2.1.3 Alignment Fiducials

The contractor shall mark on the edge of the diffraction grating blank at the points where the positive **y** and **z** axes intersect the

blank. The two fiducial marks shall be distinguishable, permanent, and documented in project reports.

2.1.4 Material

The material to be used for the diffraction grating blank shall be an ultra low expansion glass (e.g. ULE or Zerodur).

2.1.5 Ellipsoidal radii

The ellipsoidal radii along the x,y, and z axes, respectively, shall be $a = 1523.081 \pm 0.15$ mm, $b = 1672.920 \pm 0.15$ mm, and $c = 1523.081 \pm 0.15$ mm.

2.1.6 Deformation coefficient

The deformation coefficient, described above in §2.0.4, shall have the value $\epsilon_0 = 1.128E-8 \pm 0.01E-8$ mm⁻²

2.2 Figuring Tolerances

2.2.1 Figure error

The surface will be fabricated such that the peak to valley surface figure error will be 1/8 wavelength (wavelength = .6328 μ m).

2.2.2 Roughness

The microroughness goal is 2.0nm rms or less. The midfrequency error (correlation length of 1 mm) is 2.0nm rms or less.

2.3 Phase 1 -- Fabrication planning

The contractor shall prepare and submit a written fabrication and testing plan and schedule. The contractor shall provide mechanical drawings of the proposed diffraction grating blank.

2.4 Phase 2 -- Fabrication and initial testing

In this Phase, the contractor shall fabricate the diffraction grating blank to the required surface figure tolerance as above in §2.2.1. Initial tests as required to verify that the surface figure tolerance has been met shall be performed. A written report establishing that this tolerance has been met shall be prepared and submitted. This report shall include test data demonstrating the surface figure quality that was achieved.

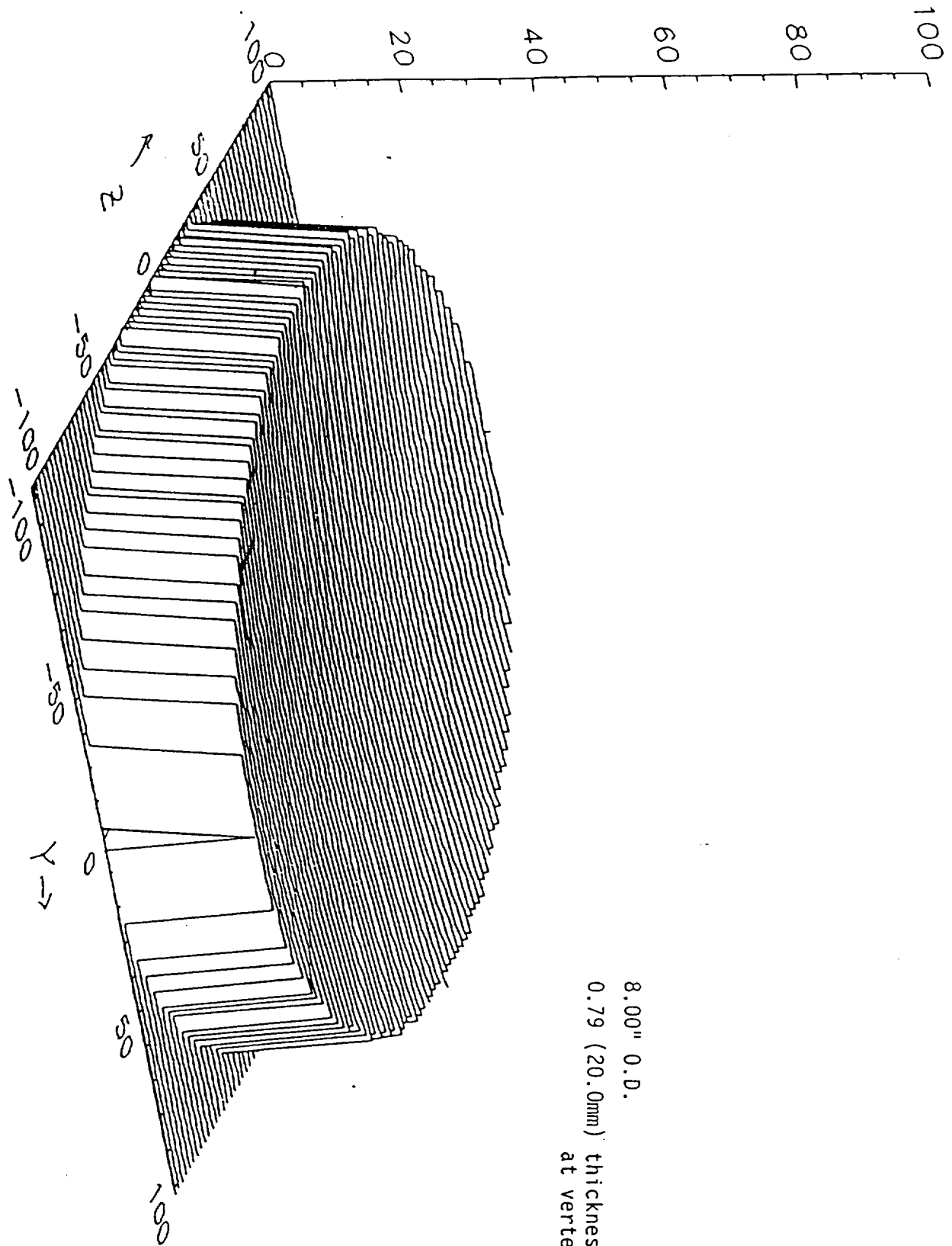
2.5 Phase 3 -- Final testing

In this phase, the completed diffraction grating blank will be tested for final surface figure, radii of curvature, flatness and parallelism of the back face, microroughness, midfrequency ripple, and mechanical dimensions. These tests shall measure these quantities to at least the precision required to ascertain whether they do or do not meet the specifications above.

2.5.1 Final testing requirements

The contractor is required to perform all necessary measurements to verify that the grating blank meets all specifications. The characterization shall include mechanical measurements, establishing overall surface figure and surface roughness, midfrequency ripple, radii of curvature, and mechanical dimensions. The contractor shall prepare and submit a written report on these tests. All test data shall be included in the report.

Drawing of the RTOP diffraction grating blank



Sag table (in mm) for RTOP grating blank

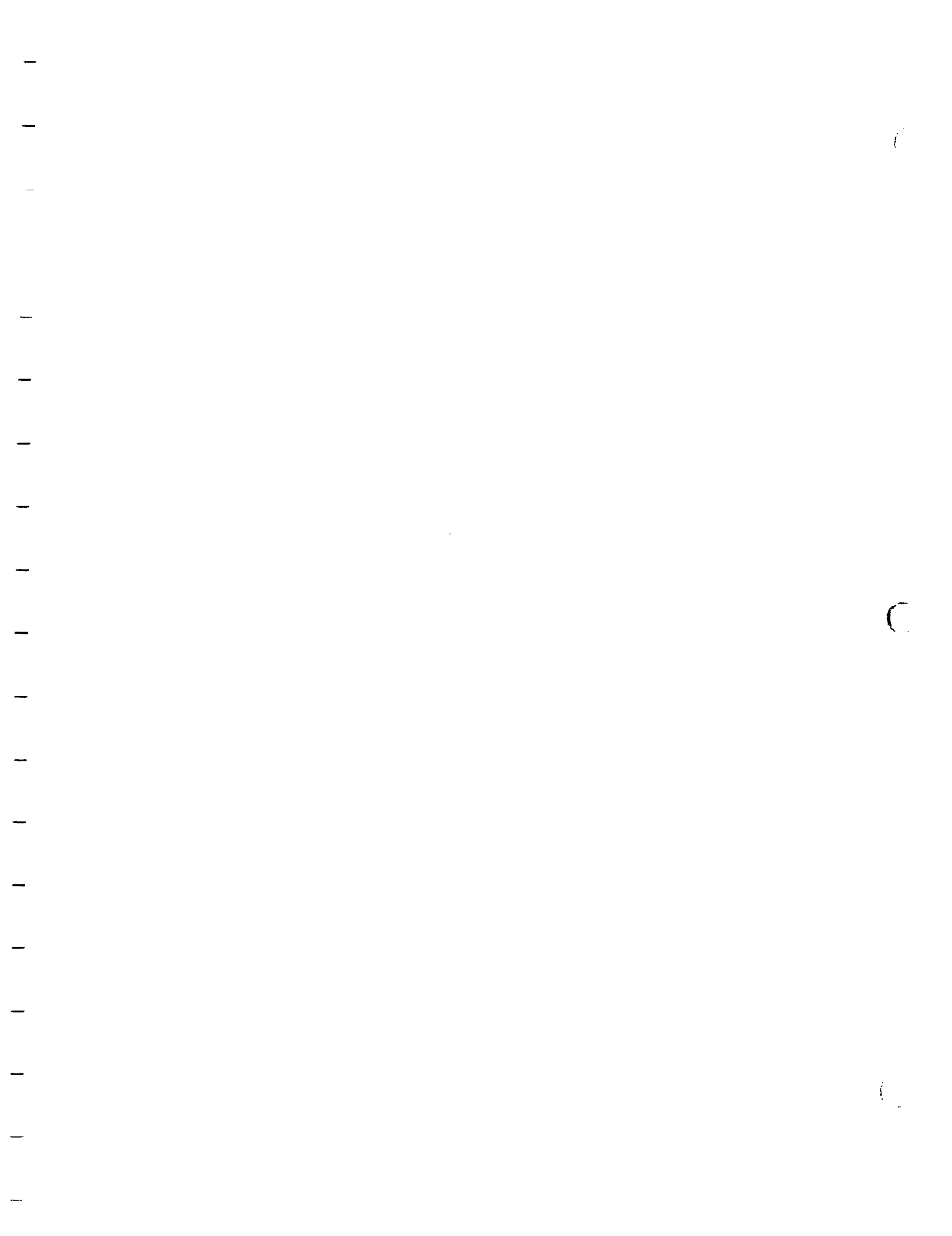
z	y	-100	-50	0	50	100
-80		4.822531	2.780211	2.102456	2.787430	4.836970
-40		3.248002	1.205098	0.525342	1.206903	3.251611
0		2.723524	0.680424	0.000000	0.680424	2.723524
40		3.248002	1.205098	0.525342	1.206903	3.251611
80		4.822531	2.780211	2.102456	2.787430	4.836970

Table of Specifications

Quantity	Value	Units	Allowable error
Surface Figure	deformed ellipsoid		
Shape of blank	203.20	mm	±0.2 mm
	(2" diameter circle)		
Material	Zerodur		
Active width	155.00	mm	±0.2 mm
Active height	155.00	mm	±0.2 mm
	(active area is elliptical with these axes)		
Thickness (@center)	20.00	mm	±1 mm
radius a (x)	1523.081	mm	±0.15 mm
radius b (y)	1672.920	mm	±0.15 mm
radius c (z)	1523.081	mm	±0.15 mm
deformation coefficient ϵ_0	1.128E-8	mm ⁻²	±1E-10mm ⁻²
Figure error (P/V)	1/8 wave	.6328 μm	
microroughness	2 nm rms goal		
(correlation length tbd)			
midfrequency roughness (1 mm correlation length)	2 nm rms goal		
Back surface shape	Flat	1/4 wave P/V	
	(normal along -x axis, to within ±15 arcseconds)		
Mechanical mounting	tbd		

Notes:

- 1) The grooves would be along the height, e.g. the longest groove is 155 mm long.





Space Optics Research Labs
An Intergraph Division

CERTIFICATE OF CONFORMANCE

MODEL NUMBER: Deformed Ellipsoidal Diffraction
Grating Blank

QUANTITY: 1

COMPANY: NASA/Goddard Space Flight Center

SORL SALES ORDER NUMBER: SN4043

PURCHASE ORDER NUMBER: NAS5-31790

DATE: November 19, 1993

Space Optics Research Labs certifies that this product complies with the material, quality, and dimensional specifications as set forth in the enclosed Quality Assurance Documentation and the above mentioned order.

A handwritten signature in cursive script, reading "Alan E. DeCew, Jr.", is written over a horizontal line.

Alan E. DeCew, Jr.
General Manager

QUALITY ASSURANCE DOCUMENTATION

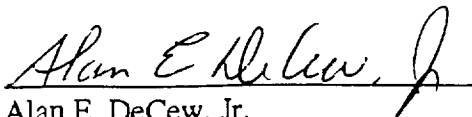
CUSTOMER: NASA/Goddard Space Flight Center

MODEL NUMBER: Deformed Ellipsoidal Diffraction Grating Blank

PURCHASE ORDER NUMBER: NAS5-31790

SALES ORDER NUMBER: SN 4043

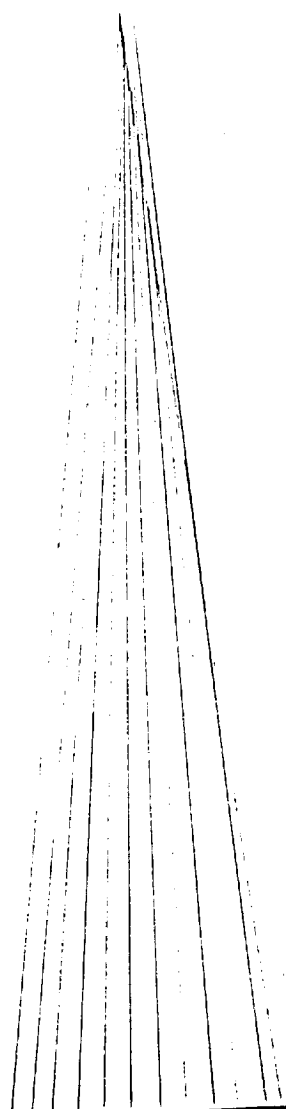
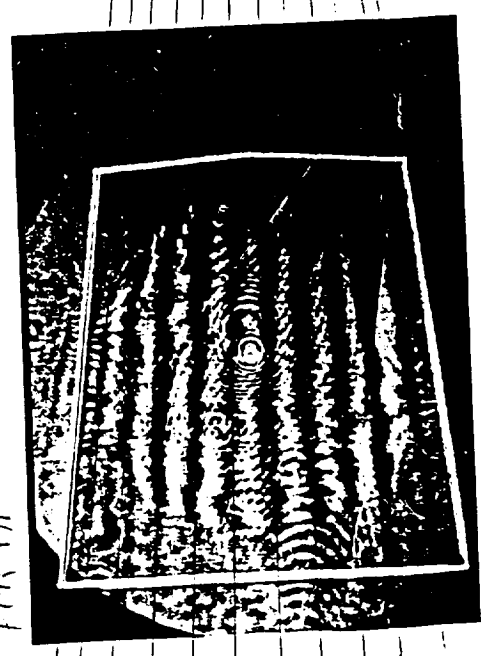
	<u>SPECIFICATION</u>	<u>ACTUAL</u>
MATERIAL:	ZERODUR [®]	ZERODUR [®]
DIAMETER:	8.000" \pm 0.005"	8.002"
VERTEX THICKNESS:	30mm +00 -10	25.45mm
CLEAR APERTURE (Elliptical):		
MAJOR AXIS:	185m	185mm
MINOR AXIS:	155mm	155mm
ELLIPSOID OF REVOLUTION (ABOUT MAJOR AXIS) RADII:		
MAJOR AXIS:	1672.92mm	Nominal \pm .1mm
MINOR AXIS:	1523.081mm	Nominal \pm .1mm
SURFACE ACCURACY:		
FIGURE:	1/8 Wave P-V @ 632.8nm over 100% C.A.	1/8 Wave P-V @ 632.8nm over 100% C.A.
MICROROUGHNESS:	20 A rms	Not Measured
MIDFREQUENCY:	20 A rms	17 A rms
COATING:	None	None
BACK SURFACE:		
FLATNESS:	1/4 Wave P-V @ 632.8nm	4 Wave P-V Concave
NORMAL TO +X AXIS:	15 arc-sec	<15 arc-sec


Alan E. DeCew, Jr.
General Manager

Date

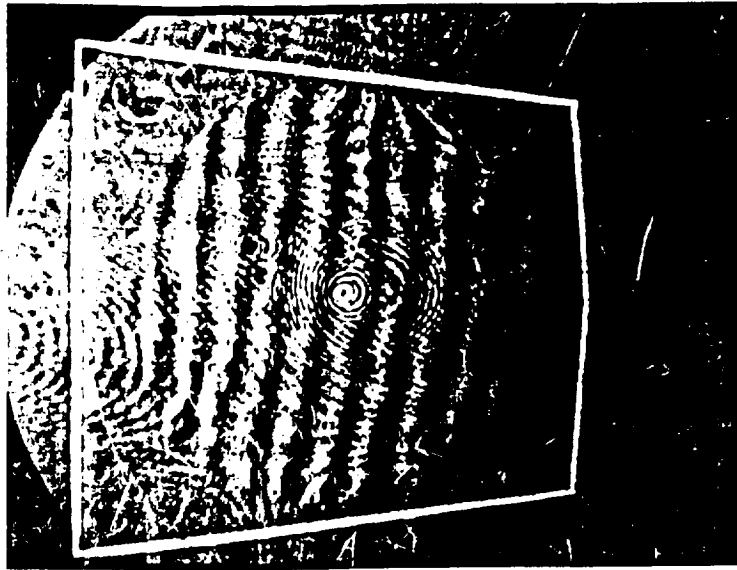
11 / 18 / 93

10-10-63
PVE
PCV IN

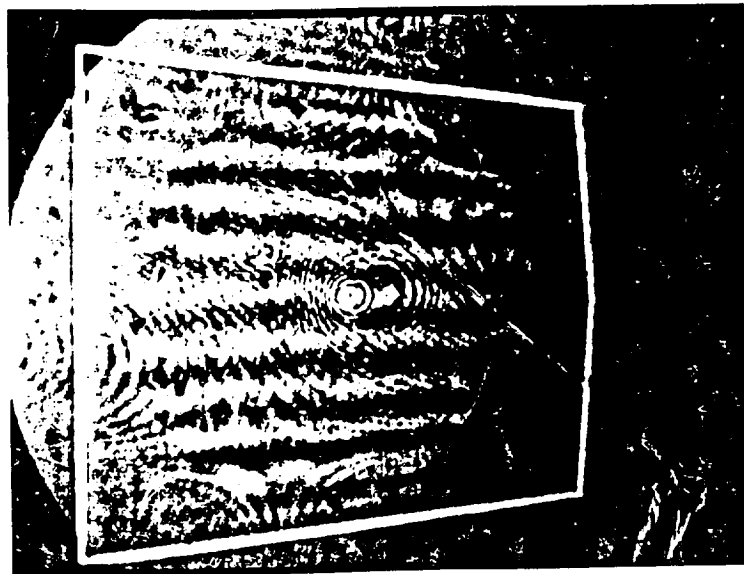


TILTED SURFACE MAKES FRINGES APPEAR TO
COME FROM A VANISHING POINT.

MANUAL REDUCTION METHOD FOR DEGB



1-73 1A54
1-73
20
20R 10



REPORT DOCUMENTATION PAGE

Form Approved
OMB No. 0704-0188

Public reporting burden for this collection of information is estimated to average 1 hour per response, including the time for reviewing instructions, searching existing data sources, gathering and maintaining the data needed, and completing and reviewing the collection of information. Send comments regarding this burden estimate or any other aspect of this collection of information, including suggestions for reducing this burden, to Washington Headquarters Services, Directorate for Information Operations and Reports, 1215 Jefferson Davis Highway, Suite 1204, Arlington, VA 22202-4302, and to the Office of Management and Budget, Paperwork Reduction Project (0704-0188), Washington, DC 20503.

1. AGENCY USE ONLY (Leave blank)		2. REPORT DATE March 1994	3. REPORT TYPE AND DATES COVERED Contractor Report	
4. TITLE AND SUBTITLE Deformed Ellipsoidal Diffraction Grating Blank			5. FUNDING NUMBERS NAS5-31790 <i>IN-35</i> <i>3348</i> <i>113P</i>	
6. AUTHOR(S) Alan E. DeCew, Jr. General Manager				
7. PERFORMING ORGANIZATION NAME(S) AND ADDRESS(ES) Space Optics Research Labs 7 Stuart Road Chelmsford, MA 01824			8. PERFORMING ORGANIZATION REPORT NUMBER	
9. SPONSORING/MONITORING AGENCY NAME(S) AND ADDRESS(ES) National Aeronautics and Space Administration Washington, D.C. 20546-0001			10. SPONSORING/MONITORING AGENCY REPORT NUMBER CR-189334	
11. SUPPLEMENTARY NOTES				
12a. DISTRIBUTION/AVAILABILITY STATEMENT Unclassified-Unlimited Subject Category 35			12b. DISTRIBUTION CODE	
13. ABSTRACT (Maximum 200 words) The Deformed Ellipsoidal Grating Blank (DEGB) is the primary component in an ultraviolet spectrometer. Since one of the major concerns for these instruments is throughput, significant efforts are made to reduce the number of components and subsequently reflections. Each reflection results in losses through absorption, and scattering. It is these two sources of photon loss that dictated the requirements for the DEGB. The first goal is to shape the DEGB in such a way that the energy at the entrance slit is focused as well as possible on the exit slit. The second goal is to produce a surface smooth enough to minimize the photon loss due to scattering. The program was accomplished in three phases. The first phase was the fabrication planning. The second phase was the actual fabrication and initial testing. The last phase was the final testing of the completed DEGB.				
14. SUBJECT TERMS Holographic Interferometry			15. NUMBER OF PAGES 112	
			16. PRICE CODE	
17. SECURITY CLASSIFICATION OF REPORT Unclassified	18. SECURITY CLASSIFICATION OF THIS PAGE Unclassified	19. SECURITY CLASSIFICATION OF ABSTRACT Unclassified	20. LIMITATION OF ABSTRACT Unlimited	